Cost-Optimal Operational Security in Transmission Grids with Embedded HVDC Systems and Energy Storage

Nico Hübner

Cost-Optimal Operational Security in Transmission Grids with Embedded HVDC Systems and Energy Storage

Cost-Optimal Operational Security in Transmission Grids with Embedded HVDC Systems and Energy Storage

Zur Erlangung des akademischen Grades eines

DOKTOR-INGENIEURS

von der KIT-Fakultät für
Elektrotechnik und Informationstechnik
des Karlsruher Instituts für Technologie (KIT)
genehmigte

DISSERTATION

von

Dipl.-Ing. *Nico Hübner*
geb. in: Bad Hersfeld, Deutschland

Tag der mündlichen Prüfung:	18.7.2019
Hauptreferent:	Prof. Dr.-Ing. Thomas Leibfried
Korreferent:	Prof. Dr. rer. pol. Wolf Fichtner

Danksagung (Acknowledgement)

Die vorliegende Arbeit entstand während meiner Tätigkeit als wissenschaftlicher Mitarbeiter am *Institut für Elektroenergiesysteme und Hochspannungstechnik* des *Karlsruher Instituts für Technologie* und wäre ohne die Unterstützung zahlreicher Personen nicht möglich gewesen.

Zunächst möchte ich mich bei meinem Doktorvater Prof. Dr.-Ing. Thomas Leibfried für die Übernahme des Hauptreferats bedanken. Die hervorragenden Arbeitsbedingungen, der bedingungslose Rückhalt und konstruktive Diskussionen trugen ebenso wie der hohe Freiheitsgrad beim Ausgestalten des Themas zum Gelingen dieser Arbeit bei.

Prof. Dr. rer. pol. Wolf Fichtner danke ich herzlich für die Übernahme des Korreferates, das Interesse an meiner Arbeit und die gründliche Lektüre.

Für fachliche Diskussionen zum Thema verteilte Optimierung und insbesondere ALADIN möchte ich mich bei Alexander Engelmann bedanken.

Die Grundlage für ein angenehmes Arbeitsumfeld haben meine ehemaligen und aktuellen Kollegen gelegt. Die Kaffeepausen sorgten besonders mit meinen Freunden und ehemaligen Kommilitonen Sebastian König, Simon Wenig und Yannick Rink immer für die nötige Abwechslung. Wichtige – häufig auch fachliche – Impulse gab mir mein langjähriger Zimmernachbar Martin Uhrig. Tobias Maier danke ich für die exzellente Vorauswahl an digitalem Informationsmaterial. Für die intensiven Kicker-Runden danke ich vor allem dem 3. Obergeschoss.

Natürlich wäre meine Arbeit ohne familiären Beistand in der Form nie möglich gewesen. Meinen Eltern möchte ich für die immer währende Unterstützung, vor allem während meines Studiums, danken. Am wichtigsten jedoch war der ständige Rückhalt meiner Frau Ann-Kathrin und seit Kurzem der kleinen Lara, die mich den Arbeitsalltag wenn notwendig immer schnell vergessen ließen.

Karlsruhe, im Juli 2019

Nico Hübner

Zusammenfassung (German Abstract)

Der politisch vorangetriebene Ausstieg aus Kohle- und Atomenergie und die damit einhergehende steigende Durchdringung von Erneuerbaren Energiequellen führt zu einer geographischen und zeitlichen Umverteilung der erzeugten elektrischen Energie. Zum einen führen beispielsweise große Windparks im Norden Deutschlands dazu, dass die erzeugte Energie unter Umständen weite Strecken zum Verbraucher im Süden zurücklegen muss und Netze lokal stark belastet werden. Zusätzliche Übertragungskapazitäten sind aufgrund ökonomischer und technischer Vorteile mit Hochspannungsgleichstromübertragung (HGÜ) zu erwarten. Zum anderen liegt es in der Natur von Wind und Sonne, dass die Stromerzeugung nicht immer zeitgleich zum Verbrauch erfolgt. Soll die Unabhängigkeit vom Leistungsaustausch mit europäischen Nachbarn zu einem gewissen Grad gewahrt bleiben, stellen Energiespeicher die einzige Möglichkeit zur Lastverschiebung dar.

Durch die veränderte Erzeugung sind bisher ungekannte Lastflusssituationen zu erwarten und es wird notwendig sein, technisch erlaubte Betriebsbereiche voll auszunutzen. Unter der Annahme, dass HGÜ-Systeme und Großspeicher in Zukunft Bestandteil unseres Energiesystems sein werden, ergeben sich für Netzbetreiber neue Möglichkeiten in der Systemführung. Des Weiteren ist es volkswirtschaftlich sinnvoll, notwendige Maßnahmen zur Sicherung der N-1 Sicherheit möglichst kostengünstig zu treffen. Deshalb handelt ein Teil dieser Arbeit vornehmlich von dem optimierten Einsatz von HGÜ-Systemen und Speichern, um teuren Kraftwerks-Redispatch zu minimieren oder ganz zu vermeiden. Es wird ein Modell vorgestellt, mit dem ein Netzbetreiber – unter Voraussetzung von entsprechenden Prognosen für Einspeisung und Last – prädiktiv die optimalen Arbeitspunkte für HGÜ und Speicher bestimmen kann, welche auch im Falle eines Leitungsausfalls nicht zu Verletzungen von thermischen Grenzen oder Spannungsbändern führen. Hierbei wird angenommen, dass nach einem Ausfall eine ausreichend schnelle Kommunikation vorhanden ist, um für die leistungselektronisch angeschlossenen Betriebsmittel neue Arbeitspunkte zu übermitteln oder zu aktivieren. Es zeigt sich, dass durch diese Flexibilität der notwendige präventive Redispatch deutlich verringert werden kann. Zudem werden Aspekte beleuchtet, wie sich beispielsweise eine Vermaschung von HGÜ-Strecken, das heißt die Bildung

von HGÜ-Netzen, auf die quasi-stationäre Netzsicherheit auswirken können.

Da einzelne Netzgebiete in einem synchronen Netz niemals isoliert betrachtet werden können, müssen benachbarte Netzbetreiber regelmäßig miteinander kommunizieren und kooperieren. Eine Optimierung nach obigem Vorbild könnte von einem zentralen Operator über Gebiets- oder Landesgrenzen hinweg erfolgen. Der Rechenaufwand wäre jedoch hoch, und politisch scheint solch eine Lösung schwer umsetzbar. Eine andere Möglichkeit ist die dezentrale Optimierung, bei der jeder Betreiber die Hoheit über sein Gebiet behält und nur dazu angehalten ist, während dem Prozess der gemeinsamen Lösungsfindung bestimmte Informationen mit den Nachbarn auszutauschen. Dies stellt den zweiten Schwerpunkt dieser Arbeit dar. Es werden Möglichkeiten aufgezeigt, wie eine verteilte Optimierung auch dann erfolgen kann, wenn benachbarte Gebiete über zusätzliche HGÜ-Verbindungen vernetzt sind. Hierbei führen die beiden implementierten Algorithmen (ADMM und ALADIN) zu einer Lösung, welche annähernd ebenso kostenoptimal ist wie eine zentral errechnete. Die sehr schnelle Konvergenz mit ALADIN lässt sich durch einen erhöhten Informationsaustausch und Rechenaufwand erkaufen. Ausführliche Berechnungen illustrieren die Performanz der Algorithmen anhand der Optimierung eines einzelnen Lastflussszenarios. Es wird jedoch auch gezeigt, dass die Entkopplung der Netzgebiete ebenso für zeitliche und N-1 sichere Probleme anwendbar ist.

Contents

Chapter 1

Introduction

Sustainability is the driver of industrialized nations around the globe to rethink our energy system. That man-made climate change is a fact, or at least the increasing variability of climate change, has found acceptance among the majority of researchers all over the world. Consequences of continued CO_2-emissions are only to be estimated – a reduction of which is our duty toward future generations. Large portions of CO_2-emissions stem from the energy sector, for example as a result of burning coal and oil to produce electricity. Given the possible alternatives, governments have started supporting the installation of renewable energy sources (RES)[1]. This trend from easily controllable power generation toward fluctuating generation with limited predictability poses new challenges to the remaining path from production to consumption. Since power from RES can be highly regional, the electrical grid might not be able to provide enough capacity for transportation. The consequence is frequent congestion management by the transmission system operator (TSO), such as generator redispatch[2]. In the long term, the costs of such measures are unacceptable for society and start gaining negative attention with the public[3].

The backbone of secure power supply – the transmission system – will inevitably undergo substantial progress to cope with already existing and continuously growing new challenges. Consequently, a radical transformation of the European power system is anticipated by the European Network of Transmission System Opera-

[1] In Germany, the installed capacity of combined photovoltaic and wind power plants grew from 26 GW to 98 GW between 2007 and 2017. The phase out of nuclear generation until 2022 has been agreed and the phase out of coal fueled generation until 2038 was recently proposed – a further increase can thus be expected.

[2] Generator redispatch: generation decrease "upstream" and generation increase "downstream" of a bottleneck to avoid overloading.

[3] In Germany, redispatch costs grew from € 132.6 million (4,370 GWh) in 2013 [9] to € 391.6 million (18,455 GWh) in 2017 [10].

tors for Electricity (ENTSO-E), which released a new Research and Innovation Roadmap 2017-2026 [30], focusing in particular on power system modernization, flexibility and efficiency.

1.1 The Future Transmission System

The development of our present transmission system involves a multitude of aspects. The most important aspects which are relevant to the scope of this thesis will be summarized below.

1.1.1 Network Enhancement

Regulatory measures will not be sufficient to cope with the challenges that are introduced by massive RES integration. The power system must be strengthened with different types of technologies.

Transfer Capacity with Benefits: VSC-based HVDC

One way to overcome costly congestion management is by installing new transmission capacities. Indeed, many kilometers of additional lines have been built, and many more are planned. Besides conventional alternating current (AC) transmission systems, a key role will be played by a new technology, namely high voltage direct current (HVDC). In fact, DC transmission is not any younger than AC technology. However, only in the past two decades, further development of semiconductors and new converter topologies have made an embedded application more attractive to transmission system operators. The transformation between AC and DC current is based on so-called voltage source converters (VSC), which are highly controllable and offer new possibilities – for example in terms of independent active and reactive power injection. VSC-based technology enables the principle of overlaying multi-terminal DC grids which will lead to a highly flexible power flow routing. The short response time facilitates efficient reactions to disturbances in the grid, such as line outages. In combination with lower energy losses over long distances compared to AC transmission, VSC-HVDC – in the following simply referred to as HVDC or DC – has a great perspective to gain importance in a future energy system mainly based on RES.

Versatile Grid Component: Energy Storage

Nevertheless, the *simultaneous* production and demand will remain crucial, even though one could argue that in a widespread network, there will always be "enough power generation somewhere". This is arguably a precarious assumption and technology to shift energy from one point in time to another will be an important

requirement for secure energy supply. The motivation to introduce energy storage systems (ESS) to level out time displacement between power production and consumption will arguably become indispensable when RES amount to at least 70-80% of electrical energy demand [92]. Despite the fact that this cannot be expected within short time, large-scale storages are already being installed all over the world, where frequency support is currently the main driver due to the ability to quickly provide positive or negative power. In addition, recent network development plan propositions in Germany include the consideration of ESS with up to 500 MW installed power in order to improve congestion management [1], that is, to provide power reserve in case of outages to relieve overloaded lines. Furthermore, it is conceivable to support the transmission system with storages from lower voltage levels, where aggregated reserve from home storage or electric cars could sum up to relevant quantities in the future. It is unlikely that ESS with such versatile application will only be employed on one field – instead, a combination will turn out to be most economic. For example, depending on the expected load flow situation, a storage system could be obliged to reserve a certain amount of positive or negative energy for possible outage scenarios and the subsequent congestion management. The remaining energy capacity could then be used for other requirements during normal operation, such as primary reserve or energy shifting for an economic RES integration.

1.1.2 Intelligent System Operation

New equipment alone will not increase system security unless controlled adequately. Thus, the potential of fast response devices will not be revealed without advanced operating strategies and an underlying high-speed communication infrastructure. Grid observability must be increased via monitoring and forecasting systems to enable advanced automatic control and intelligent decision support tools for security assessment. In addition, optimization will play an important role in order to be able to operate the system in a safe, but cost-effective state to maximize global social welfare. Automatic or triggered control actions after an outage will play a central role when exploiting security limits during normal operation in order to minimize costs. Possible curative actions must be defined in advance for each considered contingency and either be sent to the actuators after the outage or be deployed in advance and then triggered. In any case, signals must be communicated quickly and reliably, if normal operation shall rely on those curative measures.

1.1.3 Coordination of Multiple Control Areas

Integrated energy markets[4] lead to increasing cross-border trades and physical power flows. While some years ago, congestion management used to be largely a national matter, today's control areas cannot be viewed as isolated anymore. Clearly, central coordination would lead to a maximized global social welfare. However, given the expected numerous controllable and observable units, and subsequently the huge data generated, this seems out of reach. Furthermore, due to political will, it is unlikely for an operator to give up authority over a control area. Approaches will be required to maintain controller independence on the one hand, but nevertheless approaching a system operating point close to the central optimum on the other hand.

1.2 Contributions

The future transmission grid requires advanced operating schemes to optimally exploit the introduced potential of controllability, which will be addressed in this thesis. It is divided into two parts; the first part addresses the modeling and testing of an advanced optimization framework. The objective is a cost-optimal power system operation in a secure state, namely subject to stationary network constraints (for example voltage or thermal limits) and in particular N-1 security. The core feature is the efficient utilization of flexibilities provided by advanced grid equipment such as HVDC systems and energy storage. In the case of optimal storage operation, this requires RES forecasts and optimization over multiple time steps. Cost-optimality considers certain risks which can be taken by a TSO to neglect immunity against very improbable events, if the immunity would come with huge costs. Case studies in two test systems of small (5-bus) and medium size (67-bus) present comprehensive insights into the effectiveness of various control modes. The main contributions of the first part – the centralized optimization framework – are summarized to:

- Modeling of a modular framework for power flow optimization over multiple time steps and multiple topologies.
- Integration of flexibilities from energy storage and embedded HVDC systems.
- Risk-based N-1 security under consideration of various control modes (preventive, curative or preventive-curative).

The second part involves the coordination of multiple control areas. The centralized optimization problem from the first part is divided into sub-problems

[4]Europe is under steady progress toward fully coupled day-ahead and intra-day markets. In July 2018, continuous cross-zonal trading went live in 14 European countries [31].

according to geographical control areas. The model of a hybrid AC-DC grid requires certain mathematical formulations to enable a proper network decomposition. Two efficient algorithms with different properties in terms of required computation and communication are implemented and compared to push the independent sub-problems towards a central optimum. The main contributions of the second part – the distributed optimization – are summarized to:

- Detailed network decomposition for hybrid AC-DC grids.
- Implementation and comparison of two algorithms: ADMM and ALADIN.
- Coordinated multi-area operational security.

1.3 Thesis Outline

The thesis is partitioned as follows:

- Chapter 2 provides a review of requirements and definitions related to operational security in transmission systems according to ENTSO-E.
- In Chapter 3, an overview is given on recent developments in the optimization of power system operation, namely Optimal Power Flow (OPF). Schematic problem extensions relevant in the context of this thesis are highlighted.
- Mathematical formulations are presented in Chapter 4 to adequately describe the variables, constraints, and objectives of the underlying optimization problem.
- Chapter 5 presents case studies for a single time step optimization in two test systems to comprehensively highlight certain aspects, e.g. AC-DC optimal power flow or N-1 security.
- Chapter 6 presents case studies where energy storage is included, which is subsequently based on multiple time steps.
- In Chapter 7, two distributed algorithms are introduced and compared. Furthermore, a simple example is presented to illustrate the two methods.
- Chapter 8 presents the application of the algorithms from Chapter 7 to several case studies.
- In Chapter 9, the main findings are discussed and resulting conclusions are drawn.

If the reader is interested in single time step optimization with PST and HVDC only, the reader is invited to read Chapters 4 and 5. If the reader is instead interested in storage optimization, Chapters 4 and 6 are relevant. Lastly, if the reader is only interested in distributed optimization, then the reader would find Chapters 4, 7 and 8 of interest. In addition, Chapters 5 to 8 come with a short summary for an overview of the results.

Chapter 2

Operational Security in Transmission Grids

Operational security is one responsibility among many that a TSO bears. There exist different electricity markets all over the world, but usually, security aspects are not a priori respected. It is the task of a TSO to regularly check whether or not the market result, i.e. the planned dispatch, satisfies all security requirements – and to take adequate measures if that is not the case. This is done on various time scales, most importantly day-ahead and intra-day.

This chapter refers to the "UCTE Operation Handbook" [26], which is a collection of operation principles and rules for the transmission system operators in continental Europe. More specifically, Policy 3 [28] and the related Appendix [27] form the basis for the following aspects of Operational Security.

2.1 N-1 Security Principle

An important security measure is the "*N-1 principle*". Let the network consist of N elements including transmission lines, generators or bus bars. The rule guarantees that with $N-1$ elements, thus the loss of one arbitrary element, the system remains within the *Normal State*:

- "**Normal State** means the system state where the system is within operational security limits in the N-situation and after the occurrence of any contingency from the contingency list, taking into account the effect of the available Remedial Actions." [29]

A TSO can define additional sets of those operational security limits which can be accepted for a certain amount of time, e.g. allowing an increased line loading

from 100% to 120% for 15 minutes. However, if these limits are expected not be met after an incident, the system is in *Alert State*:

- "**Alert State** means the system state where the system is within operational security limits, but a contingency from the contingency list has been detected, for which in case of occurrence, the available Remedial Actions are not sufficient to keep the Normal State." [29]

N-1 calculations must be done in operational planning phase, based on forecast data, as well as in real time operation in an automatic manner.

2.1.1 ASAP Restoration

Once a contingency has occurred, potential curative remedial actions are applied and the system should be within operating limits. However, a second contingency, also referred to as N-1-1 outage, might endanger the system. Therefore, a TSO must try to restore N-1 security As Soon As Possible (ASAP). In the mean time, the system might be at risk and the new calculation must be launched immediately after the implementation of remedial actions.

2.1.2 Types of Contingencies

Tripping elements, which can not be predicted, are considered as contingencies. Each TSO creates a list of relevant contingencies which must be taken into account for the N-1 calculations. These include "normal types" such as lines, DC links, transformers or generating units, but possibly also "exceptional types" such as double circuit lines or bus bars. More severe contingencies ("out of range type"), such as a tower with more than two lines or a total substation with more than a busbar, must not necessarily be considered for N-1 calculations.

2.2 Remedial Actions

There are two categories of remedial actions:

- **Curative** actions can rapidly relieve constraints and are implemented *after* the occurrence of a contingency.
- **Preventive** actions are launched *before* an anticipated contingency.

Those actions must be prepared in advance and the effectiveness must be validated by load-flow calculations. Since remedial actions are explicitly considered during N-1 calculations, the preparation and validation is continuously repeated during operational planning phase (e.g. day-ahead) until a few hours ahead or even real time operation. Important remedial actions could include to

- change the tap position of a phase shifting transformer
- change power set points on HVDC systems
- redispatch generating units (including storage systems)
- shed loads
- change the network topology.

2.3 Risk Management

The main task of a TSO is to make the power system reliable, i.e. to ensure normal system operation, limit the number of incidents and – as far as possible – avoid major incidents. However, this need not be done at any price. Depending on the contingency, a certain risk may be taken to avoid huge costs in the case an event is very improbable to occur. The combination of *Probability* and non-served energy or expected *Loss* (commonly in MWh), is an important measure to designate a system operation at "acceptable *Risk*", and the relation can be expressed with

$$Risk = Loss * Probability. \tag{2.1}$$

In Fig. 2.1, a schematic of the risk management policy is shown. On the horizontal axis the possible incidents are assigned a certain probability, e.g. a high probability for a generator outage and a very low probability for a high voltage substation outage. On the vertical axis, the expected losses are depicted. The very left column includes Zone 1, where extreme events of very low probability have a severe impact. However, it would be too costly to cover these events with large security margins. With increasing probability of an event, an "unacceptable consequences" limit becomes active. Measures must be taken at all times to guarantee that an event will not lead to losses above this threshold, i.e. the consequences are unacceptable. For larger probabilities, a "maximum acceptable risk" is defined by the TSO. With (2.1), an iso-risk curve comes into effect, which indicates that the system should remain below that curve. For example, the system should be able to maintain the full energy supply in case of a high-probability event.

As stated before, the activation of remedial actions is incorporated in N-1 calculations. For example, even if an event puts the system at risk, indicated with (1), a curative measure is foreseen to bring it back to an acceptable risk, indicated with (2). If a curative action is not available or sufficient, a preventive action (or a combination of both) could be implemented and have the same effect.

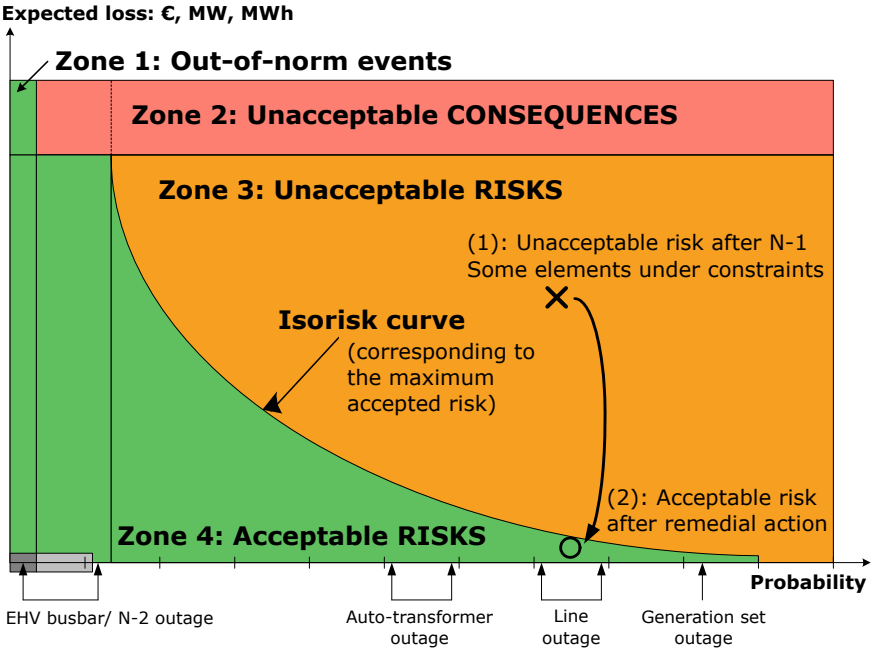

Figure 2.1: Iso-risk curve and remedial actions according to ENTSO-E [27]. With an increase of the outage probability, the acceptable losses decrease.

2.4 Summary

Continuous energy supply for any private or industrial customer is the main goal for a transmission system operator. Nevertheless, the cost for society would be unacceptable if the dimensioning and the security margins were laid out to cope with any severe outage. In those cases, energy cuts must be a valid option to maintain system security. By assigning penalty costs to a possible energy loss, a trade-off can be searched which minimizes the general expenses plus the penalties on condition that for each contingency, the risk level is not exceeded, i.e. effective costs of remedial actions are below the cost of the risk [27].

Chapter 3

Optimal Power Flow – an Overview

Reaching optimality can be easy – it always depends on the problem posed. The cheapest generator set point is straight-forward to calculate if the power network is not considered, yet it is *optimal* in relation to the posed optimality condition. Throughout this work, we consider the electrical grid as of highest interest and focus on power flow-based optimization. In particular, this means that if not mentioned explicitly, we relate to a full nonlinear load flow model. Furthermore, the following literature review lacks numerous publications which do fit into the topic but use simplified or linearized load flow models.

3.1 Optimal Power Flow (OPF)

Traditional Optimal Power Flow (OPF) goes back to the 1960s [17, 22] and has since been studied intensively under consideration of a variety of constraints, relaxations, and objective functions. A comprehensive literature review until the 1990s can be found in [62, 63]. The most common branch is undoubtedly the minimization of generator fuel costs subject to network constraints such as voltage and line flow limits. Variables x are optimized to minimize a cost function *"Costs"*, while assuring a *"Feasible Power Flow"*, i.e. remaining within *"Network Security Limits"* and respecting the *"Operational Limits of x"*. For easier reference to these

standard constraints, the set of constraints is collected in *"Basics"*:

$$\underset{x}{\text{minimize}} \quad \mathit{Costs}(x) \tag{3.1a}$$

$$\text{subject to} \quad \left.\begin{array}{l} \mathit{Feasible\ Power\ Flow} \\ \mathit{Network\ Security\ Limits} \\ \mathit{Operational\ Limits\ of\ } x \end{array}\right\} \ \mathit{Basics}(x). \tag{3.1b}$$

3.2 Dynamic Optimal Power Flow (D-OPF)

Dynamic OPF, multi-time step OPF, multi-period OPF, OPF with inter-temporal constraints, time-constrained OPF – the denomination of one and the same problem has not found consensus in research. They all describe a collection of multiple quasi-stationary time steps, which cannot be calculated independently due to inter-temporal constraints, or *"Dynamics"*[1]. The first works take the time-dependent generator scheduling for a reason to extend the OPF [18]. Then, energy constraints are added in terms of energy contracts with generators [90, 68] or with consumers [20]. With the rise of RES, energy storage has become a large topic which is discussed in Chapter 3.5.3. In D-OPF, base variables are duplicated for each time step, which is denoted with a superscript $(x^1, x^2, .., x^T)$ and T the last time step in the considered time horizon. The problem is described with

$$\underset{x^1,..,x^T}{\text{minimize}} \quad \sum_{t=1}^{T} \mathit{Costs}^t(x^t) \tag{3.2a}$$

$$\text{subject to} \quad \mathit{Basics}^t(x^t) \quad \mathit{for}\ t = 1, .., T \tag{3.2b}$$

$$\mathit{Dynamics}(x^1, .., x^T). \tag{3.2c}$$

3.3 Security-Constrained Optimal Power Flow (SC-OPF)

N-1 secure Optimal Power Flow, also called Security-Constrained Optimal Power Flow, is an extended OPF. It includes additional topology states where single elements have tripped and the controllable units can provide preventive and/or curative remedial actions to keep the system within security limits before *and* after a contingency. Since a whole list of outages is considered, preventive actions must be valid for all scenarios.

[1] We emphasize that in OPF research, this always refers to quasi-stationarity where the electrical frequency is invariant. Once frequency variation is included, it is referred to as *transient*.

3.3.1 Traditional SC-OPF

The first attempts on SC-OPF go back to the 1980s [2, 65] and recent developments can be found in [16, 15]. Here, a superscript describes either variables from the base case (x^0), or variables from one of the C contingencies ($x^1, .., x^C$). So-called *"N-1 Coupling"*-constraints relate the controllable units or states from before to after an outage. Thus, they describe whether or not those variables are allowed to change their set point. The "traditional" objective is to minimize the costs in the base case, i.e. preventive remedial actions. The problem can be written as

$$\underset{x^0,..,x^C}{\text{minimize}} \quad \mathit{Costs}^0(x^0) \tag{3.3a}$$

$$\text{subject to} \quad \mathit{Basics}^c(x^c) \quad \mathit{for}\ c = 0, 1, .., C \tag{3.3b}$$

$$\mathit{N\text{-}1\ Coupling}(x^0, .., x^C). \tag{3.3c}$$

3.3.2 Risk-based SC-OPF

In problem (3.3), every contingency, regardless of the probability, must be covered by the security margins. No energy loss is allowed, even if necessary preventive actions are unreasonably expensive. To cope with these circumstances, and motivated by the risk management policy from ENTSO-E [27], a risk-based OPF formulation is of interest. This is a young, but growing research field and various formulations are proposed. Additional risk constraints can be added [14, 81, 82], and the violation of operating security limits can be allowed [49, 91]. However, as an example, it can be hard to assign costs to voltage limit violations. Therefore, it is reasonable to require operational security limits to be held at all time and to only use the non-served energy as costly flexibility that a TSO can choose to take a risk on. This is in line with [67, 66] where, however, additional scenarios with a probability-weighted variation in the load or RES profile is added.

To account for a risk-based formulation, the objective function is augmented by the cost of curative actions and non-served energy. The costs arising after an outage c are weighted with a probability p^c. The probability of a certain outage is a parameter, which must be estimated by the responsible TSO. The problem can be written to

$$\underset{x^0,..,x^C}{\text{minimize}} \quad \mathit{Costs}^0(x^0) + \sum_{c=1}^{C} p^c \cdot \mathit{Costs}^c(x^c) \tag{3.4a}$$

$$\text{subject to} \quad \mathit{Basics}^c(x^c) \quad \mathit{for}\ c = 0, 1, .., C \tag{3.4b}$$

$$\mathit{N\text{-}1\ Coupling}(x^0, .., x^C). \tag{3.4c}$$

3.4 Security-Constrained Dynamic Optimal Power Flow (SC-D-OPF)

Recent works have sought to combine both N-1 security with the optimization of multiple time steps. First research in that area was done in 2013 by [67], where not only power but also necessary energy reserves can be determined to ensure N-1 security. In [23], successive linear algorithms and approximated power flows are used to solve large-scale SC-D-OPF problems in a European context. The authors of [76] propose an SC-D-OPF model including uncertainty of wind power or equipment availability, which is solved in a two-stage stochastic program. In [37], SC-D-OPF is used as inner iteration in a hierarchical approach to optimize a central deployment signal which is sent to the units able to provide a reserve. Furthermore, [66, 55, 86] are described in the ESS-section 3.5.3.

Consequently combining the approaches from D-OPF and SC-OPF, two superscripts (t, c) denote time step and contingency in SC-D-OPF, subsequently resulting in $(x^{1,0}, .., x^{1,C}, .., x^{T,0}, .., x^{T,C})$. The full problem contains both dynamic constraints over all base cases and security constraints for each time step:

$$\underset{\substack{x^{1,0},..,x^{1,C},..,\\ x^{T,0},..,x^{T,C}}}{\text{minimize}} \quad \sum_{t=1}^{T} \mathit{Costs}^{t,0}(x^{t,0}) + \sum_{t=1}^{T}\sum_{c=1}^{C} p^{t,c} \cdot \mathit{Costs}^{t,c}(x^{t,c}) \tag{3.5a}$$

$$\text{subject to} \quad \mathit{Basics}^{t,c}(x^{t,c}) \quad \mathit{for}\ c = 0, 1, .., C\ \mathit{and}\ t = 1, .., T \tag{3.5b}$$

$$\mathit{N\text{-}1\ Coupling}^{t}(x^{t,0}, .., x^{t,C}) \quad \mathit{for}\ t = 1, .., T \tag{3.5c}$$

$$\mathit{Dynamics}(x^{1,0}, .., x^{T,0}). \tag{3.5d}$$

An overview of the schematic modeling of different OPF variations is given in Fig. 3.1.

3.5 Integration of Additional Assets

With a future energy system based on RES, the need for additional assets at hand of a TSO is unarguable. We distinguish between

- **AC power flow routing**: traditional Phase Shifting Transformers (PST) or power electronic devices such as Flexible AC Transmission Systems (FACTS) allow for an optimization of voltage magnitude and angle which affects active and reactive power flow over a certain line and subsequently in the network;
- **HVDC systems**: embedded HVDC systems add transmission capacity on the one hand, and – with VSC-based technology – independent active and reactive power control on the other hand;

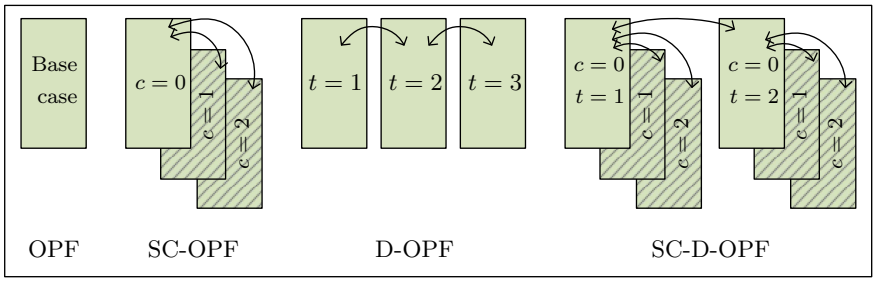

Figure 3.1: From left to right: Basic OPF, N-1-secure OPF with two contingencies, Dynamic OPF with three time steps, N-1-secure dynamic OPF with two contingencies and two time steps.

- **Energy Storage Systems**: fluctuating RES production and load can be leveled out by shifting energy over time, and congested lines can be relieved with positive and negative active power reserve.

If OPF-based control is used by a TSO, the above-stated additional flexibilities should be considered in the calculations to enable a cost-optimal solution.

3.5.1 AC Power Flow Routing

Variable tap transformers have been integrated into power system planning and operation for a long time and are considered as standard equipment of a TSO. In [71], PSTs are integrated in a large-scale OPF and [64] implements various additional constraints on tap changing. The author in [79] uses PSTs to intensively study effects on the Belgian (and bordering) transmission system. Power electronic based flexible AC transmission systems are used to optimize active power flow [40] and OPF is used in [3] to search for optimal locations of Unified Power Flow Controllers (UPFC).

N-1 Security

Suitable UPFC models for the incorporation in SC-OPF are derived in [56], and [50] presents an SC-OPF with controllable discrete transformer taps.

3.5.2 HVDC Systems

Probably the first to include VSC-based HVDC systems into OPF calculations was [72] in 2007. Initially, converter losses are neglected, but [87] closes the gap. In [13], different control strategies are applied to the VSCs in a meshed DC grid

to minimize steady-state losses and in [58], AC-DC OPF is used to calculate an optimal VSC schedule. Shortly after in 2014, [73] claimed to present the first VSC-based AC-DC OPF in a fully meshed DC network. New programming approaches are presented in [6] and AC-DC OPF is used in [35] to evaluate the economic benefit of installing VSC-based HVDC systems in existing AC grids, followed by other power flow studies.

N-1 Security

After the AC-DC OPF had established, the focus logically turned towards N-1 security. In [88], the positive effect of allowing curative actions by the HVDC system are examined, however, the AC grid is linearized. In [74], this drawback is removed, and the authors in [12] also include short term post-contingency corrective control and a risk-based objective. Most recently, further applications, for example to robust approaches [59] or optimized generator redispatch [102], are presented among others.

3.5.3 Energy Storage Systems

The first D-OPF applications including energy storage focused on hydrothermal power plants and the related time-dependent water reservoirs [84, 78]. Starting 2011, battery storage was used to cope with distributed RES [54] and to optimally control active distribution networks [38, 42]. Isolated microgrids are optimized with D-OPF in [70], and robust formulations follow in [48].

N-1 Security

Using distributed batteries for N-1 security was presented in 2015 by [85]. However, a linearized AC network is considered and furthermore, the state of charge of the battery is neglected – the author assumes that there is always enough energy reserve for the curative actions. In [11], AC power flow is considered and, to some extent, the state of charge of the batteries. The base case, i.e. the available energy for a particular outage, cannot be optimized and is assumed as given.

A concept to include the inter-temporal dependencies for the base case is presented in [66], and actual case studies and the impact on storage operation are shown in [55]. In [86], the base case storage operation is included into a N-1 secure day-ahead unit commitment problem considering a linearized network model, which is solved in two iterative stages, i.e. before and after the contingency.

Table 3.1: Literature overview on OPF types with ESS and/or HVDC.

OPF type	Extensions	Literature
OPF	HVDC	[72, 87, 6, 13, 58, 73, 35]
SC-OPF	HVDC	[88, 74, 12, 102]
SC-OPF	ESS	[85, 11]
D-OPF	ESS	[54, 38, 70, 42, 48]
D-OPF	ESS & HVDC	[95]
SC-D-OPF	ESS	[66, 55, 86]
SC-D-OPF	ESS & HVDC	[99]

3.5.4 HVDC and ESS

Despite the fact that both HVDC and ESS seem to deserve close attention when optimizing power system operation, only a few works exist to combine the advantages of both assets. In [95], a D-OPF is applied to a hybrid AC-DC grid with ESS and in [99], the framework is extended to cope with N-1 security.

An overview of the relevant works which incorporate HVDC and/or ESS for different OPF applications is given in Table 3.1. In the case of OPF with HVDC and D-OPF with ESS, only a selection of the most relevant and high-quality papers is displayed.

3.6 Handling Discrete Variables

Some variables are of discrete nature and form a major concern for solution strategies. As of today, there are no solvers available to efficiently handle the possibly most challenging optimization problem with the properties of being large-scale, nonlinear, non-convex and mixed integer. One basically has the choice between linearizing the model and maintaining the discrete variables, or to relax the discrete variables into continuous ones and maintain system nonlinearity. Either way, a trade-off must be accepted and global optimality is a goal that will probably never be reached under guarantee. The most important mixed integer variables and constraints are described in the following.

Generator Operating Constraints

Thermal power generation is based on comparatively slow processes. Beside the ramp rate, which can be modeled continuously, a power plant might be subject to minimum up or down times. Furthermore, startup and shutdown costs might play a role, which were considered in a Mixed Integer Linear Program (MILP)

as early as 1962 [39]. However, the so-called unit commitment problem is often neglected in OPF-based investigations by reasoning that the generators are either fast enough (e.g. gas turbines) or known to be on-/offline. In the latter case, an online generator could simply be subject to a minimum power generation limit. A reasonable trade-off is to compute a two-stage optimization: first with an MILP, and second a continuous nonlinear problem (NLP) with a given generator commitment.

Transformer Taps or Shunt Steps

Transformer taps and shunt steps usually do not directly contribute to the cost function. Furthermore, the discrete steps are small compared to the covered range of the variable. For example, a transformer tap could lie between $\pm 20\,\%$ with a step size of $2\,\%$ and therefore, relaxation to a continuous variable seems to be a reasonable approach. In [71] it is shown for a large-scale network under various loading conditions that the effects of discretization are very small. Nevertheless, good care must be taken in order not to provoke an infeasible power flow situation. Rounding strategies are widely used, i.e. the resulting continuous value is rounded to the closest valid discrete step. An additional simulation should be done to verify the feasibility of the modified power flow. With multiple discrete units, this step could be repeated by only rounding and fixing the units which are closest to a valid value, until all units are fixed [50].

Optimal Transmission Switching

As stated in Chapter 2.2, a change in topology is a possible remedial action for a TSO. In some situations, it can be beneficial to switch out overloaded lines or to switch in other lines for stress relief. The decision which line to switch in or out is inevitably binary. Therefore, a true optimization is only possible with a simplified network model [36] loosing crucial information on voltage magnitudes and reactive power. Similar to the generator commitment, a two-stage process with a MILP in the first stage and an NLP in the second stage can lead to acceptable results.

3.7 Solving the Continuous Problem

Considering the full AC power balance, this is a nonlinear and non-convex optimization problem which is not easy to solve, but powerful methods have been developed to tackle the problem efficiently these days, even at large-scale. Most state-of-the-art continuous NLP solvers are based on primal-dual interior point methods with logarithmic barrier functions to treat inequality constraints (early

works from [89, 83, 77]). A general NLP has the form

$$\begin{aligned} \underset{x}{\text{minimize}} \quad & f(x) && \text{(3.6a)} \\ \text{subject to} \quad & g(x) = 0 && \text{(3.6b)} \\ & h(x) \leq 0, && \text{(3.6c)} \end{aligned}$$

where cost function $f(x)$, equality constraints $g(x)$ and inequality constraints $h(x)$ are assumed to be twice continuously differentiable. To handle inequalities efficiently, slack variables s are introduced to form equalities instead. With a logarithmic barrier function to penalize slack variables, the problem is formed to

$$\begin{aligned} \underset{x}{\text{minimize}} \quad & f(x) - \gamma \sum_{j=1}^{n_\text{i}} \ln(s_j) && \text{(3.7a)} \\ \text{subject to} \quad & g(x) = 0 && \text{(3.7b)} \\ & h(x) + s = 0 && \text{(3.7c)} \\ & s \geq 0, && \text{(3.7d)} \end{aligned}$$

with n_i the number of inequality constraints. The barrier coefficient γ holds the inequality constraints away from zero in the first iterations to avoid early convergence into local minima. Eventually, γ is reduced to zero and the problem (3.7) approaches the original one (3.6). With the assignment of dual multipliers λ to the equality constraints and κ to the inequality constraints, the Lagrangian of (3.7) for a given γ is formed to

$$\mathcal{L}^\gamma(x, \lambda, \kappa, s) = f(x) + \kappa^\mathsf{T} \left(h(x) + s\right) + \lambda^\mathsf{T} g(x) - \gamma \sum_{j=1}^{n_\text{i}} \ln(s_j). \tag{3.8}$$

The optimal solution and thus a stationary point of the Lagrangian is found when $\nabla \mathcal{L}^\gamma(x, \lambda, \kappa, s) = 0$, that is,

$$\begin{aligned} 0 &= \nabla_x f(x) + \lambda^\mathsf{T} \nabla_x g(x) + \kappa^\mathsf{T} \nabla_x h(x) && \text{(3.9a)} \\ 0 &= \kappa^\mathsf{T} - \gamma e^\mathsf{T} [s]^{-1} && \text{(3.9b)} \\ 0 &= g^\mathsf{T}(x) && \text{(3.9c)} \\ 0 &= h^\mathsf{T}(x) + s^\mathsf{T}. && \text{(3.9d)} \end{aligned}$$

Here, ∇_x is the gradient operator with respect to x; e is an all ones vector of appropriate size; and $[s]$ forms a diagonal matrix with vector s on the diagonal. Newton steps are used to linearize and solve problem (3.9) iteratively. Non-negativity of s and κ, that is,

$$\begin{aligned} 0 &\leq s && \text{(3.10a)} \\ 0 &\leq \kappa, && \text{(3.10b)} \end{aligned}$$

must be assured by appropriate Newton update step sizes. Note that (3.9) together with (3.7) are called Karush-Kuhn-Tucker (KKT)-conditions [53]. Depending on the solver, different rules are applied for the reduction of γ and the Newton update step sizes. Throughout this thesis, it is used IPOPT [80] for solving continuous nonlinear problems.

Chapter 4

Optimization Framework Model

In this chapter, we derive all the necessary models and formulations for the optimization framework. In Chapter 4.1, we describe the basic constraints for optimal power flow in AC-DC grids for one time step and one topology (OPF). Next, we extend the model by multiple topologies in Chapter 4.2, which leads to an N-1 secure OPF (SC-OPF). In Chapter 4.3 we add a dynamic dimension to cope with power fluctuations and energy-related restrictions (D-OPF). Finally, we build up the full optimization problem (SC-D-OPF) in Chapter 4.4. All OPF variants and extensions are designed in a modular way, such that a reduction to a customized problem remains possible.

Notation

In the modeling sections 4.1 and 4.2, our focus lies on a comprehensive description and we omit indices where not necessary. Variables without running subscript should therefore not be viewed as a vector but rather as a representative variable for a certain type. For example, instead of $X_{\mathrm{G}i}^2 \leq 1, \ \forall i$ we can write $X_{\mathrm{G}}^2 \leq 1$. Superscripts (t, c) are used to denote a time step t and a topology scenario c. However, many constraints are valid for all t or all c. Therefore, the superscripts are omitted unless the constraint requires a differentiation between different t's (e.g. dynamics) or c's (e.g. N-1 security).

Furthermore, we collect elements of the same type (e.g. generators, loads, converters, etc.) in a set $\mathcal{E}^{\mathrm{X}}$, where X is an identifier for the respective type. The subset $\mathcal{E}_i^{\mathrm{X}}$ then collects those elements of $\mathcal{E}^{\mathrm{X}}$, which are connected to node i. An illustrative example of some set definitions is shown in Fig. 4.1.

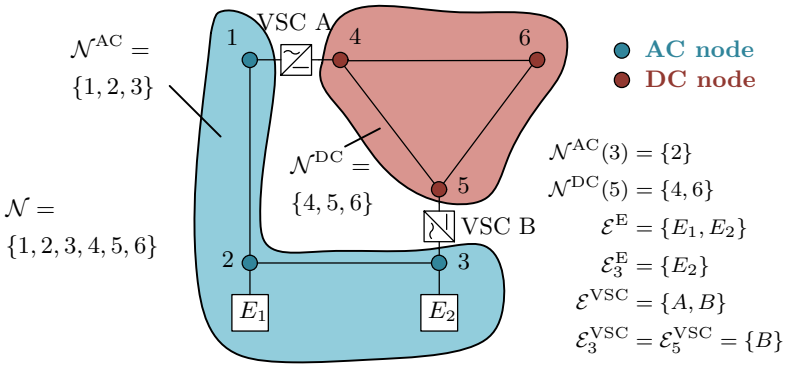

Figure 4.1: Illustrative example of node set ($\mathcal{N}$) and element set ($\mathcal{E}$) definitions.

4.1 Base Case

Consider an electrical network with a total of N nodes, also referred to as buses, which are collected in the set $\mathcal{N} = \{1, ..., N\}$. We distinguish two types of nodes: alternating current (AC) nodes with a corresponding complex voltage V_{AC} and direct current (DC) nodes with a corresponding real voltage V_{DC}. The subsets $\mathcal{N}^{\mathrm{AC}} \subseteq \mathcal{N}$ and $\mathcal{N}^{\mathrm{DC}} \subset \mathcal{N}$ identify the membership of a node in $\mathcal{N}$. A node can only be of one type, thus $\mathcal{N}^{\mathrm{AC}} \cup \mathcal{N}^{\mathrm{DC}} = \mathcal{N}$ and $\mathcal{N}^{\mathrm{AC}} \cap \mathcal{N}^{\mathrm{DC}} = \emptyset$. Electrical neighbors of an AC node $i \in \mathcal{N}^{\mathrm{AC}}$ (excluding node i itself) are collected in $\mathcal{N}^{\mathrm{AC}}(i)$. Analogously, $\mathcal{N}^{\mathrm{DC}}(i)$ collects all DC neighbors of $i \in \mathcal{N}^{\mathrm{DC}}$.

4.1.1 AC Branches

All branches connecting two AC nodes $i, j \in \mathcal{N}^{\mathrm{AC}}$, i.e. AC lines and transformers, are modeled with an ideal transformer in series with a standard π-model. The transformer has a complex tap ratio $\psi_{\mathrm{PST}} = \tau e^{\mathrm{j}\theta}$ and the π-model consists of a series admittance y_{S} and parallel admittances y_{P} (see Fig. 4.2). With $\psi^*_{\mathrm{PST}} = \tau e^{-\mathrm{j}\theta}$, the current balances at both sides of the π-model are

$$0 = \psi^*_{\mathrm{PST}} I_{\mathrm{Br}ij} - y_{\mathrm{P}} \frac{V_{\mathrm{AC}i}}{\psi_{\mathrm{PST}}} - y_{\mathrm{S}} \Big(\frac{V_{\mathrm{AC}i}}{\psi_{\mathrm{PST}}} - V_{\mathrm{AC}j} \Big) \tag{4.1a}$$

$$0 = I_{\mathrm{Br}ji} - y_{\mathrm{P}} V_{\mathrm{AC}j} - y_{\mathrm{S}} \Big(V_{\mathrm{AC}j} - \frac{V_{\mathrm{AC}i}}{\psi_{\mathrm{PST}}} \Big). \tag{4.1b}$$

Thus, the calculation of an outgoing current from a node depends on the location of the ideal transformer. Depending on whether we compute our current injection

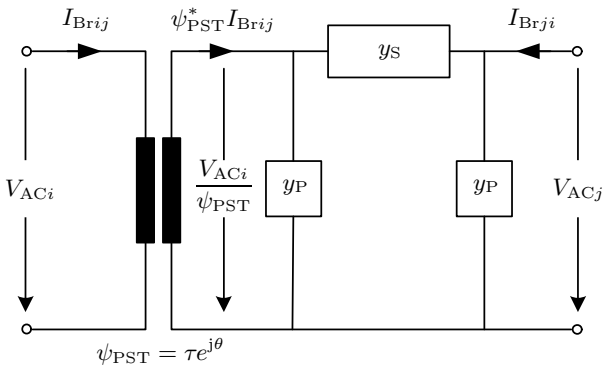

Figure 4.2: Branch model between AC nodes i and j, which consists of a pi-model for a transmission line and an ideal transformer.

at the transformer side, i.e. a flow $i \to j$, or at the opposite side, i.e. a flow $j \to i$, and with $y_{\mathrm{SP}} = y_{\mathrm{S}} + y_{\mathrm{P}}$, we have

$$I_{\mathrm{Br}ij} = \frac{y_{\mathrm{SP}}}{\psi_{\mathrm{PST}}\psi^*_{\mathrm{PST}}} V_{\mathrm{AC}i} - \frac{y_{\mathrm{S}}}{\psi^*_{\mathrm{PST}}} V_{\mathrm{AC}j} \tag{4.2a}$$

$$I_{\mathrm{Br}ji} = y_{\mathrm{SP}} V_{\mathrm{AC}j} - \frac{y_{\mathrm{S}}}{\psi_{\mathrm{PST}}} V_{\mathrm{AC}i}. \tag{4.2b}$$

In the case of a transmission line, the tap ratio is set to $\psi_{\mathrm{PST}} = 1\angle 0^\circ$ which deactivates the transformer. If we consider a controllable phase shifting transformer (PST), we collect the complex tap ratios in $\mathcal{E}^{\mathrm{PST}}$ and include the variables into the optimization. Note that in the example above, we have $\mathcal{E}^{\mathrm{PST}}_i = \{\psi_{\mathrm{PST}}\}$ and $\mathcal{E}^{\mathrm{PST}}_j = \{\}$, since the transformer is located at node i. Complex tap ratio limits are formulated with

$$\underline{\psi}_{\mathrm{PST}} \leq \psi_{\mathrm{PST}} \leq \overline{\psi}_{\mathrm{PST}}, \tag{4.3}$$

which includes limits on both magnitude and angle. As discussed in Chapter 3.6, this is a relaxed formulation of the actual discrete tap ratios in order to comply with the continuous model.

To limit the flow from i to j, we may include a bound on active power $\overline{P}_{\mathrm{Br}ij}$, on apparent power $\overline{S}_{\mathrm{Br}ij}$ or apparent current $\overline{I}_{\mathrm{Br}ij}$. In that case, we consider one of the following 3 constraints:

$$|V_{\mathrm{AC}i} I^*_{\mathrm{Br}ij}|^2 \leq \overline{S}^2_{\mathrm{Br}ij} \tag{4.4a}$$

$$\Re\left(V_{\mathrm{AC}i} I^*_{\mathrm{Br}ij}\right) \leq \overline{P}_{\mathrm{Br}ij} \tag{4.4b}$$

$$|I_{\mathrm{Br}ij}|^2 \leq \overline{I}^2_{\mathrm{Br}ij}. \tag{4.4c}$$

4.1.2 Loads and Shunts

Generally, we model the electrical demand – collected in $\mathcal{E}^{\mathrm{D}}$ – as a constant power sink for both active and reactive power:

$$S_{\mathrm{D}} = P_{\mathrm{D}} + \mathrm{j}Q_{\mathrm{D}}. \tag{4.5}$$

However, shunts – collected in $\mathcal{E}^{\mathrm{Shunt}}$ – are modeled with a constant complex admittance y_{Sh}, which is directly connected to a node and where the withdrawn power is

$$S_{\mathrm{Sh}} = y_{\mathrm{Sh}} V_{\mathrm{AC}}^2. \tag{4.6}$$

Thus, constant impedance loads can be included indirectly.

Load Shedding

It might become necessary to shed loads if a secure system operation can not be assured otherwise. Therefore, we allow a maximal demand reduction $\overline{P}_{\mathrm{D,Shed}} \leq P_{\mathrm{D}}$ for a specified set of loads. We assume a constant power factor $\cos\phi$ and with $\frac{Q}{P} = \tan\phi$, the reactive power demand is reduced proportionally to the active power reduction:

$$0 \leq P_{\mathrm{D,Shed}} \leq \overline{P}_{\mathrm{D,Shed}} \tag{4.7a}$$

$$Q_{\mathrm{D,Shed}} = P_{\mathrm{D,Shed}} \frac{Q_{\mathrm{D}}}{P_{\mathrm{D}}}. \tag{4.7b}$$

Sheddable loads are collected in $\mathcal{E}^{\mathrm{D,Shed}} \subseteq \mathcal{E}^{\mathrm{D}}$.

4.1.3 Generators

We model a generator with two independent active and reactive power sources $(P_{\mathrm{G}}, Q_{\mathrm{G}})$. Both must satisfy operational upper and lower limits

$$\underline{P}_{\mathrm{G}} \leq P_{\mathrm{G}} \leq \overline{P}_{\mathrm{G}} \tag{4.8a}$$

$$\underline{Q}_{\mathrm{G}} \leq Q_{\mathrm{G}} \leq \overline{Q}_{\mathrm{G}}. \tag{4.8b}$$

The model of a renewable energy source (RES) is derived either from (4.5) via a negative load or from (4.8) via a generator subject to varying upper power limits – depending on whether the RES is considered controllable or not. All controllable generators are collected in the set $\mathcal{E}^{\mathrm{G}}$.

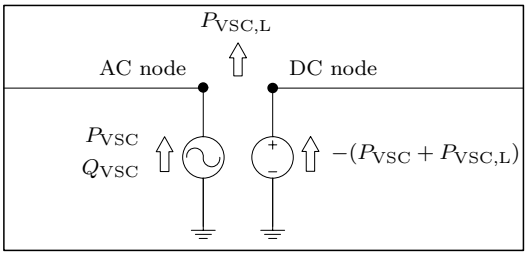

Figure 4.3: VSC model between AC and DC node. Coupling via an active power balance respecting the converter losses.

Redispatch

Usually, an economic dispatch is calculated where the objective depends on the total power output of a generator. If we seek to derive an optimal redispatch however, a day-ahead dispatch $P_{\mathrm{G,Disp}}$ is given and we minimize the deviation from it. This is modeled with two strictly non-negative variables for upward ($P_{\mathrm{G,Up}}$) and downward deviation ($P_{\mathrm{G,Down}}$); the resulting injected power P_{G} becomes

$$P_{\mathrm{G}} = P_{\mathrm{G,Disp}} + P_{\mathrm{G,Up}} - P_{\mathrm{G,Down}} \tag{4.9a}$$

$$0 \leq P_{\mathrm{G,Up}} \tag{4.9b}$$

$$0 \leq P_{\mathrm{G,Down}}. \tag{4.9c}$$

The two separate variables allow for the assignment of different cost functions to an increase or decrease of generator output. Additionally, model (4.9) can be used for RES curtailment. In that case, we interpret a power reduction $P_{\mathrm{G,Down}}$ as costly curtailment. We collect redispatchable generators in the set $\mathcal{E}^{\mathrm{G,Redisp}} \subseteq \mathcal{E}^{\mathrm{G}}$. Note that the remaining generators are called dispatchable, thus $\mathcal{E}^{\mathrm{G}} - \mathcal{E}^{\mathrm{G,Redisp}} = \mathcal{E}^{\mathrm{G,Disp}}$.

4.1.4 AC-DC Converter

As proposed in [58, 73, 4], the converter model is a simplified VSC model based on two generators, see Fig. 4.3. Active and reactive power output on the AC side are denoted with $(P_{\mathrm{VSC}}, Q_{\mathrm{VSC}})$, and a positive value of P_{VSC} denotes a power flow from DC to AC. Several limits can be defined for active, reactive and apparent AC power output:

$$\underline{P}_{\mathrm{VSC}} \leq P_{\mathrm{VSC}} \leq \overline{P}_{\mathrm{VSC}} \tag{4.10a}$$

$$\underline{Q}_{\mathrm{VSC}} \leq Q_{\mathrm{VSC}} \leq \overline{Q}_{\mathrm{VSC}} \tag{4.10b}$$

$$P_{\mathrm{VSC}}^2 + Q_{\mathrm{VSC}}^2 \leq \overline{S}_{\mathrm{VSC}}^2. \tag{4.10c}$$

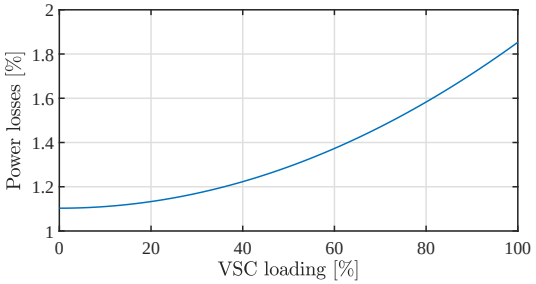

Figure 4.4: VSC loss curve for $\alpha_{\mathrm{VSC,L}} = 0.01103$ and $\gamma_{\mathrm{VSC,L}} = 0.0075$ relative to installed apparent capacity.

Losses are modeled with a quadratic function depending on the apparent power. This approximates ohmic losses which depend on the square of the current at nearly constant voltage. The transferred active power is reduced by the term $P_{\mathrm{VSC,L}}$, where $\alpha_{\mathrm{VSC,L}}$ and $\gamma_{\mathrm{VSC,L}}$ are converter specific loss parameters:

$$P_{\mathrm{VSC,L}} = \left(\alpha_{\mathrm{VSC,L}} + \gamma_{\mathrm{VSC,L}} \frac{P_{\mathrm{VSC}}^2 + Q_{\mathrm{VSC}}^2}{\overline{S}_{\mathrm{VSC}}^2}\right) \overline{S}_{\mathrm{VSC}}. \tag{4.11}$$

An exemplary loss curve is shown in Fig. 4.4. Note that a converter connecting AC node i with DC node j is element of both sets $\mathcal{E}_i^{\mathrm{VSC}}$ *and* $\mathcal{E}_j^{\mathrm{VSC}}$.

4.1.5 DC Branches

If a branch connects two DC nodes $i, j \in \mathcal{N}^{\mathrm{DC}}$, the model is a simple conductance g_{DC}. Thus, the current flowing from i to j is

$$I_{\mathrm{DCBr}ij} = g_{\mathrm{DC}} \cdot (V_{\mathrm{DC}i} - V_{\mathrm{DC}j}). \tag{4.12}$$

DC branch flows are limited via active power bounds

$$V_{\mathrm{DC}i} I_{\mathrm{DCBr}ij} \leq \overline{P}_{\mathrm{DCBr}ij}. \tag{4.13}$$

4.1.6 AC Network

Active and reactive power balance of an AC node $i \in \mathcal{N}^{\mathrm{AC}}$ is given by

$$\Re\Big(V_{\mathrm{AC}i} \sum_{j \in \mathcal{N}^{\mathrm{AC}}(i)} I_{\mathrm{Br}ij}^*\Big) = P_{\mathrm{AC}i} \tag{4.14a}$$

$$\Im\Big(V_{\mathrm{AC}i} \sum_{j \in \mathcal{N}^{\mathrm{AC}}(i)} I_{\mathrm{Br}ij}^*\Big) = Q_{\mathrm{AC}i} \tag{4.14b}$$

with branch currents $I_{\mathrm{Br}ij}$ from (4.2). Here, $(P_{\mathrm{AC}i}, Q_{\mathrm{AC}i})$ are active and reactive injected power at node i, respectively, which will be defined in Chapter 4.4.3. Voltage magnitudes are limited by

$$\underline{V}_{\mathrm{AC}} \leq |V_{\mathrm{AC}}| \leq \overline{V}_{\mathrm{AC}}, \tag{4.15}$$

and both magnitude and angle are fixed for one node per synchronous area:

$$V_{\mathrm{AC}ref} = 1.0 \text{ pu} \angle 0^{\circ}. \tag{4.16}$$

4.1.7 DC Network

Equivalently to the AC side, active power balance of a DC node $i \in \mathcal{N}^{\mathrm{DC}}$ is given by

$$V_{\mathrm{DC}i} \sum_{j \in \mathcal{N}^{\mathrm{DC}}(i)} I_{\mathrm{DCBr}ij} = P_{\mathrm{DC}i}, \tag{4.17}$$

with branch currents $I_{\mathrm{DCBr}ij}$ from (4.12) and $P_{\mathrm{DC}i}$ the injected power at node i, which will be explained in Chapter 4.4.3. Again, voltages are limited by

$$\underline{V}_{\mathrm{DC}} \leq V_{\mathrm{DC}} \leq \overline{V}_{\mathrm{DC}} \tag{4.18}$$

and the voltage magnitude of one node per inter-connected DC system is fixed:

$$V_{\mathrm{DC}ref} = 1.0 \text{ pu}. \tag{4.19}$$

4.2 Incorporation of N-1 Security

Reliability is a key requirement for electricity supply. Therefore, transmission grids need to be fault-tolerant up to a certain extent. A secure operation can be achieved when operating points are determined not only for a normal and fault-free scenario but also under consideration of equipment outages. To implement this extension, the original problem set up is duplicated and then included with a modified topology, e.g. with a certain line out of operation. Thus, the optimization problem includes *both* the base case *and* the N-1 cases which allows for a simultaneous calculation of coupled set points. The different topologies are collected in $\mathcal{C} = \{0, 1, ..., C\}$, where "0" denotes the base case with full topology and C is the number of considered contingencies. The branch current formulation (4.2) can be maintained by setting $y_{\mathrm{P}} = y_{\mathrm{S}} = 0$. Furthermore, controllable devices from the duplicate must be coupled to the original base case in order to prevent sudden set point changes which could not be performed in reality. The coupling is explained in the following.

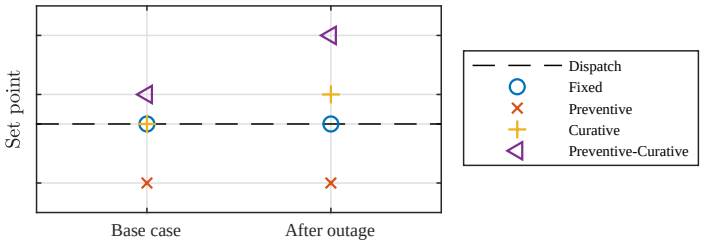

Figure 4.5: Relation between power set points before and after a contingency for different coupling modes.

4.2.1 Coupling of Fast Response Units

Devices which are connected via power electronics, i.e. storage systems and AC-DC converters, are highly controllable and can change power set points in milliseconds. The main issue might be communication delays, but the time delay is negligible since steady-state network constraints (e.g. voltage or current limitations) are allowed to be violated during the first seconds or even minutes after a failure. Similarly, a controllable PST requires communication but only seconds for the actual act of tap change. Therefore, those units do not require coupling constraints if they are equipped with the necessary communication and if the TSO seeks to use the flexibility as a curative measure. However, it is of interest how this additional flexibility affects the system behavior and the resulting operating cost compared to a less intelligent system. To highlight these aspects, the coupling of fast units can be restricted as well and we distinguish four different coupling modes, which are shown in Fig. 4.5.

In *Fixed* mode, the unit is not controllable at all and set points are equal to previously calculated values. In *Preventive* mode, the base case variable is preventively optimized to satisfy the outage scenario with the very same operating set point. In *Curative* mode, the base case values are fixed to constant values from previous calculations as in *Fixed* mode, but the units are variable after the outage. In *Preventive-Curative* mode, base case and outage scenario are both assumed controllable. To allow for flexible coupling, the following constraints are introduced for a contingency c:

$$-R_{\text{N-1,VSC}} \leq P^0_{\text{VSC}} - P^c_{\text{VSC}} \leq R_{\text{N-1,VSC}} \tag{4.20a}$$

$$-R_{\text{N-1,PST}} \leq \psi^0_{\text{PST}} - \psi^c_{\text{PST}} \leq R_{\text{N-1,PST}} \tag{4.20b}$$

$$-R_{\text{N-1,ESS}} \leq P^0_{\text{ESS,C}} - P^c_{\text{ESS,C}} \leq R_{\text{N-1,ESS}} \tag{4.20c}$$

$$-R_{\text{N-1,ESS}} \leq P^0_{\text{ESS,D}} - P^c_{\text{ESS,D}} \leq R_{\text{N-1,ESS}}. \tag{4.20d}$$

Variables $(P_{\text{ESS,C}}, P_{\text{ESS,D}})$ are related to energy storage charging and discharg-

Table 4.1: Generalization of coupling modes from before (state variables X^0_{type}) to after (with allowed deviation $R_{\text{N-1},type}$) an outage, with $type \in \{\text{VSC}, \text{PST}, \text{ESS}\}$.

Coupling mode	X^0_{type}	$R_{\text{N-1},type}$
Fixed ("*Fixed*-...")	= const.	$= 0$
Preventive ("*Prev*-...")	–	$= 0$
Curative ("*Cura*-...")	= const.	> 0
Preventive-curative ("*Prev*-*Cura*-...")	–	> 0

ing, respectively, and are further discussed in Chapter 4.3. The ramp limits $R_{\text{N-1},type} \geq 0$ are set according to Table 4.1, where X^0_{type} stands for the related base case variables of the unit *type*. To allow a unit to freely move its set point from before to after a contingency, the ramp can be set to $R_{\text{N-1},type} = \infty$.

4.2.2 Coupling of Generators

Generally, generators are modeled analogously to fast response units, except that ramp rates are chosen much slower. But, this work focuses on the use of smart assets for curative measures. Therefore, throughout this work, generators will be operated in preventive mode. However, a topology change after an outage leads inevitably to a change in network losses. To maintain power balance in the grid, the generated power must be adaptable up to a small degree[1]. Therefore, the ramp rate from before to after a contingency should be $R_{\text{N-1,G}} > 0$, even in preventive mode. The coupling equations for generators are formed to

$$-R_{\text{N-1,G}} \leq P^0_{\text{G}} - P^c_{\text{G}} \leq R_{\text{N-1,G}}, \tag{4.21}$$

where P^0_{G} is the power output of a generator in the base case, and P^c_{G} is the power output of the same generator after an outage c. Note that from a mathematical perspective, one cannot distinguish between necessary power adaption due to a change in losses resulting from a new topology, and "desired" set point change to reduce costs. Thus, if a generator shall only be accessible for power balance needs, ramp limits must be chosen carefully in order to guarantee a feasible power flow in the new topology on the one hand, but no obscuration of results on the other hand. In reality, where the nominal frequency is never exactly met, power balance is automatically achieved by frequency-triggered primary control.

[1] Many works in literature neglect this fact. It can easily be overseen if higher or lower voltages lead to the exact same network losses after the outage.

4.3 Quasi-Stationary Dynamics

System state and load flow situation are inevitably subject to changes in power demand and renewable generation. Some operational constraints are not entirely time-independent and hence require the consideration of a forecast on multiple time steps. To this end, we define a set of considered time steps $\mathcal{T} = \{1, 2, .., T\}$. In this thesis, steady state power flow equations are used for each time step and thus only slow dynamics are considered. Those inter-temporal constraints are presented in the following.

4.3.1 Energy Storage System

Energy storage has dynamic behavior in the sense that the state of charge depends on time. If we consider upper and lower limits, the ability to charge or discharge an ESS is heavily time-dependent since the ESS might be empty or full. Therefore, the energy level of a storage E^t_{ESS} after time step t depends on the energy level after the previous time step E^{t-1}_{ESS} and the incremental charged or discharged energy ΔE^t_{ESS} between those two time steps:

$$E^t_{\text{ESS}} = E^{t-1}_{\text{ESS}} + \Delta E^t_{\text{ESS}}. \tag{4.22}$$

Note that the initial energy E^0_{ESS} is not a variable, since the actual state is assumed to be known. An ESS is modeled with two power injection variables to facilitate the consideration of efficiencies below 100 %. Storage efficiency for discharging ($\eta_{\text{ESS,D}}$) and charging ($\eta_{\text{ESS,C}}$) is assumed to be constant. With charging power $P_{\text{ESS,C}}$ and discharging power $P_{\text{ESS,D}}$, the incremental energy stored in the ESS during a time interval Δt is in general given by

$$\Delta E^t_{\text{ESS}} = (\eta_{\text{ESS,C}} P^t_{\text{ESS,C}} - \frac{1}{\eta_{\text{ESS,D}}} P^t_{\text{ESS,D}}) \Delta t^t. \tag{4.23}$$

The time span between $t-1$ and t, Δt^t, is assumed variable over time and is also marked with a superscript t. This generalization is useful to implement a variable resolution on the discretized time scale.

Lastly, limits on power and energy must be fulfilled:

$$\underline{E}_{\text{ESS}} \leq E_{\text{ESS}} \leq \overline{E}_{\text{ESS}} \tag{4.24a}$$

$$\underline{P}_{\text{ESS,C}} \leq P_{\text{ESS,C}} \leq \overline{P}_{\text{ESS,C}} \tag{4.24b}$$

$$\underline{P}_{\text{ESS,D}} \leq P_{\text{ESS,D}} \leq \overline{P}_{\text{ESS,D}} \tag{4.24c}$$

$$\underline{Q}_{\text{ESS}} \leq Q_{\text{ESS}} \leq \overline{Q}_{\text{ESS}}. \tag{4.24d}$$

Note that the lower limit on active power is usually zero. However, a flexible bound can prove useful to force a certain power set point. Furthermore, a minimum or

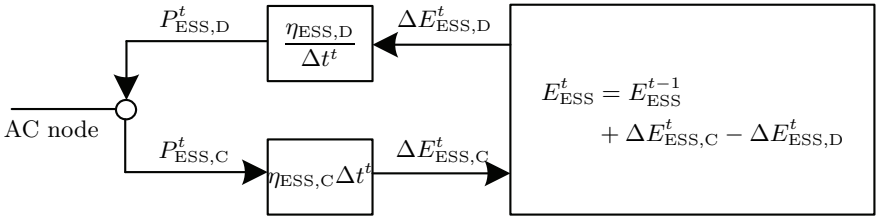

Figure 4.6: Model of energy storage system with two independent power variables for charging and discharging.

maximum energy level can be defined for the end of an optimization horizon by adapting energy limits accordingly.

The storage model is illustrated in Fig. 4.6. Observing the possible loop flow, a general issue becomes apparent. In continuous optimization, it is not possible to properly avoid a simultaneous charge and discharge, which would otherwise be done with binary constraints[2]. Therefore, the objective must be chosen such that it is never advantageous to burn energy, which would be the case with non-zero losses in the storage model by simultaneously charging and discharging. For the same reason one must be careful if a maximal energy below the upper limit is desired for the end of horizon. Depending on the scenario, it could be cost-optimal to reach that goal by burning energy instead of less charging beforehand.

N-1 Security

The stored energy after an outage depends on the time of occurrence. To this end, we define a parameter $0 \leq \xi \leq 1$ which subtracts[3] a portion of the incremental energy of the current base case. This parameter is inherently unknown, but a TSO has the choice of assuming the occurrence at the beginning of a new time step ($\xi = 0$), at the end ($\xi = 1$) or at some point in time between. The storage energy after a contingency is defined for $c > 0$ to

$$E^{t,c}_{\mathrm{ESS}} = E^{t,0}_{\mathrm{ESS}} - (1-\xi)\Delta E^{t,0}_{\mathrm{ESS}} + \Delta E^{t,c}_{\mathrm{ESS}}, \tag{4.25}$$

which means, for example, that

$$E^{t,c}_{\mathrm{ESS}} = \begin{cases} E^{t-1,0}_{\mathrm{ESS}} + \Delta E^{t,c}_{\mathrm{ESS}} & \text{if } \xi = 0 \\ E^{t,0}_{\mathrm{ESS}} + \Delta E^{t,c}_{\mathrm{ESS}} & \text{if } \xi = 1. \end{cases} \tag{4.26}$$

[2] A possible complementary constraint is $P_{\mathrm{ESS,D}} \cdot P_{\mathrm{ESS,C}} = 0$. Although being continuous variables, the binary behavior introduces bad convergence properties.

[3] The reason for "starting" at the end of the time step is a more readable problem description if all variables only depend on t.

4.3.2 Generator Ramping

Depending on fuel type and technology, thermal power plants need time to ramp the power output up or down. Therefore, the change in generator power output from time step $t-1$ to t is limited upwards by $R_{\mathrm{T}+,\mathrm{G}} \geq 0$ and downwards by $R_{\mathrm{T}-,\mathrm{G}} \geq 0$. The ramp rates are given per hour and must be multiplied with the length of the respective time interval:

$$-R_{\mathrm{T}-,\mathrm{G}}\Delta t^t \leq P_{\mathrm{G}}^t - P_{\mathrm{G}}^{t-1} \leq R_{\mathrm{T}+,\mathrm{G}}\Delta t^t. \tag{4.27}$$

Similarly to the storage initial energy, P_{G}^0 is assumed to be a known input.

4.4 Problem Set Up

In terms of modeling, the incorporation of N-1 security and the consideration of dynamics have strong similarities. In both variants, the problem is extended by duplicating and adding a modified version of the base case network to the original problem. While the network topology is modified for N-1 security, varying load and RES scenarios are used for the dynamics. The principle of the problem synthesis is shown in Fig. 3.1. Since each added extension requires the same types of variables, the original identifiers are kept and the respective time step and contingency are denoted with a superscript tuple (t, c). However, it might be of interest not to include N-1 security for every time step. For instance, forecast values far ahead in the future might be known to be inexact but relevant enough for a storage system to anticipate large energy deficits or excesses. For that time step, an N-1 secure operating point is of limited relevance since it will most probably be subject to changes after updated forecasts[4] and a reduction of problem complexity can be achieved by neglecting contingencies far ahead in future. Therefore, we split the total number of time steps T into $T_{\text{N-1}}$ N-1 secure time steps and $T_{\text{N-0}}$ N-0 secure time steps, leading to $T = T_{\text{N-1}} + T_{\text{N-0}}$. We further define the set of N-1 secure time steps:

$$\mathcal{T}_{\text{N-1}} = \{1, 2, .., T_{\text{N-1}}\}. \tag{4.28}$$

The collection of valid tuples, i.e. considered scenarios, then becomes

$$\mathcal{S} = \Big\{(t_1, c), (t_2, 0),\ \ \forall t_1 \in \mathcal{T}_{\text{N-1}}, \forall t_2 \in \mathcal{T} \setminus \mathcal{T}_{\text{N-1}}, \forall c \in \mathcal{C}\Big\}. \tag{4.29}$$

As an example, a comprehensive problem set up is shown in Fig. 4.7.

[4] See also the explanation of Receding Horizon Control in Chapter 6.1.

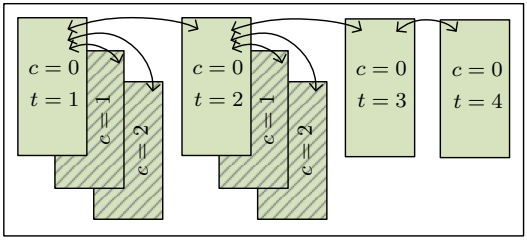

Figure 4.7: Exemplary framework with $T_{\text{N-1}} = 2$, $T = 4$ and $\mathcal{C} = \{0, 1, 2\}$ to include N-1 security with two contingencies only for the first two out of four time steps. The full scenario set is then defined to $\mathcal{S} = \{(1,0), (1,1), (1,2), (2,0), (2,1), (2,2), (3,0), (4,0)\}$.

4.4.1 Optimization Variables

Each state can be assigned to a specific node. The states assigned to an AC node i for scenario (t, c) are

$$\begin{aligned} s^{t,c}_{\text{AC}i} = \Big\{ \big(&V^{t,c}_{\text{AC}i}, P^{t,c}_{\text{G}j}, Q^{t,c}_{\text{G}j}, P^{t,c}_{\text{VSC}k}, Q^{t,c}_{\text{VSC}k}, E^{t,c}_{\text{ESS}l}, P^{t,c}_{\text{ESS}l,\text{C}}, P^{t,c}_{\text{ESS}l,\text{D}}, Q^{t,c}_{\text{ESS}l}, \\ &P^{t,c}_{\text{G}m,\text{Up}}, P^{t,c}_{\text{G}m,\text{Down}}, P^{t,c}_{\text{D}n,\text{Shed}}, \psi^{t,c}_{\text{PST}io}\big), \quad \forall j \in \mathcal{E}^{\text{G}}_i, \forall k \in \mathcal{E}^{\text{VSC}}_i, \\ &\forall l \in \mathcal{E}^{\text{ESS}}_i, \forall m \in \mathcal{E}^{\text{G,Redisp}}_i, \forall n \in \mathcal{E}^{\text{D,Shed}}_i, \forall (i,o) \in \mathcal{E}^{\text{PST}}_i \Big\}, \end{aligned} \tag{4.30}$$

and the states assigned to a DC node i are

$$s^{t,c}_{\text{DC}i} = \big\{ \big(V^{t,c}_{\text{DC}i}, P^{t,c}_{\text{G}j}\big), \forall j \in \mathcal{E}^{\text{G}}_i \big\}. \tag{4.31}$$

Note that usually we do not connect generators to a DC node. However, the supported possibility will prove useful for later purposes in distributed optimization. We generalize the node states to

$$s^{t,c}_i = \begin{cases} s^{t,c}_{\text{AC}i} & \text{if } i \in \mathcal{N}^{\text{AC}} \\ s^{t,c}_{\text{DC}i} & \text{if } i \in \mathcal{N}^{\text{DC}}. \end{cases} \tag{4.32}$$

Finally, the optimization variables for scenario (t, c) in a network with node set $\mathcal{N}$ are given by

$$x^{t,c}_{\mathcal{N}} = \big\{ (s^{t,c}_i), \forall i \in \mathcal{N} \big\} \tag{4.33}$$

4.4.2 Objective

The objective usually consists of generator fuel cost functions. Furthermore, we allow for a small weight to reactive power injections in order to numerically improve the problem condition. Note that we distinguish between cost functions for dispatchable generators ($\mathcal{E}^{\mathrm{G,Disp}}$) and redispatchable generators ($\mathcal{E}^{\mathrm{G,Redisp}}$). The local cost function at node i is

$$\begin{aligned} f_i(s_i^{t,c}) = & \sum_{j \in \mathcal{E}_i^{\mathrm{G,Disp}}} \left(a_{\mathrm{G}j} (P_{\mathrm{G}j}^{t,c})^2 + b_{\mathrm{G}j} P_{\mathrm{G}j}^{t,c} \right) \\ & + \sum_{j \in \mathcal{E}_i^{\mathrm{G,Redisp}}} \left(a_{\mathrm{G}j,\mathrm{Up}} (P_{\mathrm{G}j,\mathrm{Up}}^{t,c})^2 + b_{\mathrm{G}j,\mathrm{Up}} P_{\mathrm{G}j,\mathrm{Up}}^{t,c} \right) \\ & + \sum_{j \in \mathcal{E}_i^{\mathrm{G,Redisp}}} \left(a_{\mathrm{G}j,\mathrm{Down}} (P_{\mathrm{G}j,\mathrm{Down}}^{t,c})^2 + b_{\mathrm{G}j,\mathrm{Down}} P_{\mathrm{G}j,\mathrm{Down}}^{t,c} \right) \\ & + \sum_{j \in \mathcal{E}_i^{\mathrm{ESS}}} \left(a_{\mathrm{ESS}j,\mathrm{D}} (P_{\mathrm{ESS}j,\mathrm{D}}^{t,c})^2 + b_{\mathrm{ESS}j,\mathrm{D}} P_{\mathrm{ESS}j,\mathrm{D}}^{t,c} \right) \\ & + \sum_{j \in \mathcal{E}_i^{\mathrm{ESS}}} \left(a_{\mathrm{ESS}j,\mathrm{C}} (P_{\mathrm{ESS}j,\mathrm{C}}^{t,c})^2 + b_{\mathrm{ESS}j,\mathrm{C}} P_{\mathrm{ESS}j,\mathrm{C}}^{t,c} \right) \\ & + \sum_{j \in \mathcal{E}_i^{\mathrm{D,Shed}}} \left(a_{\mathrm{D}j,\mathrm{Shed}} (P_{\mathrm{D}j,\mathrm{Shed}}^{t,c})^2 + b_{\mathrm{D}j,\mathrm{Shed}} P_{\mathrm{D}j,\mathrm{Shed}}^{t,c} \right) \\ & + a_{\mathrm{q}i} \sum_{j \in \mathcal{E}_i^{\mathrm{G}}} (Q_{\mathrm{G}j}^{t,c})^2 + a_{\mathrm{q}i} \sum_{j \in \mathcal{E}_i^{\mathrm{VSC}}} (Q_{\mathrm{VSC}j}^{t,c})^2. \end{aligned} \tag{4.34}$$

If the minimization of line loading is desired instead of the fuel costs, we form

$$f_i(s_i^{t,c}) = \sum_{(i,j) \in \mathcal{E}_i^{\mathrm{CL}}} \frac{|V_{\mathrm{AC}i}^{t,c} (I_{\mathrm{Br}ij}^{t,c})^*|^2}{\overline{S}_{\mathrm{Br}ij}^2}, \tag{4.35}$$

with $\mathcal{E}_i^{\mathrm{CL}}$ the set of considered lines connected to node i.

Finally, the total cost function of scenario (t, c) in a network with node set $\mathcal{N}$ is formed to

$$Costs_{\mathcal{N}}^{t,c}(x_{\mathcal{N}}^{t,c}) \equiv \sum_{i \in \mathcal{N}} f_i(s_i^{t,c}). \tag{4.36}$$

4.4.3 Constraints

The basic constraints in scenario (t, c) over node set $\mathcal{N}$ include all time-independent equations, such as power balance and operational limits for AC and DC grid:

$$Basics^{t,c}_{\mathcal{N}}(x^{t,c}_{\mathcal{N}}) \equiv \Bigg\{$$

$$V^{t,c}_{\mathrm{AC}i} \sum_{l \in \mathcal{N}^{\mathrm{AC}}(i)} \left(I^{t,c}_{\mathrm{Br}il}\right)^* = P^{t,c}_{\mathrm{AC}i} + \mathrm{j}Q^{t,c}_{\mathrm{AC}i} \tag{4.37a}$$

$$\underline{V}_{\mathrm{AC}i} \leq |V^{t,c}_{\mathrm{AC}i}| \leq \overline{V}_{\mathrm{AC}i}, \tag{4.37b}$$

$$|V^{t,c}_{\mathrm{AC}i}\left(I^{t,c}_{\mathrm{Br}il}\right)^*|^2 \leq \overline{S}^2_{\mathrm{Br}il}, \quad \forall l \in \mathcal{N}^{\mathrm{AC}}(i) \tag{4.37c}$$

$$\underline{\psi}_{\mathrm{PST}il} \leq \psi^{t,c}_{\mathrm{PST}il} \leq \overline{\psi}_{\mathrm{PST}il}, \quad \forall (i,l) \in \mathcal{E}^{\mathrm{PST}}_i \tag{4.37d}$$

$$0 \leq P^{t,c}_{\mathrm{D}l,\mathrm{Shed}} \leq \overline{P}^{t,0}_{\mathrm{D}l,\mathrm{Shed}} \quad \forall l \in \mathcal{E}^{\mathrm{D,Shed}}_i \tag{4.37e}$$

$$\underline{P}_{\mathrm{G}l} \leq P^{t,c}_{\mathrm{G}l} \leq \overline{P}_{\mathrm{G}l}, \tag{4.37f}$$

$$\underline{Q}_{\mathrm{G}l} \leq Q^{t,c}_{\mathrm{G}l} \leq \overline{Q}_{\mathrm{G}l}, \quad \forall l \in \mathcal{E}^{\mathrm{G}}_i \tag{4.37g}$$

$$P^{t,c}_{\mathrm{G}l} = P^{t,0}_{\mathrm{G}l,\mathrm{Disp}} + P^{t,c}_{\mathrm{G}l,\mathrm{Up}} - P^{t,c}_{\mathrm{G}l,\mathrm{Down}}, \tag{4.37h}$$

$$P^{t,c}_{\mathrm{G}l,\mathrm{Up}}, P^{t,c}_{\mathrm{G}l,\mathrm{Down}} \geq 0, \quad \forall l \in \mathcal{E}^{\mathrm{G,Redisp}}_i \tag{4.37i}$$

$$\underline{E}_{\mathrm{ESS}l} \leq E^{t,c}_{\mathrm{ESS}l} \leq \overline{E}_{\mathrm{ESS}l}, \tag{4.37j}$$

$$\underline{P}^{t,c}_{\mathrm{ESS}l,\mathrm{C}} \leq P^{t,c}_{\mathrm{ESS}l,\mathrm{C}} \leq \overline{P}^{t,c}_{\mathrm{ESS}l,\mathrm{C}}, \tag{4.37k}$$

$$\underline{P}^{t,c}_{\mathrm{ESS}l,\mathrm{D}} \leq P^{t,c}_{\mathrm{ESS}l,\mathrm{D}} \leq \overline{P}^{t,c}_{\mathrm{ESS}l,\mathrm{D}}, \tag{4.37l}$$

$$\underline{Q}_{\mathrm{ESS}l} \leq Q^{t,c}_{\mathrm{ESS}l} \leq \overline{Q}_{\mathrm{ESS}l}, \quad \forall l \in \mathcal{E}^{\mathrm{ESS}}_i \tag{4.37m}$$

$$V^{t,c}_{\mathrm{DC}j} \sum_{l \in \mathcal{N}^{\mathrm{DC}}(i)} I^{t,c}_{\mathrm{DCBr}jl} = P^{t,c}_{\mathrm{DC}j} \tag{4.37n}$$

$$V^{t,c}_{\mathrm{DC}j} I^{t,c}_{\mathrm{DCBr}jl} \leq \overline{P}_{\mathrm{DCBr}jl}, \quad \forall l \in \mathcal{N}^{\mathrm{DC}}(j) \tag{4.37o}$$

$$\underline{V}_{\mathrm{DC}j} \leq V^{t,c}_{\mathrm{DC}j} \leq \overline{V}_{\mathrm{DC}j}, \tag{4.37p}$$

$$\underline{P}_{\mathrm{VSC}l} \leq P^{t,c}_{\mathrm{VSC}l} \leq \overline{P}_{\mathrm{VSC}l} \tag{4.37q}$$

$$\underline{Q}_{\mathrm{VSC}l} \leq Q^{t,c}_{\mathrm{VSC}l} \leq \overline{Q}_{\mathrm{VSC}l} \tag{4.37r}$$

$$P^{t,c}_{\mathrm{VSC}l} + Q^{t,c}_{\mathrm{VSC}l} \leq \overline{S}^2_{\mathrm{VSC}l}, \quad \forall l \in \mathcal{E}^{\mathrm{VSC}}_i \tag{4.37s}$$

$$V^{t,c}_{\mathrm{AC}l} = 1\angle 0, \tag{4.37t}$$

$$V^{t,c}_{\mathrm{DC}l} = 1, \quad \forall l \in \mathcal{N}^{\mathrm{Ref}} \tag{4.37u}$$

$$\forall i \in \mathcal{N}^{\mathrm{AC}}, \forall j \in \mathcal{N}^{\mathrm{DC}} \Bigg\}.$$

In (4.37a), we sum up the power injections into an AC node i with

$$\begin{aligned} P^{t,c}_{\mathrm{AC}i} = &\sum_{j\in\mathcal{E}^{\mathrm{G}}_i} P^{t,c}_{\mathrm{G}j} + \sum_{j\in\mathcal{E}^{\mathrm{VSC}}_i} P^{t,c}_{\mathrm{VSC}j} + \sum_{j\in\mathcal{E}^{\mathrm{ESS}}_i} (P^{t,c}_{\mathrm{ESS}j,\mathrm{D}} - P^{t,c}_{\mathrm{ESS}j,\mathrm{C}}) \\ &- \sum_{j\in\mathcal{E}^{\mathrm{D}}_i} P^{t,c}_{\mathrm{D}j} + \sum_{j\in\mathcal{E}^{\mathrm{D,Shed}}_i} P^{t,c}_{\mathrm{D}j,\mathrm{Shed}} - \sum_{j\in\mathcal{E}^{\mathrm{Shunt}}_i} \Re\left(y^{t,0}_{\mathrm{Sh}j}(V^{t,c}_{\mathrm{AC}i})^2\right) \end{aligned} \tag{4.38a}$$

$$\begin{aligned} Q^{t,c}_{\mathrm{AC}i} = &\sum_{j\in\mathcal{E}^{\mathrm{G}}_i} Q^{t,c}_{\mathrm{G}j} + \sum_{j\in\mathcal{E}^{\mathrm{VSC}}_i} Q^{t,c}_{\mathrm{VSC}j} + \sum_{j\in\mathcal{E}^{\mathrm{ESS}}_i} Q^{t,c}_{\mathrm{ESS}j} \\ &- \sum_{j\in\mathcal{E}^{\mathrm{D}}_i} Q^{t,c}_{\mathrm{D}j} + \sum_{j\in\mathcal{E}^{\mathrm{D,Shed}}_i} Q^{t,c}_{\mathrm{D}j,\mathrm{Shed}} - \sum_{j\in\mathcal{E}^{\mathrm{Shunt}}_i} \Im\left(y^{t,0}_{\mathrm{Sh}j}(V^{t,c}_{\mathrm{AC}i})^2\right) \end{aligned} \tag{4.38b}$$

Accordingly, in (4.37n) the power injection into a DC node j is

$$P^{t,c}_{\mathrm{DC}j} = \sum_{l\in\mathcal{E}^{\mathrm{G}}_j} P^{t,c}_{\mathrm{G}l} + \sum_{l\in\mathcal{E}^{\mathrm{VSC}}_j} (P^{t,c}_{\mathrm{VSC}l} + P^{t,c}_{\mathrm{VSC}l,\mathrm{L}}). \tag{4.39}$$

The constraints, which couple all N-1 cases to the base case in time step t, are collected in

$$\begin{aligned} &\textit{N-1 Coupling}^t_{\mathcal{N}}(x^{t,0}_{\mathcal{N}}, .., x^{t,C}_{\mathcal{N}}) \equiv \Bigg\{ \\ &\quad - R_{\text{N-1,G}l} \le P^{t,0}_{\mathrm{G}l} - P^{t,c}_{\mathrm{G}l} \le R_{\text{N-1,G}l}, \quad \forall l \in \mathcal{E}^{\mathrm{G}}_i && (4.40a)\\ &\quad - R_{\text{N-1,VSC}} \le P^{t,0}_{\mathrm{VSC}l} - P^{t,c}_{\mathrm{VSC}l} \le R_{\text{N-1,VSC}}, \quad \forall l \in \mathcal{E}^{\mathrm{VSC}}_j && (4.40b)\\ &\quad E^{t,c}_{\mathrm{ESS}l} = E^{t,0}_{\mathrm{ESS}l} - (1-\xi)\Delta E^{t,0}_{\mathrm{ESS}l} + \Delta E^{t,c}_{\mathrm{ESS}l}, && (4.40c)\\ &\quad - R_{\text{N-1,ESS}} \le P^{t,0}_{\mathrm{ESS}l,\mathrm{C}} - P^{t,c}_{\mathrm{ESS}l,\mathrm{C}} \le R_{\text{N-1,ESS}}, && (4.40d)\\ &\quad - R_{\text{N-1,ESS}} \le P^{t,0}_{\mathrm{ESS}l,\mathrm{D}} - P^{t,c}_{\mathrm{ESS}l,\mathrm{D}} \le R_{\text{N-1,ESS}}, \quad \forall l \in \mathcal{E}^{\mathrm{ESS}}_i && (4.40e)\\ &\quad - R_{\text{N-1,PST}} \le \psi^{t,0}_{\mathrm{PST}il} - \psi^{t,c}_{\mathrm{PST}il} \le R_{\text{N-1,PST}}, \quad \forall (i,l) \in \mathcal{E}^{\mathrm{PST}}_i && (4.40f)\\ &\quad \forall i \in \mathcal{N}^{\mathrm{AC}}, \forall j \in \mathcal{N}^{\mathrm{DC}}, \forall c \in \mathcal{C} \setminus 0 \Bigg\}. \end{aligned}$$

Table 4.2: Problem composition depending on total number of time steps T and N-1 secure time steps $T_{\text{N-1}}$.

OPF Type	$T_{\text{N-1}}$	T
OPF	0	1
D-OPF	0	> 1
SC-OPF	1	1
SC-D-OPF	$1 \leq T_{\text{N-1}} \leq T$	> 1

The dynamic constraints connect the base cases of all time steps. They are collected in

$$
\begin{aligned}
\mathit{Dynamics}_{\mathcal{N}}(x_{\mathcal{N}}^{1,0}, .., x_{\mathcal{N}}^{T,0}) \equiv \Bigg\{ & \\
& E_{\text{ESS}j}^{1,0} = E_{\text{ESS}j}^{0,0} + \Delta E_{\text{ESS}j}^{1,0}, && \text{(4.41a)} \\
& E_{\text{ESS}j}^{t,0} = E_{\text{ESS}j}^{t-1,0} + \Delta E_{\text{ESS}j}^{t,0}, \quad \forall j \in \mathcal{E}_i^{\text{ESS}} && \text{(4.41b)} \\
& -R_{\text{T}-,\text{G}j}\Delta t^{1,0} \leq P_{\text{G}j}^{1,0} - P_{\text{G}j}^{0,0} \leq R_{\text{T}+,\text{G}j}\Delta t^{1,0}, && \text{(4.41c)} \\
& -R_{\text{T}-,\text{G}j}\Delta t^{t,0} \leq P_{\text{G}j}^{t,0} - P_{\text{G}j}^{t-1,0} \leq R_{\text{T}+,\text{G}j}\Delta t^{t,0}, \quad \forall j \in \mathcal{E}_i^{\text{G}} && \text{(4.41d)} \\
& \forall i \in \mathcal{N}^{\text{AC}}, \forall t \in \mathcal{T} \setminus 1 \Bigg\}.
\end{aligned}
$$

4.4.4 General Optimization Problem

Due to the generic form, the above-formulated optimization variables, objective function and constraint regions are still accessible for variations of the node set, which will be of use in the distributed optimization. According to Chapter 3.4, we form the most general risk-based SC-D-OPF problem for a node set $\mathcal{N}$ and scenario set $\mathcal{S}$ to

$$
\begin{aligned}
\underset{x_{\mathcal{N}}^{t,c},\ \forall (t,c)\in\mathcal{S}}{\text{minimize}} \quad & \sum_{(t,c)\in\mathcal{S}} p^{t,c}\, \mathit{Costs}_{\mathcal{N}}^{t,c}(x_{\mathcal{N}}^{t,c}) && \text{(4.42a)} \\
\text{subject to} \quad & \mathit{Basics}_{\mathcal{N}}^{t,c}(x_{\mathcal{N}}^{t,c}),\ \forall (t,c) \in \mathcal{S} && \text{(4.42b)} \\
& \textit{N-1 Coupling}_{\mathcal{N}}^{t}(x_{\mathcal{N}}^{t,0}, .., x_{\mathcal{N}}^{t,C}),\ \forall t \in \mathcal{T}_{\text{N-1}} && \text{(4.42c)} \\
& \mathit{Dynamics}_{\mathcal{N}}(x_{\mathcal{N}}^{1,0}, .., x_{\mathcal{N}}^{T,0}) && \text{(4.42d)}
\end{aligned}
$$

Note that we derive a simplified problem by defining $(T_{\text{N-1}}, T)$ and subsequently the scenario tuples in $\mathcal{S}$ (4.29) appropriately, see Table 4.2 for some examples.

Chapter 5

Case Studies: Single-Time Step Optimization

In this chapter, power flow optimization is investigated under the consideration of full control over phase shifting transformers (PST) and embedded HVDC systems. Step by step, we highlight different aspects in an illustrative 5-bus and a more realistic 67-bus test system. The focus lies on the optimization of a single time step.

5.1 5-Bus System

To demonstrate the functionalities of various OPF approaches, we use the illustrative 230 kV (AC) 5-bus test system from [57] (Fig.5.1a) and extend it with a 300 kV (DC) 3-bus multi-terminal DC grid (Fig. 5.1b). The largest generator, i.e. *G4* with 600 MW installed power, is interpreted as a wind park and its power injection is prioritized by assigning a low fuel price. Thus, there are 3 conventional generators and total active load is 1000 MW. The bipolar HVDC grid consists of 3 DC nodes in delta connection, which are linked to AC nodes via AC-DC converters. Nominal converter rating is $\overline{S}_{\mathrm{VSC}} = 100$ MVA and VSC loss parameters are set to $(\alpha_{\mathrm{VSCL}}, \gamma_{\mathrm{VSCL}}) = (0.01103, 0.0075)$. The allowed voltage ranges lie between 0.9 and 1.1 pu on the AC side, and between 0.95 and 1.05 pu on the DC side. The complete case data is shown in Appendix A.

5.1.1 OPF with PST and HVDC

In this section, we will show the effects on power flow when extending an AC grid with DC systems and/or PSTs. For that purpose, we compute traditional OPF's,

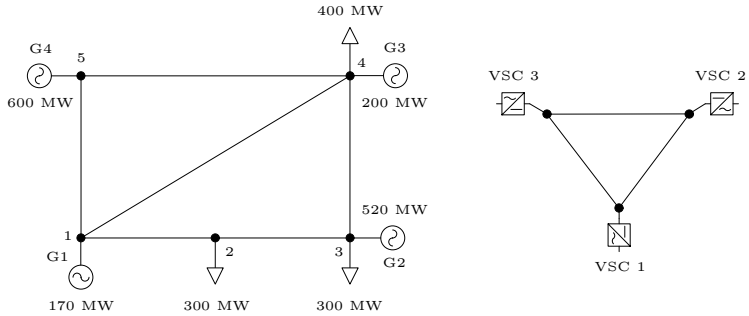

(a) 5-bus AC system. **(b)** 3-bus DC system.

Figure 5.1: AC and DC test systems. More details in Appendix A.

which means over one time step and without N-1 security. First, a PST is added to a pure AC grid and second, a PST is added to an AC-DC grid. Recall from Chapter 3.1 that the OPF problem for a single time step without N-1 Security has the form

$$\underset{x}{\text{minimize}} \quad \mathit{Costs}(x) \tag{5.1a}$$

$$\text{subject to} \quad \mathit{Basics}(x), \tag{5.1b}$$

or, in a more general form for time step and contingency scenario $(t, c) = (1, 0)$:

$$\underset{x^{1,0}}{\text{minimize}} \quad \mathit{Costs}^{1,0}(x^{1,0}) \tag{5.2a}$$

$$\text{subject to} \quad \mathit{Basics}^{1,0}(x^{1,0}). \tag{5.2b}$$

Throughout Chapter 5.1.1, we use linear cost functions as depicted in Table A.4. Furthermore, we remove upper power limits for conventional generators in order to allow for a more meaningful interpretation of the results when new equipment is introduced. For illustration reasons, we tighten the flow limits of *Line 1-2* and *5-4* to a maximal apparent power of 240 MVA and 180 MVA, respectively. Note that an overlined value in a figure stands for a binding constraint, i.e. an upper or lower limit which is reached.

AC Grid with and without PST

In an AC grid, the state variables consist of generator power output and voltages:

$$x^{1,0} = \left\{P^{1,0}_{\mathrm{G1}}, .., P^{1,0}_{\mathrm{G4}}, Q^{1,0}_{\mathrm{G1}}, .., Q^{1,0}_{\mathrm{G4}}, V^{1,0}_{\mathrm{AC1}}, .., V^{1,0}_{\mathrm{AC5}}\right\}. \tag{5.3}$$

As described above, we choose a linear cost function which is written to

$$Costs^{1,0}(x^{1,0}) = \left(0.15P_{\mathrm{G1}}^{1,0} + 0.3P_{\mathrm{G2}}^{1,0} + 0.4P_{\mathrm{G3}}^{1,0} + 0.05P_{\mathrm{G4}}^{1,0}\right)\frac{€}{\mathrm{h}}. \tag{5.4}$$

The constraint set consists of nodal power balance, voltage limits, generator limits and branch flow limits:

$$\begin{aligned}
Basics^{1,0}(x^{1,0}) \equiv \Bigg\{ & \\
& P_{\mathrm{G1}}^{1,0} + \mathrm{j}Q_{\mathrm{G1}}^{1,0} = V_{\mathrm{AC1}}^{1,0}\big((y_{\mathrm{SP12}}^{1,0} + y_{\mathrm{SP14}}^{1,0} + y_{\mathrm{SP15}}^{1,0})V_{\mathrm{AC1}}^{1,0} \\
& \qquad - y_{\mathrm{S12}}^{1,0}V_{\mathrm{AC2}}^{1,0} - y_{\mathrm{S14}}^{1,0}V_{\mathrm{AC4}}^{1,0} - y_{\mathrm{S15}}^{1,0}V_{\mathrm{AC5}}^{1,0}\big)^*, && \text{(5.5a)} \\
& -3 - \mathrm{j}0.99 = V_{\mathrm{AC2}}^{1,0}\big((y_{\mathrm{SP21}}^{1,0} + y_{\mathrm{SP23}}^{1,0})V_{\mathrm{AC2}}^{1,0} \\
& \qquad - y_{\mathrm{S21}}^{1,0}V_{\mathrm{AC1}}^{1,0} - y_{\mathrm{S23}}^{1,0}V_{\mathrm{AC3}}^{1,0}\big)^*, && \text{(5.5b)} \\
& \quad \vdots \\
& P_{\mathrm{G4}}^{1,0} + \mathrm{j}Q_{\mathrm{G4}}^{1,0} = V_{\mathrm{AC5}}^{1,0}\big((y_{\mathrm{SP51}} + y_{\mathrm{SP54}})V_{\mathrm{AC5}}^{1,0} \\
& \qquad - y_{\mathrm{S51}}V_{\mathrm{AC1}}^{1,0} - y_{\mathrm{S54}}V_{\mathrm{AC4}}^{1,0}\big)^*, && \text{(5.5c)} \\
& 0 \le P_{\mathrm{G}i}^{1,0}, \quad \forall i \in \{1,..,4\}, && \text{(5.5d)} \\
& -1.3 \le Q_{\mathrm{G1}}^{1,0} \le 1.3, && \text{(5.5e)} \\
& \quad \vdots \\
& -4.5 \le Q_{\mathrm{G4}}^{1,0} \le 4.5, && \text{(5.5f)} \\
& V_{\mathrm{AC1}}^{1,0} = 1, && \text{(5.5g)} \\
& 0.9 \le |V_{\mathrm{AC}i}^{1,0}| \le 1.1, \quad \forall i \in \{2,..,5\}, && \text{(5.5h)} \\
& |V_{\mathrm{AC1}}^{1,0}\big(y_{\mathrm{SP12}}V_{\mathrm{AC1}}^{1,0} - y_{\mathrm{S12}}V_{\mathrm{AC2}}^{1,0}\big)^*|^2 \le 2.4, && \text{(5.5i)} \\
& |V_{\mathrm{AC2}}^{1,0}\big(y_{\mathrm{SP21}}V_{\mathrm{AC2}}^{1,0} - y_{\mathrm{S21}}V_{\mathrm{AC1}}^{1,0}\big)^*|^2 \le 2.4, && \text{(5.5j)} \\
& |V_{\mathrm{AC5}}^{1,0}\big(y_{\mathrm{SP54}}V_{\mathrm{AC5}}^{1,0} - y_{\mathrm{S54}}V_{\mathrm{AC4}}^{1,0}\big)^*|^2 \le 1.8, && \text{(5.5k)} \\
& |V_{\mathrm{AC4}}^{1,0}\big(y_{\mathrm{SP45}}V_{\mathrm{AC4}}^{1,0} - y_{\mathrm{S45}}V_{\mathrm{AC5}}^{1,0}\big)^*|^2 \le 1.8 \Bigg\}. && \text{(5.5l)}
\end{aligned}$$

OPF results are shown in Fig. 5.2. Despite the cheapest price, wind power can not fully be integrated without PST, see Fig. 5.2a. Only 525 MW out of 600 MW are injected due to active line limits. Expensive generation must be ordered from generators *G2* and *G3*, leading to operating costs of 19,153.7 €/h.

In the next step, we introduce a PST between *Node 1* and *5*. The state variable $\psi_{\mathrm{PST15}}^{1,0}$ is added to $x^{1,0}$. Since we activate the ideal transformer, the admittances

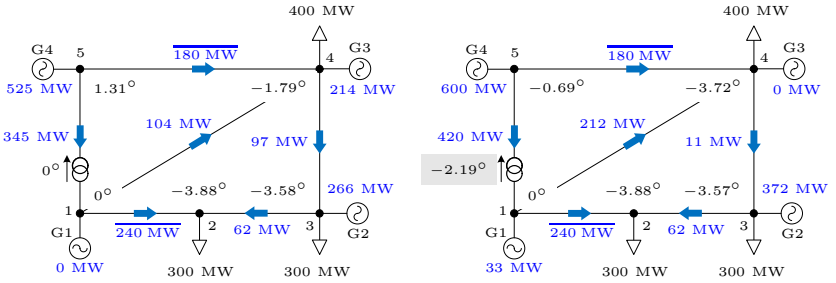

(a) Non-adjustable PST: 19,153.7 €/h. **(b)** Adjustable PST: 14,666.1 €/h.

Figure 5.2: OPF results in a pure AC grid.

between *Node 1* and *5* become dependent on the complex tap ratio:

$$y_{\text{SP15}} \leftarrow \frac{y_{\text{SP15}}}{\psi_{\text{PST15}}\psi^{*}_{\text{PST15}}} \tag{5.6a}$$

$$y_{\text{S15}} \leftarrow \frac{y_{\text{S15}}}{\psi^{*}_{\text{PST15}}} \tag{5.6b}$$

$$y_{\text{S51}} \leftarrow \frac{y_{\text{S51}}}{\psi_{\text{PST51}}}. \tag{5.6c}$$

Tap ratio limits are set to $1.0\angle\pm10^{\circ}$, i.e. only the phase shifting angle is considered in the optimization. Thus, the constraint set (5.5) is augmented by

$$-10^{\circ} \leq \angle\psi^{1,0}_{\text{PST15}} \leq 10^{\circ} \tag{5.7a}$$

$$1.0 \leq |\psi^{1,0}_{\text{PST15}}| \leq 1.0. \tag{5.7b}$$

The result is an angle reduction by -2.19° in the stressed network area at *Node 5*, where the wind power is injected, see Fig. 5.2b. Subsequently, the angle difference between *Node 1* and *4* is increased, which allows for a larger power flow between those two nodes. This sets free enough capacity to integrate the full amount of available wind power and the power transferred from *Node 1* to *Node 4* is increased from 104 MW to 212 MW. Meanwhile, angle difference and power flow from *Node 1* towards *Node 2* and *3* remain unchanged. As a consequence of the additional power transferred to *Node 4*, the expensive generator *G3* is relieved and power can be ordered from *G2* and *G1*, which results in operating costs of 14,666.1 €/h.

AC-DC Grid with and without PST

Next, the 3-bus HVDC system is added to the original case without PST. *VSC 3* is connected to the wind power node with a capacity of 100 MVA in order to cope

with the remaining wind power which would otherwise be curtailed. The state variables $x^{1,0}$ are augmented by

$$\left\{V_{\mathrm{DC1}}^{1,0},..,V_{\mathrm{DC3}}^{1,0},P_{\mathrm{VSC1}}^{1,0},..,P_{\mathrm{VSC3}}^{1,0},Q_{\mathrm{VSC1}}^{1,0},..,Q_{\mathrm{VSC3}}^{1,0}\right\}, \tag{5.8}$$

which includes VSC power set points and DC voltages. The power output from VSCs must be added to the AC side nodal power balance. For example, active power balance of *Node 2* (5.5b) becomes

$$\begin{aligned}-3-\mathrm{j}0.99+&P_{\mathrm{VSC1}}^{1,0}+\mathrm{j}Q_{\mathrm{VSC1}}^{1,0}=\\ &V_{\mathrm{AC2}}^{1,0}\left((y_{\mathrm{SP21}}^{1,0}+y_{\mathrm{SP23}}^{1,0})V_{\mathrm{AC2}}^{1,0}-y_{\mathrm{S21}}^{1,0}V_{\mathrm{AC1}}^{1,0}-y_{\mathrm{S23}}^{1,0}V_{\mathrm{AC3}}^{1,0}\right)^{*}.\end{aligned} \tag{5.9}$$

Nodal DC power balances – which include the VSC loss function –, DC voltage limits and VSC power limits are new constraints which must be added to (5.5):

$$\begin{aligned}&P_{\mathrm{VSC1}}^{1,0}+\left(0.011+0.008\frac{P_{\mathrm{VSC1}}^{2}+Q_{\mathrm{VSC1}}^{2}}{100}\right)=\\ &\qquad V_{\mathrm{DC1}}^{1,0}\left((g_{\mathrm{DC12}}^{1,0}+g_{\mathrm{DC13}}^{1,0})V_{\mathrm{DC1}}^{1,0}-g_{\mathrm{DC12}}^{1,0}V_{\mathrm{DC2}}^{1,0}-g_{\mathrm{DC13}}^{1,0}V_{\mathrm{DC3}}^{1,0}\right)\end{aligned} \tag{5.10a}$$

$$\begin{aligned}&P_{\mathrm{VSC2}}^{1,0}+\left(0.011+0.008\frac{P_{\mathrm{VSC2}}^{2}+Q_{\mathrm{VSC2}}^{2}}{100}\right)=\\ &\qquad V_{\mathrm{DC2}}^{1,0}\left((g_{\mathrm{DC21}}^{1,0}+g_{\mathrm{DC23}}^{1,0})V_{\mathrm{DC2}}^{1,0}-g_{\mathrm{DC21}}^{1,0}V_{\mathrm{DC1}}^{1,0}-g_{\mathrm{DC23}}^{1,0}V_{\mathrm{DC3}}^{1,0}\right)\end{aligned} \tag{5.10b}$$

$$\begin{aligned}&P_{\mathrm{VSC3}}^{1,0}+\left(0.011+0.008\frac{P_{\mathrm{VSC3}}^{2}+Q_{\mathrm{VSC3}}^{2}}{100}\right)=\\ &\qquad V_{\mathrm{DC3}}^{1,0}\left((g_{\mathrm{DC31}}^{1,0}+g_{\mathrm{DC32}}^{1,0})V_{\mathrm{DC3}}^{1,0}-g_{\mathrm{DC31}}^{1,0}V_{\mathrm{DC1}}^{1,0}-g_{\mathrm{DC32}}^{1,0}V_{\mathrm{DC2}}^{1,0}\right)\end{aligned} \tag{5.10c}$$

$$V_{\mathrm{DC1}}^{1,0}=1 \tag{5.10d}$$

$$0.95\leq V_{\mathrm{DC}i}^{1,0}\leq 1.05,\quad \forall i\in\{2,3\} \tag{5.10e}$$

$$(P_{\mathrm{VSC}i}^{1,0})^{2}+(Q_{\mathrm{VSC}i}^{1,0})^{2}\leq 1,\quad \forall i\in\{1,2,3\}. \tag{5.10f}$$

Figure 5.3a shows, that wind power is fully integrated and the DC system transfers 100 MW from *Node 1* to *4*. Subsequently, expensive power generation from generator *G3* is reduced and operational costs sum up to 15,835.4 €/h. However, generator *G3* is still needed since the power flows on the AC lines, and accordingly the angle differences, remain similar to the original case. Only an additional PST can resolve this issue and fully relieve the most expensive generator *G3*, see Fig. 5.3b. Here, the DC system changes the power injection toward *Node 2* instead of *Node 4*, since *Line 1-4* is capable of feeding large amounts of power towards *Node 4*.

Increased Converter Capacity

Lastly, we are interested in the effect of an HVDC system with non-restricting capacity. We set the converter power to 500 MVA and subsequently, large amounts

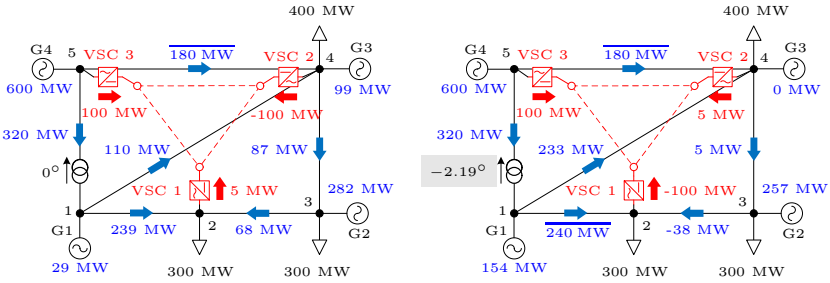

(a) Non-adjustable PST: 15,835.4 €/h. **(b)** Adjustable PST: 12,999.5 €/h.

Figure 5.3: OPF results with 100 MVA DC system.

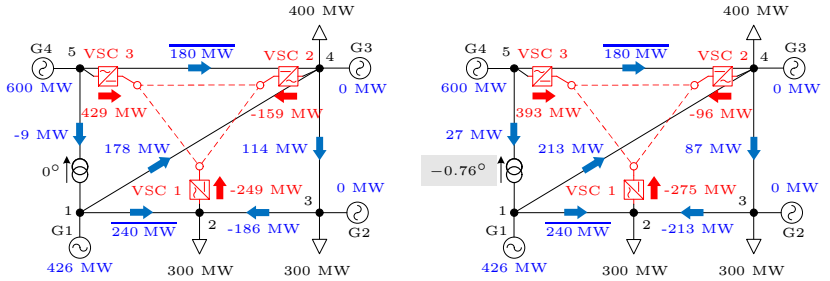

(a) Non-adjustable PST: 9,387.4 €/h. **(b)** Adjustable PST: 9,384.6 €/h.

Figure 5.4: OPF results with 500 MVA DC system.

of power are distributed via the DC system to support the AC bottlenecks, see Fig.5.4a. Power is not only injected into the AC system by *VSC 2*, as with the smaller DC system, but also with *VSC 1*. In the region "downstream" from the constrained *Line 1-2*, the second most expensive generator *G2* is relieved and the full amount of power can be ordered from the cheaper generator *G1*, leading to operational costs of 9,387.4 €/h. Since we are already dispatching the two cheapest generators, an additional PST is not expected to improve the power flow dramatically. Still, losses are reduced by 0.1 MW when setting a shifting angle of $\psi_{\text{PST15}} = -0.76°$. Interestingly, this is achieved by shifting the power transfer back to the AC system, see Fig.5.4b. Angles are manipulated such that *Line 1-4* can carry more power without violating thermal limits of the constrained lines, which reduces the power withdrawal of *VSC 3* by 36 MW.

5.1.2 SC-OPF with Varying PST Control

In this section, we investigate the effect of a PST on N-1 security. To this end, besides the base case (index "0"), we add a second topology incorporating the outage of *Line 1-2* (index "1") to the set of contingencies $\mathcal{C} = \{0, 1\}$. Subsequently, the optimization variables are extended to $x = \{x^{1,0}, x^{1,1}\}$. Recall from Chapter 3.3.1 that a traditional SC-OPF with one contingency is expressed by

$$\begin{aligned}
\underset{x^{1,0},x^{1,1}}{\text{minimize}} \quad & \mathit{Costs}^{1,0}(x^{1,0}) && \text{(5.11a)}\\
\text{subject to} \quad & \mathit{Basics}^{1,0}(x^{1,0}) && \text{(5.11b)}\\
& \mathit{Basics}^{1,1}(x^{1,1}) && \text{(5.11c)}\\
& \mathit{N\text{-}1\ Coupling}(x^{1,0}, x^{1,1}). && \text{(5.11d)}
\end{aligned}$$

The basic constraints must be fulfilled both in the base case, where $(t, c) = (1, 0)$ – see (5.11b) – , and after the contingency, where $(t, c) = (1, 1)$ – see (5.11c). Additionally, security constraints (5.11c) describe the transition between the two states. In this section, we use the redispatch formulation for all generators, which means $\mathcal{E}^{\mathrm{G,Redisp}} = \mathcal{E}^{\mathrm{G}}$ and $\mathcal{E}^{\mathrm{G,Disp}} = \emptyset$. We use the OPF result from Fig. 5.3b as generator dispatch. The redispatch requires new generator state variables, namely $P_{\mathrm{G}i,\mathrm{Up}}$ and $P_{\mathrm{G}i,\mathrm{Down}}$ for generator i. Together with the constant input $P_{\mathrm{G}i,\mathrm{Disp}}$, they define $P_{\mathrm{G}i}$:

$$P_{\mathrm{G}i} = P_{\mathrm{G}i,\mathrm{Disp}} + P_{\mathrm{G}i,\mathrm{Up}} - P_{\mathrm{G}i,\mathrm{Down}}. \tag{5.12}$$

Consequently, $P_{\mathrm{G}i}$ can be substituted in the constraints. For example, with a dispatch of $P_{\mathrm{G1,Disp}}$ =154 MW for generator *G1*, the power balance of *Node 1* (5.5a) becomes

$$\begin{aligned}
1.54 + & P^{1,0}_{\mathrm{G1,Up}} - P^{1,0}_{\mathrm{G1,Down}} + \mathrm{j}Q^{1,0}_{\mathrm{G1}} = \\
& V^{1,0}_{\mathrm{AC1}}\big((y^{1,0}_{\mathrm{SP12}} + y^{1,0}_{\mathrm{SP14}} + y^{1,0}_{\mathrm{SP15}})V^{1,0}_{\mathrm{AC1}} - y^{1,0}_{\mathrm{S12}}V^{1,0}_{\mathrm{AC2}} - y^{1,0}_{\mathrm{S14}}V^{1,0}_{\mathrm{AC4}} \\
& - y^{1,0}_{\mathrm{S15}}V^{1,0}_{\mathrm{AC5}}\big)^*.
\end{aligned} \tag{5.13}$$

In the case of an outage of *Line 1-2*, we set $y^{1,1}_{\mathrm{S12}} = y^{1,1}_{\mathrm{P12}} = 0$ and the power balance for $(t, c) = (1, 1)$ becomes

$$\begin{aligned}
1.54 + P^{1,1}_{\mathrm{G1,Up}} - & P^{1,1}_{\mathrm{G1,Down}} + \mathrm{j}Q^{1,1}_{\mathrm{G1}} = \\
& V^{1,1}_{\mathrm{AC1}}\big((y^{1,1}_{\mathrm{SP14}} + y^{1,1}_{\mathrm{SP15}})V^{1,1}_{\mathrm{AC1}} - y^{1,1}_{\mathrm{S14}}V^{1,1}_{\mathrm{AC4}} - y^{1,1}_{\mathrm{S15}}V^{1,1}_{\mathrm{AC5}}\big)^*.
\end{aligned} \tag{5.14}$$

We define cost functions for both positive redispatch (upwards) and negative redispatch (downwards). We choose to minimize the total amount of positive redispatch, which is achieved by using the same cost function for each generator. Since we only consider line outages, power balance will only change in terms of

network losses. Thus, each positive redispatch induces an almost equivalent negative redispatch from a different generator. It might occur that losses in a certain network region decrease after the outage. Instead of forcing the same amount of power injection from the generators, we incentive a power reduction by using negative cost functions for the negative redispatch. In absolute values, however, these must be smaller than the ones for positive redispatch[1]. The cost coefficients for this section are given in Table A.4 and the cost function is written to

$$\begin{aligned} \mathit{Costs}^{1,0}(x^{1,0}) = \big(&1P^{1,0}_{\mathrm{G1,Up}} - 0.02P^{1,0}_{\mathrm{G1,Down}} + 1P^{1,0}_{\mathrm{G2,Up}} - 0.02P^{1,0}_{\mathrm{G2,Down}} \\ &+ 1P^{1,0}_{\mathrm{G3,Up}} - 0.02P^{1,0}_{\mathrm{G3,Down}} + 1P^{1,0}_{\mathrm{G4,Up}} - 0.01P^{1,0}_{\mathrm{G4,Down}}\big)\frac{€}{\mathrm{h}}. \end{aligned} \tag{5.15}$$

The positive wind redispatch costs can be considered hypothetical since it is usually already fully dispatched. We slightly increase the negative wind redispatch costs to avoid curtailment where conventional generators could provide the reserve as well. Thus, it is cheaper to use negative redispatch from conventional generators than from wind power plants.

We run generators in a preventive mode, i.e. the power output set points must be valid throughout all considered scenarios. However, to cope with changing system losses, we allow for each generating unit to adapt its power set point from the base case to a contingency by ± 1 MW. Contrarily, we assume the DC system highly controllable (*Preventive-Curative-DC* mode). Hence, a TSO can freely adapt the power set points before and after a contingency. The coupling constraints are defined as

$$\begin{aligned} &\textit{N-1 Coupling}^1(x^{1,0}, x^{1,1}) \equiv \Bigg\{ \\ &\quad -0.01 \leq (P^{1,0}_{\mathrm{G}i\mathrm{,Up}} - P^{1,0}_{\mathrm{G}i\mathrm{,Down}}) - (P^{1,1}_{\mathrm{G}i\mathrm{,Up}} - P^{1,1}_{\mathrm{G}i\mathrm{,Down}}) \leq 0.01 \qquad \text{(5.16a)} \\ &\quad -\infty \leq P^{1,0}_{\mathrm{VSC}j} - P^{1,1}_{\mathrm{VSC}j} \leq \infty, \qquad \text{(5.16b)} \\ &\quad \forall i \in \{1,..,4\}, \forall j \in \{1,2,3\} \Bigg\}. \end{aligned}$$

In the following figures, a power value in black denotes a non-controllable dispatch, and a power value in blue color denotes the controllable deviation from it. The impact of PST is investigated by means of *Fixed-*, *Preventive-* and *Preventive-Curative-PST* modes.

[1] Otherwise, a simultaneous upward and downward redispatch, compensating each other in sum, would have negative costs and thus be cheaper than no redispatch (with no costs).

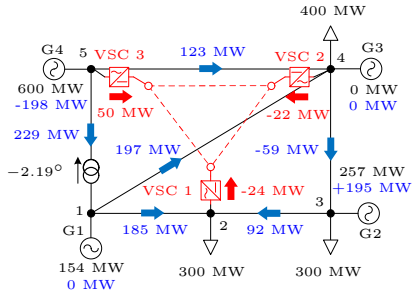

(a) Base case. Preventive generator redispatch of +195/-198 MW.

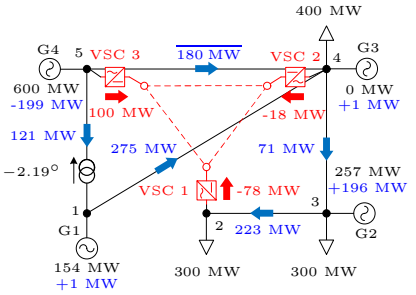

(b) After outage of *Line 1-2*. Generators within ±1 MW compared to base case.

Figure 5.5: SC-OPF results in *Fixed-PST* mode, where the PST angle is non-controllable. The optimization comprises both (a) and (b).

Fixed-PST Mode

We perform a redispatch where a TSO does not have control over the PST. To use the same dispatch throughout the next cases and to foster a fair comparison, we use the optimal value from Fig. 5.3b as a fixed shifting angle. In Fig. 5.5, results are shown for both before and after the outage of *Line 1-2*. In Fig.5.5a, it can be seen that the generators are preventively redispatched, namely the power output of generator *G2* is increased by 195 MW and the wind generator *G4* is curtailed by -198 MW. Subsequently, all AC lines and VSCs are loaded far from their thermal limits. This margin allows for safe operation after the outage where 185 MW must be re-routed at *Node 1*, see Fig. 5.5b. Additionally, the withdrawn power of *VSC 3* is increased by 50 MW to relieve the stressed network area. With the same generator set points (±1 MW), all operational constraints are satisfied while *Line 4-5* and *VSC 3* are fully loaded.

Preventive-PST Mode

Next, we give the TSO the ability to preventively adapt the PST taps, see Fig. 5.6. One optimal phase shift angle is calculated which must remain valid before and after the contingency. Thus, security constraints (5.16) are augmented by

$$0 \leq \angle\psi^{1,0}_{\mathrm{PST15}} - \angle\psi^{1,1}_{\mathrm{PST15}} \leq 0. \tag{5.17}$$

Similar to the OPF results, the voltage angle in the wind region is decreased by $-5.42°$ to allow for a larger flow on *Line 1-4* and avoid wind curtailment. Nevertheless, generator *G1* is preventively redispatched by -54 MW to reduce load on the constrained *Line 5-4*, see Fig. 5.6a. Subsequently, the two remaining

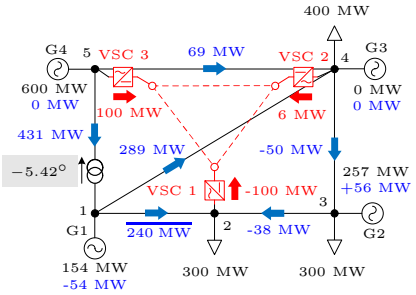

(a) Base case. Preventive generator redispatch of +56/-54 MW.

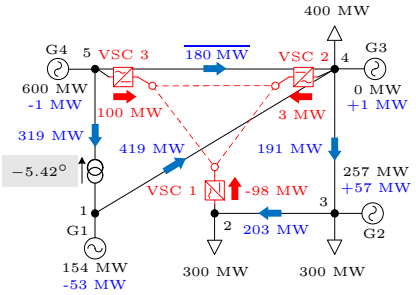

(b) After outage of *Line 1-2*. Generators within ±1 MW compared to base case.

Figure 5.6: SC-OPF results in *Preventive-PST* mode, where the controllable PST angle is valid for both topologies. The optimization comprises both (a) and (b).

AC lines *5-4* and *1-4* are able to carry an additional 240 MW after the line outage in Fig. 5.6b.

Preventive-Curative-PST Mode

Finally, we allow the TSO to adapt the PST angle after the contingency as well, which gives the most available flexibility. In our case, a PST angle adaption of up to 10° is allowed:

$$-10^\circ \leq \angle\psi^{1,0}_{\text{PST15}} - \angle\psi^{1,1}_{\text{PST15}} \leq 10^\circ. \tag{5.18}$$

With $\angle\psi^{1,0}_{\text{PST15}} = -2.21^\circ$, the optimal PST angle in the base case is very close to the OPF result of -2.19°, see Fig. 5.7a. Both constrained lines are fully loaded with a small generator redispatch of +10/-9 MW. By increasing the phase shift angle after the outage to $\angle\psi^{1,1}_{\text{PST15}} = -6.31^\circ$, *Line 1-4* takes over the full amount of power flowing previously on *Line 1-2*. Subsequently, the power set points of the generators can be held within the ±1 MW-tolerance.

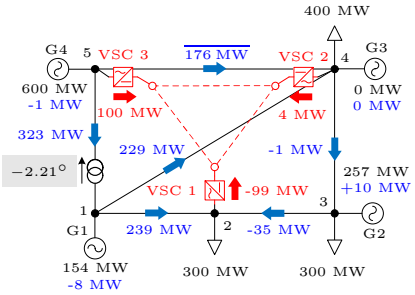

(a) Base case. Preventive generator redispatch of +10/-9 MW.

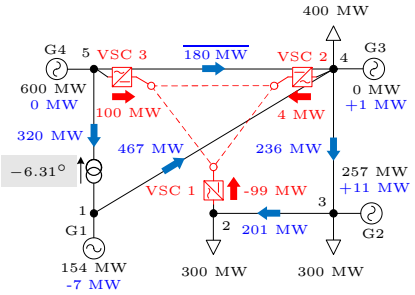

(b) After outage of *Line 1-2*. Generators within ±1 MW compared to base case.

Figure 5.7: SC-OPF results in *Preventive-Curative-PST* mode, where the PST angle is independently controllable before and after the outage. The optimization comprises both (a) and (b).

5.1.3 Risk-based SC-OPF

In this chapter, we illustrate the effect of varying outage probabilities and load shedding costs in a risk-based SC-OPF. Recall from Chapter 3.3.2 that a risk-based SC-OPF with one contingency is expressed by

$$\underset{x^{1,0},x^{1,1}}{\text{minimize}} \quad \mathit{Costs}^{1,0}(x^{1,0}) + p^{1,1} \cdot \mathit{Costs}^{1,1}(x^{1,1}) \tag{5.19a}$$

$$\text{subject to} \quad \mathit{Basics}^{1,0}(x^{1,0}) \tag{5.19b}$$

$$\mathit{Basics}^{1,1}(x^{1,1}) \tag{5.19c}$$

$$\mathit{N\text{-}1\ Coupling}^{1}(x^{1,0}, x^{1,1}). \tag{5.19d}$$

In contrast to the traditional SC-OPF, the cost after an outage is incorporated into the objective. It is weighted with a probability factor $p^{1,1}$, which is defined by the TSO depending on the type of contingency. For the analysis, we use a pure AC topology with original line flow limits of 400 MVA for *Line 1-2*, and 240 MVA for *Line 5-4*. Wind power is reduced to 500 MW and the PST is deactivated. We use generator dispatch set points $(P_{\text{G1,Disp}}, P_{\text{G2,Disp}}, P_{\text{G3,Disp}}) = (170\,\text{MW}, 230\,\text{MW}, 100\,\text{MW})$ and power limits are activated. As before, we treat *Line 1-2* as a possible contingency. Additionally, we allow the curtailment of the load at *Node 2* at costs of 1000 €/MWh. Consequently, $P^{1,0}_{\text{D2,Shed}}$ and $P^{1,1}_{\text{D2,Shed}}$ denote the curtailed load before and after the contingency and are added to the state vectors $x^{1,0}$ and $x^{1,1}$, respectively. As an example, the power balance of

Node 2 (5.5b) after the outage, i.e. $(t, c) = (1, 1)$, becomes

$$-3 + P^{1,1}_{\mathrm{D2,Shed}} + \mathrm{j}(-0.99 + P^{1,1}_{\mathrm{D2,Shed}} \frac{0.99}{3}) = V^{1,1}_{\mathrm{AC2}} \left(y^{1,1}_{\mathrm{SP23}} V^{1,1}_{\mathrm{AC2}} - y^{1,1}_{\mathrm{S23}} V^{1,1}_{\mathrm{AC3}} \right)^*. \tag{5.20}$$

Here, admittances between *Node 2* and *Node 1* are zero. The new decision variables are limited by the nominal load of 300 MW:

$$0 \leq P^{1,0}_{\mathrm{D2,Shed}}, P^{1,1}_{\mathrm{D2,Shed}} \leq 3. \tag{5.21}$$

Generator redispatch costs remain at 100 €/MWh, i.e. one tenth of the load shedding costs. Therefore, the cost of the base case ($c = 0$) or the contingency case ($c = 1$) is described with

$$\begin{aligned} \mathit{Costs}^{1,c}(x^{1,c}) = \big(& 1P^{1,c}_{\mathrm{G1,Up}} - 0.02P^{1,c}_{\mathrm{G1,Down}} + 1P^{1,c}_{\mathrm{G2,Up}} - 0.01P^{1,c}_{\mathrm{G2,Down}} \\ & + 1P^{1,c}_{\mathrm{G3,Up}} - 0.02P^{1,c}_{\mathrm{G3,Down}} + 1P^{1,c}_{\mathrm{G4,Up}} - 0.01P^{1,c}_{\mathrm{G4,Down}} \\ & + 10P^{1,c}_{\mathrm{D2,Shed}} \big) \frac{€}{\mathrm{h}}. \end{aligned} \tag{5.22}$$

The expectation to a risk-based optimization in this system is clear: as long as the contingency probability $p^{1,1}$ is below 10 %, preventive generator redispatch is more expensive than the weighted costs of an energy loss after the outage. Thus, the risk is taken and no redispatch is activated. With an increasing probability assumption, the risk-based costs grow too large and preventive redispatch should be initiated to avoid a possible load curtailment.

In Fig. 5.8a, our assumption is in general confirmed. However, generator redispatch seems to be triggered with a delay, being fully deployed not before the probability has risen to over 10.08 %. This is due to the fact that the generator is not located directly at the load and the power must be transported over a non-lossless line. Thus, slightly more than 1 MW of redispatch is needed to replace 1 MW of shedded load. The non-linear losses lead to a transition zone, where it is cost-optimal to share the necessary power injection between generator and load. If we place the generator right at *Node 2*, where the sheddable load is connected, we observe that the threshold probability is exactly met, see Fig. 5.8b.

Remarks on Implementation

Note that when allowing load shedding after an outage, there must be sufficient negative reserve in the system to reduce the injected power by the amount of lost load and maintain power balance[2], which might stand in contrast to preventive control where generator power set points are not allowed to change after an outage.

[2] In reality, this is automatically achieved by frequency control.

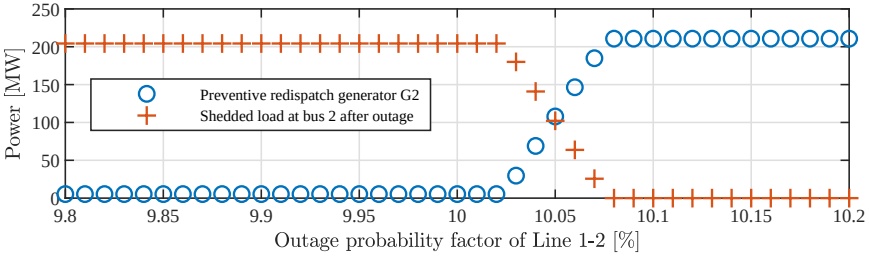

(a) Generator *G2* connected at *Node 3*.

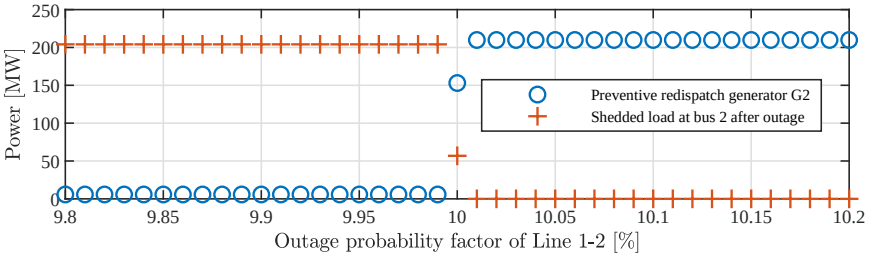

(b) Generator *G2* connected at *Node 2*.

Figure 5.8: Risk-based SC-OPF with preventive redispatch costs of 100 €/MWh and load shedding costs of 1000 €/MWh. The choice between generator redispatch and load shedding depends on the assumed outage probability.

This must be handled with care – especially in small systems where the curative reserve is limited due to the relatively small installed generator capacity. In our example, we allow wind power and generator *G1* to decrease power injection after the outage. Furthermore, we set the generator redispatch costs in the outage scenario to zero for illustration reasons. Normally, those costs are weighted and then included in the cost function as well[3], which would subsequently lead to a small shift toward delayed generator redispatch.

[3] If the objective has no components based on a power injection, multiple solutions lead to the same costs. For example, a slight increase in power injection could be compensated with lower voltages and subsequently higher losses, but have the same costs and thus appear of equal priority to the solver. Many solutions of equal priority lead to an ill-conditioned optimization problem and possibly to divergence in large systems.

5.2 67-Bus System

In [75], a hybrid AC-DC benchmark system is presented. The AC system has a voltage level of 400 kV and is built up of 3 control areas complemented by an offshore area; it consists of 67 nodes and 102 lines, see Fig. 5.9 and more details in Appendix B. Here, a set of critical line contingencies is provided and marked in red; all AC line flow limits are set to 2300 MVA. Power is produced by 17 conventional generators and 3 wind parks to satisfy a total demand of 11.8 GW, see Tables B.1 and B.5. The bipolar DC system has a nominal voltage of ±500 kV and is connected via 9 VSCs. Different DC topologies connecting the VSCs can be examined. In this work, we consider two different stages. *DC-Stage 1* represents 3 parallel DC systems consisting of 2-4 serial terminals directed from North to South, which includes in total 6 DC lines (Fig. 5.10a). *DC-Stage 2* is an advanced topology with additional meshing, where a total of 11 DC lines are included (Fig. 5.10b). In both stages, full selectivity is assumed. That is, if a DC line or a VSC fails, the fault is considered isolated and the remaining grid components remain operable. The rated converter power is $\overline{S}_{\mathrm{VSC}} = 1800\,\mathrm{MVA}$ for all VSCs and loss parameters are set to $(\alpha_{\mathrm{VSCL}}, \gamma_{\mathrm{VSCL}}) = (0.01103, 0.0075)$. There exists a desired power imbalance between the individual areas to force a considerable long-distance power transfer.

5.2.1 OPF with Varying Objectives

In our first study, we will investigate how DC systems can affect the AC power flow in different manners depending on the objective function. We use the original AC benchmark system in combination with *DC-Stage 2* (Fig. 5.10b). Furthermore, a generator redispatch is performed ($\mathcal{E}^{\mathrm{G,Redisp}} = \mathcal{E}^{\mathrm{G}}$) and the dispatch set points are taken from [75], see Table B.8. We investigate 3 objective functions:

- **Network losses:** assigning the same cost per MWh to each generator yields in a minimized total power injection and subsequently minimized losses. Additionally, as described in Chapter 5.1.2, we assign negative costs to negative redispatch:

$$Costs^{1,0} = \Big(\sum_{i \in \mathcal{E}^{\mathrm{G,Redisp}}} 1 P^{1,0}_{\mathrm{G}i,\mathrm{Up}} - \sum_{i \in \mathcal{E}^{\mathrm{G,Redisp}}} 0.1 P^{1,0}_{\mathrm{G}i,\mathrm{Down}} \Big) \frac{\text{€}}{\mathrm{h}}. \tag{5.23}$$

- **Loading critical lines:** generator reserve costs are set to zero and instead, the square of apparent power flowing over a chosen set of AC lines $\mathcal{E}^{\mathrm{CL}}$ is added to the objective function:

$$Costs^{1,0} = \sum_{(i,j) \in \mathcal{E}^{\mathrm{CL}}} \frac{|V^{1,0}_{\mathrm{AC}i} (I^{1,0}_{\mathrm{Br}ij})^*|^2}{\overline{S}^2_{\mathrm{Br}ij}} \frac{\text{€}}{\mathrm{h}}. \tag{5.24}$$

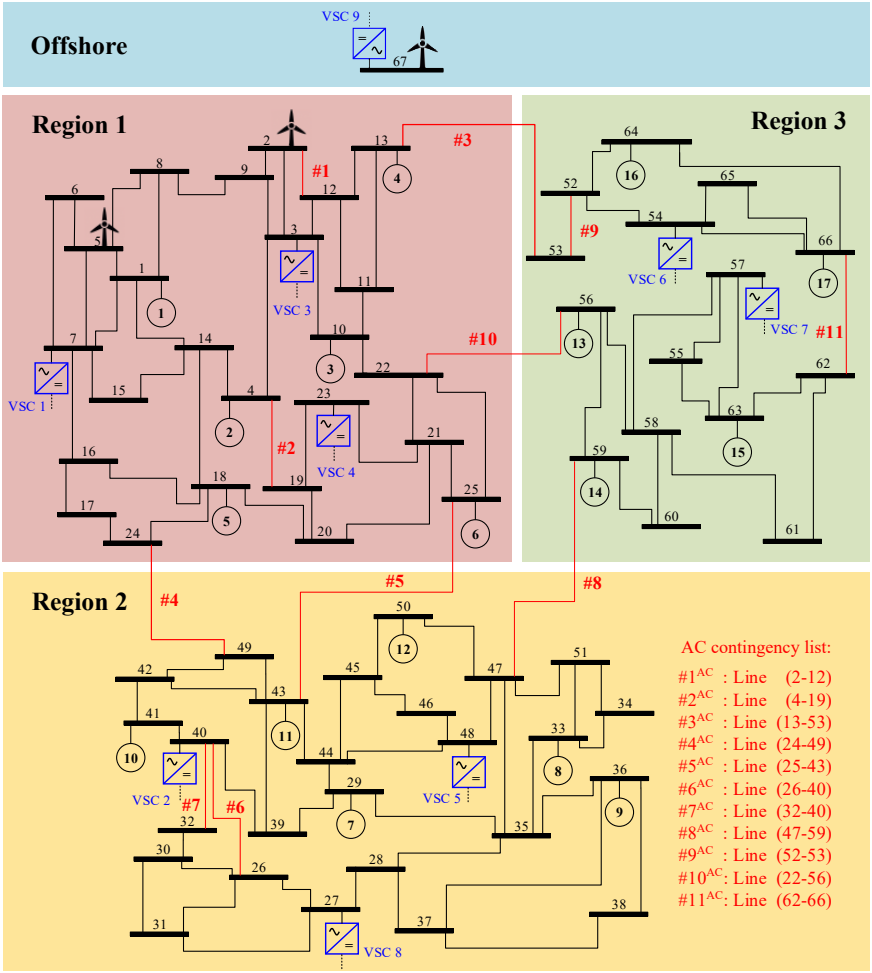

Figure 5.9: AC-Topology of 67-bus test system with 3 control areas and an offshore connection. VSCs are marked in blue and possible AC contingencies are marked in red. The illustration is taken from [75] with modifications.

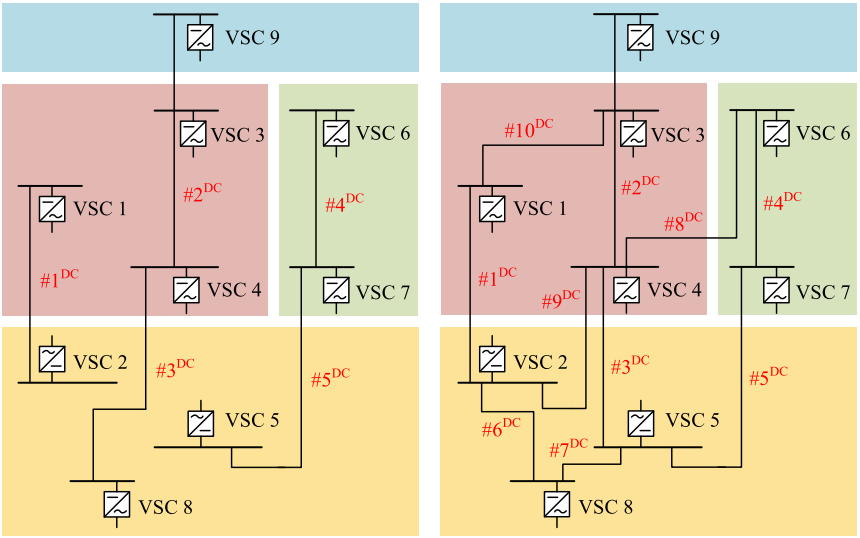

(a) DC-Topology *"DC-Stage 1"*. **(b)** DC-Topology *"DC-Stage 2"*.

Figure 5.10: Different DC topologies for 67-bus test system. Possible DC contingencies are marked in red.

Critical lines are marked in red in Fig. 5.9. Since the generators do not appear in the objective and redispatch would be cost-free, we restrict generator actions by modeling a distributed slack. With

$$P^{1,0}_{\mathrm{G}i,\mathrm{Up}} - P^{1,0}_{\mathrm{G}i,\mathrm{Down}} = P^{1,0}_{\mathrm{G}j,\mathrm{Up}} - P^{1,0}_{\mathrm{G}j,\mathrm{Down}}, \quad \forall i,j \in \mathcal{E}^{\mathrm{G,Redisp}} \wedge i \neq j, \tag{5.25}$$

generators are forced to provide the same amount of positive or negative reserve each and are consequently only employed to secure power balance.

- **Loading all lines:** the critical line set $\mathcal{E}^{\mathrm{CL}}$ is extended to *all* AC lines.

The two latter objectives are motivated by a TSO, which seeks to increase the security margins in the AC network without performing full N-1 security studies. The resulting differences are reflected naturally in the network losses and the power flow over the critical lines. As expected, total network losses are the lowest (374 MW) when using the first objective, see Fig. 5.11. However, it is notable that losses in the AC system are the lowest when minimizing the load on all AC lines. This comes at costs of higher losses in the DC system, which is employed to

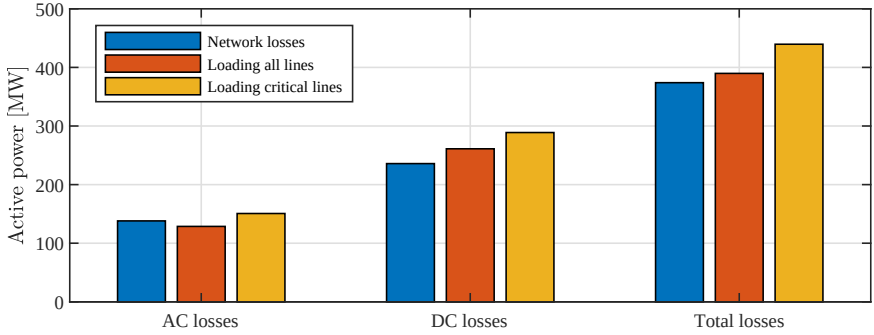

Figure 5.11: Network losses for different objective functions.

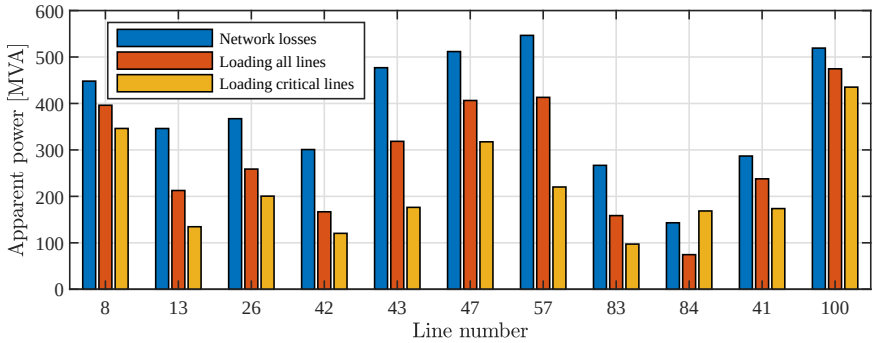

Figure 5.12: Power flow on critical lines for different objective functions.

relieve the AC side. The highest losses (440 MW) occur when minimizing loading on critical AC lines only since there is no incentive to reduce currents in any other parts of the network.

Line apparent power flow is shown in Fig. 5.12. As expected, the power flows are reduced if the loading is added to the objective. However, loading on critical lines can remain significantly larger if the remaining AC lines in the network are added to the objective as well.

The power transfer over the DC system can be observed in Fig. 5.13, where power set points of the VSCs are depicted. Negative values denote a power transfer from AC to DC and positive values from DC to AC. When minimizing losses, a total power of about 3.65 GW is injected into the DC system and transferred to other AC locations. When AC lines are meant to be relieved, the DC system is utilized for the power transfer instead, which can be observed in Fig. 5.13. The need for

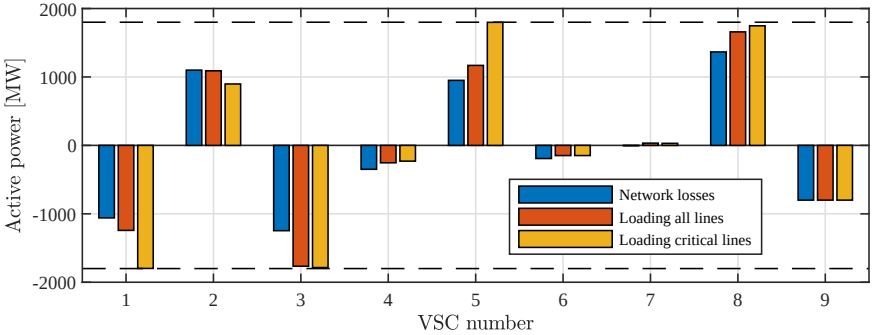

Figure 5.13: Power set points of converters for different objective functions. Positive value: power flow from DC to AC, negative value: power flow from AC to DC.

a power transfer shift from AC to DC is the largest (4.76 GW) when only critical line loading is penalized. This is due to the fact that those lines include important connections between North and South. Those tie lines are relieved to a maximum by using the full capacity of *VSC 1* and *3* to extract power from the AC side and re-inject it with *VSC 5* and *8* on the opposite side of the tie lines.

To conclude, the loading on critical lines can substantially be reduced by utilizing the DC system to relieve stressed AC network areas. As a consequence, however, grid losses are increased in both AC and DC system.

5.2.2 SC-OPF with AC Contingencies and Varying DC Control Modes

In this section, we investigate the use of HVDC curative control in order to reduce generator redispatch. We use *DC-Stage 1* to increase the network stress level, see Fig. 5.10a. Furthermore, AC line flow, DC line flow, and VSC capacity limits are reduced to 1200 MVA. Active power demand in *Region 2* and *Region 3* is increased by 18 %, see Table B.5, which leads to a total load of 13.6 GW. Additionally, higher costs are assigned to generators in *Region 2* (see Table B.6). The scenario list $\mathcal{C} = \{0, 1, .., 11\}$ includes all lines which are marked red in Fig. 5.9. The order remains identical, e.g. index 1 ($\in \mathcal{C}$), also referred to as outage $\#1^{\mathrm{AC}}$ or AC outage #1, represents an outage of *Line 2-12*. Lastly, a conventional AC-DC OPF is performed to obtain generator dispatch set points, see Table B.8.

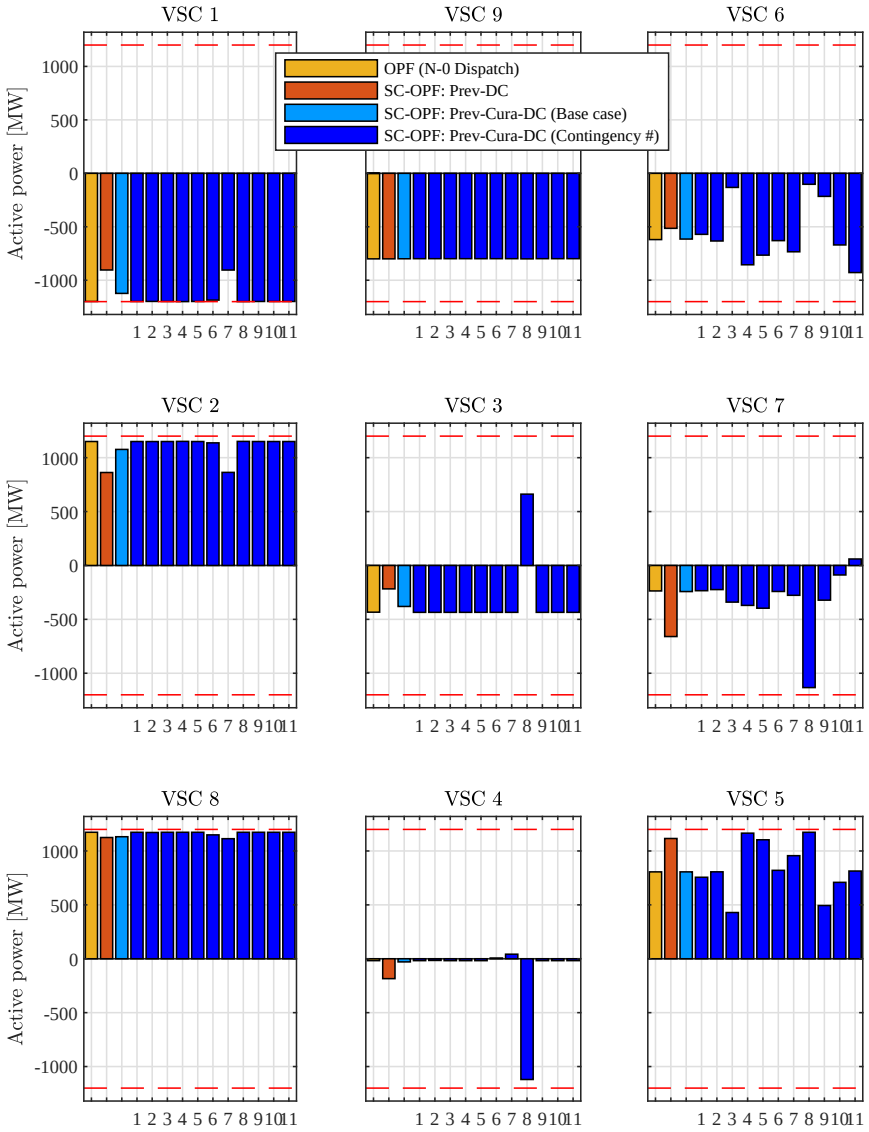

Figure 5.14: VSC active power set points after dispatch (yellow) and two N-1 secure redispatch optimizations with different DC control modes: *Preventive-DC* (red) and *Preventive-Curative-DC* (blue).

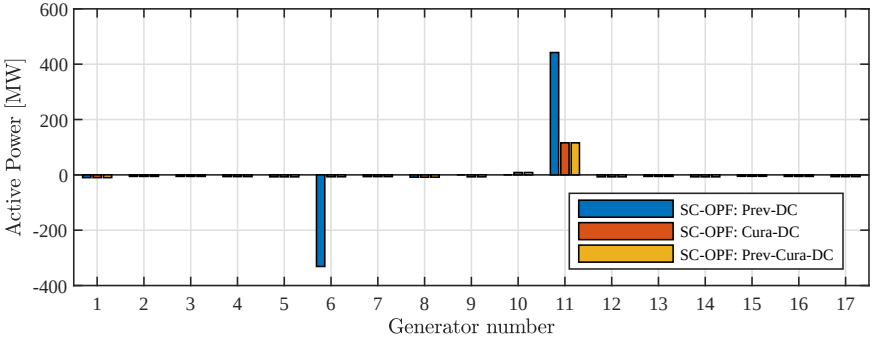

Figure 5.15: Preventive redispatch of each generator in 3 SC-OPF optimizations with varying DC control modes.

VSC power set points

In Fig. 5.14, active power set points are shown for each converter. The originally computed dispatch (yellow) is compared with two different redispatch optimizations – one set point with *Preventive-DC* (red) and in total 12 set points with *Preventive-Curative-DC* (blue). Here, we can differentiate between the base case (light blue) and the 11 contingencies (dark blue). The left DC link (*VSC 1* to *VSC 2*) is fully loaded during dispatch and after most outages, thus, the link cannot provide much flexibility. An exception is formed by a necessary power reduction after outage $\#7^{\mathrm{AC}}$, which is a line directly connected to *VSC 2*. In *Preventive-DC* mode, the link is slightly relieved due to a generator redispatch. Similar operation can be stated for the receiving end of the middle DC link, namely *VSC 8*. However, the link includes *two* converters in *Region 1*, namely *VSC 3* and *4*, which vary their set points significantly in case of outage $\#8^{\mathrm{AC}}$. The total transmitted power toward *VSC 8* remains similar, but the injected power is shifted between *VSC 3* and *VSC 4*. After outage $\#8^{\mathrm{AC}}$, *VSC 3* even reverses the power flow direction from DC to AC in order to feed large power amounts from *VSC 4* into the DC system, which, in turn, relieves the AC side close to the outage. Similarly, *VSC 6* and *VSC 7* shift power set points and in case of outage $\#8^{\mathrm{AC}}$, where the nearby located *VSC 7* is almost fully loaded to absorb power from the AC side. However, unlike the middle link, the total power transferred to *VSC 5* does fluctuate depending on the contingency scenario.

Generator Redispatch

In Fig. 5.15, preventive redispatch is shown for each generator. In *Preventive-DC* mode, total upwards and downwards redispatch are +442 MW and -420 MW,

respectively. The deviation in absolute value stems from changing system losses the generators need to cope with. When using *Preventive-Curative-DC* mode, the amount of generator redispatch is reduced to +124/-104 MW[4]. Thus, an amount of around ±320 MW can be avoided only by adjusting HVDC set points after an outage. For comparison, the *Curative-DC* mode is added. However, it can be seen that in this particular case, the effect of fixing the base case set points is negligible in terms of preventive generator redispatch. Since the base case has no constraining issues, all that matters is whether or not the HVDC set points are allowed to change after an outage to cope with a stressed N-1 scenario.

Remark on Contingency Filtering

The above-made observations are based on a calculation, where all critical contingencies are included. However, the full list is not necessarily required for an optimal redispatch. In Fig. 5.16 (top), we perform optimizations with different subsets of the full contingency list. Interestingly, a very similar amount of generator redispatch is triggered when only outages $\#3^{\mathrm{AC}}$, $\#7^{\mathrm{AC}}$ and $\#8^{\mathrm{AC}}$ are included. This reveals that some contingencies, or rather combinations of contingencies, are dominant in a network. For example, outages $\#4^{\mathrm{AC}}$ and $\#5^{\mathrm{AC}}$ are undoubtedly important AC tie lines for a North to South power transfer. However, if $\#8^{\mathrm{AC}}$ is respected, the redispatch is distributed such that outages $\#4^{\mathrm{AC}}$ and $\#5^{\mathrm{AC}}$ are automatically covered as well. After all, the weak impact of single outages ($\mathcal{C} = \{3\}$, $\{7\}$ or $\{8\}$) shows that it might not be trivial to find a worst-case combination. Figure 5.16 (bottom) shows that reducing the full contingency set by single lines can indicate which outages play a dominant role, but clearly requires calculations with large contingency sets in the first place. In other words, an offline contingency analysis can be crucial to saving computation time, but a good knowledge of the network and load flow patterns is necessary to reduce the full list to an adequate subset in order to avoid huge numbers of combinatoric calculations.

5.2.3 SC-OPF with DC Contingencies and Varying DC Topologies

Contingencies may occur not only on the AC side. The DC system as well is prone to failures and possible DC line or converter outages must be taken into account. Regarding the DC control mode, preventive control seems unreasonable. For example, if a converter fails and the remaining ones need to maintain the same power set points, huge security margins are required. Therefore, we assume *Preventive-Curative-DC* mode in this section. In order to cause generator redis-

[4] Observing that the remaining redispatch of around ±100 MW is distributed among all generators, one can presume that each generator provides small curative action by abusing the allowed 1 % "primary reserve".

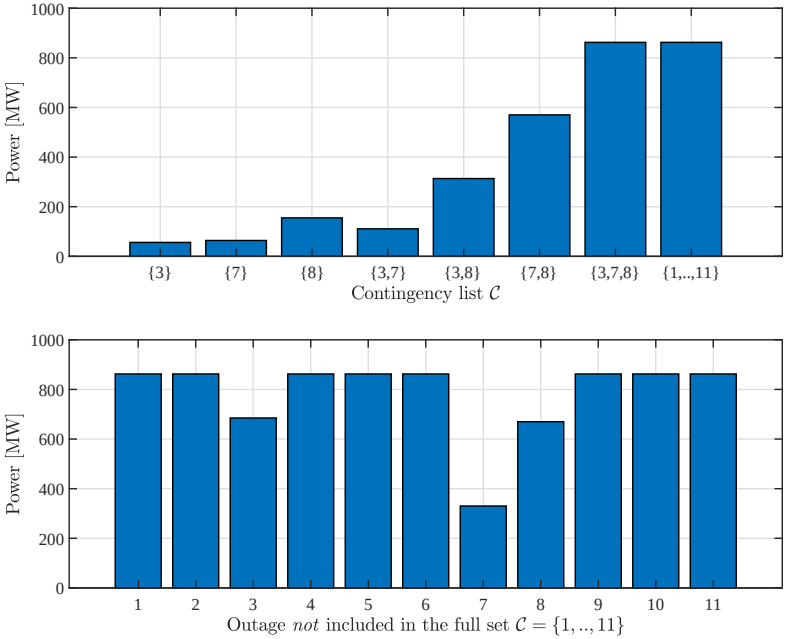

Figure 5.16: Absolute preventive generator redispatch (upwards plus downwards) with different contingency sets in *Preventive-DC* mode.

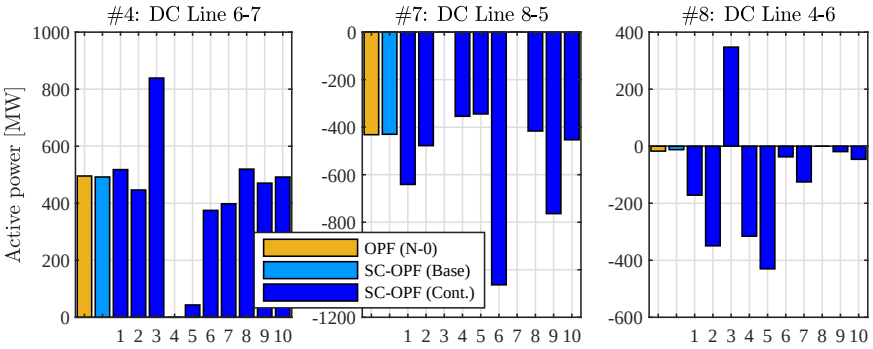

Figure 5.17: DC line flows with *DC-Stage 2* and contingency list *DC Lines*.

patch in curative mode as well, we increase the capacity of each generator by 10 %, see Table B.2. This leads to a higher power transfer from North to South since cheap generation in the North can be dispatched more extensively. Generator dispatch set points are shown in Table B.8. We define 3 different types of contingency sets:

- "*AC Lines*": All 11 critical AC lines from the previous sections.
- "*DC Lines*": All DC lines in the system, except between *VSC 3* and *VSC 9*.
- "*VSCs*": All VSCs in the system, except *VSC 9*.

Note that in bipolar DC systems, the loss of a full branch would, in fact, imply the outage of both positive and negative system. However, we assume the same power transfer capacity for AC branch, DC branch and VSC. Thus, to foster a fair comparison between outage severity regarding necessary preventive generator redispatch, we assume monopolar DC systems.

DC Line Flow

As an excerpt, DC line flow is shown for 3 exemplary lines in Fig. 5.17. Power is compared for a conventional AC-DC OPF and the various scenarios of an SC-OPF (base case and 10 contingencies). For example, *DC Line 6-7* almost doubles the carried power after contingency $\#3^{\mathrm{DC}}$. The reason is that a part of the power transferred from *Region 1* to *Region 2* must be re-routed via *Region 3*. On the other hand, line flow is negligible if $\#4^{\mathrm{DC}}$ fails. In that case, *DC Line 6-7* has no more connection toward *Region 2* as a power receiver. Similarly, *DC Line 8-5* takes over power from failing $\#6^{\mathrm{DC}}$ – which is also feeding *VSC 8* during the base

case – and is relieved if outage $\#3^{\mathrm{DC}}$, previously sending power from *Region 1*, occurs. An interesting behavior can be observed for *DC Line 4-6*. During the base case, this horizontal line between *Region 1* and *Region 3* practically does not carry any power. However, depending on the location of a contingency, the line is used to transfer power in both directions. If $\#3^{\mathrm{DC}}$ fails, over 300 MW are transferred from *Region 1* toward *Region 3*. On the other hand, if $\#2^{\mathrm{DC}}$, $\#4^{\mathrm{DC}}$ or $\#10^{\mathrm{DC}}$ fail, a similar amount of power is directed the other way from *Region 3* toward *Region 1*. This underlines the additional flexibility which is obtained by meshing a power network. Lines which might not be relevant for general power transfer between different price regions might gain importance in case of failures when they are operated as a sort of power by-pass.

DC-Stage 1 vs. DC-Stage 2

We now turn the focus toward the difference between non-meshed and meshed DC systems. Figure 5.18 depicts total preventive generator redispatch, i.e. the sum of absolute upward and downward redispatch, for different contingency sets and DC topologies. Note that the dispatch is computed separately for the two topologies in order to load the DC systems to a maximum and foster a fair comparison, see Table B.8. It is notable that with *DC-Stage 1*, the amount of redispatch lies between 1200-1400 MW regardless of the type of contingencies. Contrarily, the type of contingency has severe impact on redispatch in a meshed *DC-Stage 2*. If the contingency set consists of VSCs, redispatch almost reaches the same amount as with *DC-Stage 1*. This is mainly due to the fact that if *VSC 2*, *5* or *8* fail, there is no alternative way of providing the missing power in *Region 2*, since the AC tie lines are usually highly loaded as well. Contrarily, redispatch is reduced to a minimum when only DC lines are considered as possible outages. The meshed network provides enough flexibility and by-passes to overcome line outages. As seen in the previous section, power can effectively be re-directed by adapting the converter set points. Similarly, *DC-Stage 2* improves the power flow situation in the case of AC line contingencies, where the necessary generator redispatch is reduced from strongly. However, it is still required an amount of 700 MW redispatch, since a power transfer shift from the AC to the DC system is also limited by free VSC capacity “behind” the AC bottleneck.

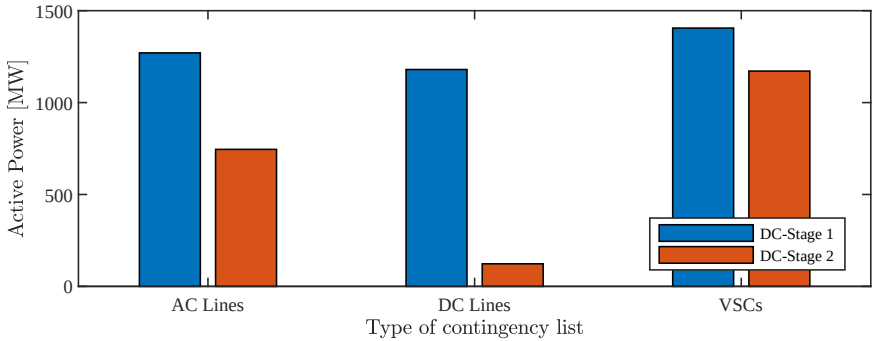

Figure 5.18: Total preventive generator redispatch for different types of contingencies and DC topologies.

5.3 Summary

The main findings of this chapter are:

- **OPF with HVDC and PST** — the effectiveness of a PST is large when parallel lines tend to be loaded unevenly. In that case, DC systems provide only limited flexibility and need to be dimensioned comparatively large. However, it is clear that a PST cannot replace network extension if the total transfer capacity is insufficient.

- **SC-OPF with PST** — the amount of necessary preventive generator redispatch decreases with higher degrees of PST flexibility. This statement is generally valid, however, a quantification depends highly on the considered system and assumptions made.

- **Risk-based SC-OPF** — the "choice" between preventive generator redispatch and curative load shedding depends on the probability assigned to the contingency and the distance between concerned generator and load.

- **Objectives with HVDC** — different goals can be reached when employing HVDC. Objectives such as minimization of network losses or AC line loading lead to differing optimal operating points.

- **SC-OPF with HVDC** — curatively controllable HVDC set points can reduce preventive generator redispatch. Power injections are shifted from one VSC to another to relieve specific AC network areas in the case of an outage. However, this requires free VSC capacity during normal operation.

- **Contingency list** — a shrunk contingency list can massively reduce computational effort without changing the result. However, the choice is not straightforward since the isolated effects of single contingencies do not reflect the impact of possible worst-case combinations.
- **DC-side contingencies** — outages of VSCs weigh heavy, especially if all VSCs in the same price region are fully loaded and there is no alternative power by-pass. The impact of DC line outages depends on the degree of selectivity and meshing.
- **Meshed DC-topology** — even if total transfer capacity is not necessarily increased, meshing a DC network introduces advantageous power flow flexibility regarding N-1 security and subsequently the reduction of generator redispatch. To resolve DC-side contingencies, this requires a high degree of selectivity which implies costs for additional fault handling hardware.

Chapter 6

Case Studies: Multi-Time Step Optimization with Energy Storage Systems

In this chapter, the asset of a TSO is extended by energy storage systems. Since storage operation is highly dependent on time to respect energy constraints, the optimization must be based on a forecast of load and renewables. Therefore, it comprises multiple time steps to obtain an optimal storage power trajectory.

6.1 Receding Horizon Control with Averaged Forecast

At any time, the power system is subject to fluctuations in load and generation. Weather and load predictions can never be exact and forecast errors grow with the time distance from the present. One can determine an optimal control sequence for the entire day, however, optimality or even feasibility can be lost a few hours (or minutes) later. Therefore, frequent forecast updates and renewed optimizations are crucial in a real system. One method is Receding Horizon Control (RHC), also referred to as rolling horizon, which stems from model predictive control theory. The principle is to calculate an optimal sequence over a certain optimization horizon and apply it to a limited number of time steps. Then, a forecast update is received and a new optimization is performed. The number of optimized time steps – depending on the time resolution and the desired optimization horizon – defines the computational effort, which can rapidly increase. As stated above, forecast values farther ahead in the future are more likely to be erroneous, which reduces the necessity of a high granularity. Thus, we use a decreasing forecast granularity, which reduces the total number of time steps included in the optimization. However, we assume that an incoming forecast is

entirely based on a 15 min resolution. Therefore, the values are averaged if longer time intervals are desired.

Example

The method shall be illustrated with an exemplary optimization process comprising four different resolution intervals. Note that in the following, all values are normalized per hour. Let the first resolution interval be defined by interval length $T^1_{\mathrm{RHC}} = 8$ and resolution $\Delta t^1_{\mathrm{RHC}} = 0.25$, i.e. the first 8 hours of the forecast remain unchanged in the highest 15 min resolution. Hours 9-16 are averaged on an hourly basis, leading to $(T^2_{\mathrm{RHC}}, \Delta t^2_{\mathrm{RHC}}) = (8, 1)$ and thus 8 instead of 32 time steps. Hours 17-24 are averaged on a 4-hour basis, $(T^3_{\mathrm{RHC}}, \Delta t^3_{\mathrm{RHC}}) = (8, 4)$, and the second day, i.e. hours 25-48, are averaged on a 12-hour basis, $(T^4_{\mathrm{RHC}}, \Delta t^4_{\mathrm{RHC}}) = (24, 12)$. In total, the number of time steps is reduced from 192 to 44. In the example, we use a sample rate of $R_{\mathrm{RHC}} = 8$. That is, calculated values are applied for the first 8 hours, the optimization window moves forward 8 hours, and the second calculation is performed with an updated forecast. To fully describe an RHC scheme, the notation

$$RHC = [(T^1_{\mathrm{RHC}}, \Delta t^1_{\mathrm{RHC}}), (T^2_{\mathrm{RHC}}, \Delta t^2_{\mathrm{RHC}}), ..., (T^N_{\mathrm{RHC}}, \Delta t^N_{\mathrm{RHC}})@R_{\mathrm{RHC}}] \quad (6.1)$$

is used for N different intervals. In our example, this leads to

$$RHC = [(8, 0.25), (8, 1), (8, 4), (24, 12)@8], \quad (6.2)$$

which describes a total time horizon of $T_{\mathrm{RHC}} = \sum_{i=1}^{N} T^i_{\mathrm{RHC}} = 48$ hours and a number of $T = \sum_{i=1}^{N} T^i_{\mathrm{RHC}} / \Delta t^i_{\mathrm{RHC}} = 44$ time steps.
The optimization process is illustrated in Fig. 6.1. Vertical solid lines indicate the actual optimization window, which contain the original load or wind forecast (black trajectories) in the original resolution of 15 minutes. Vertical dashed lines mark the adapted time steps according to the above-described time step reduction. As a result, the colored lines represent the averaged values of the respective profile between two new time steps. Clearly, the deviation in terms of power values becomes relatively large in the second 24 hours. Nevertheless, crucial information for storage operation is maintained: there tends to be a lack of energy as the demand is expected to exceed renewable generation.

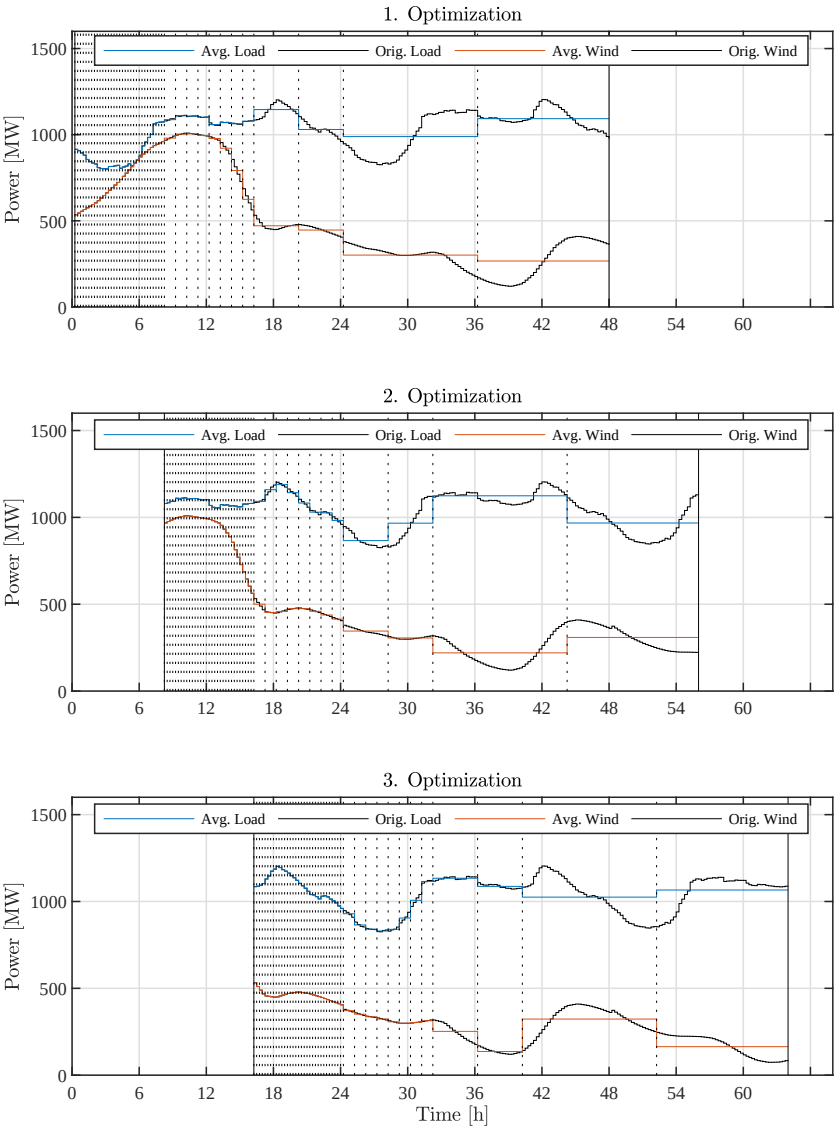

Figure 6.1: Three consecutive optimizations in receding horizon control with averaged forecasts and 4 different resolution intervals, $RHC = [(8, 0.25), (8, 1), (8, 4), (24, 12)@8]$.

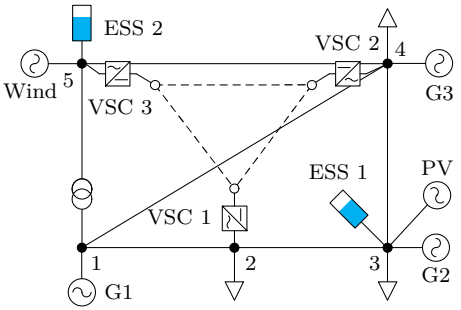

Figure 6.2: Extended 5-bus AC-DC system with two ESSs and a PV park.

6.2 5-Bus System

Two energy storage systems with characteristics from Table A.6 and a PV park are connected to the existing system, see Fig. 6.2. Generator cost functions remain unchanged from Chapter 5, see Table A.4. Forecast power profiles are taken from the Belgian transmission system operator *Elia*, which provides detailed RES generation and load data on its website. Original profiles are shown in Fig. C.1 and Fig. C.4; adapted profiles for usage in the 5-bus test system are shown in Fig. C.2 and Fig. C.5. Here, the first PV peak is ignored since it coincides with the wind peak which would heavily overload the system. Due to an increased peak demand and peak RES generation, we use the original line flow limits of 400 MVA for *Line 1-2* and 240 MVA for *Line 4-5*, respectively. Furthermore, the capacity of each VSC is set to 200 MVA.

6.2.1 Dispatch with D-OPF

We perform an N-0 dispatch with settings $RHC = [(4, 0.25), (8, 1), (12, 4)@2]$, which leads to $(T_{\text{N-1}}, T) = (0, 27)$ for each optimization. Line flow limits are reduced to 70% of the original limits. This setting imitates a day-ahead market-based dispatch with network constraints under consideration of the following 24 hours for a more economic storage operation[1]. The computation of such dispatch demonstrates the functionality of the models, however, it could be used any other market mechanism to generate the necessary input for subsequent redispatch studies.

[1]With an increasing RES integration, we must expect a more important role of storage during dispatch.

Recall from Chapter 4.3 that a D-OPF for T time steps is expressed by

$$\begin{aligned}
\underset{x^{1,0},..,x^{T,0}}{\text{minimize}} \quad & \sum_{t=1}^{T} \mathit{Costs}^{t,0}(x^{t,0}) && \text{(6.3a)}\\
\text{subject to} \quad & \mathit{Basics}^{1,0}(x^{1,0}) && \text{(6.3b)}\\
& \vdots \\
& \mathit{Basics}^{T,0}(x^{T,0}) && \text{(6.3c)}\\
& \mathit{Dynamics}(x^{1,0},..,x^{T,0}). && \text{(6.3d)}
\end{aligned}$$

The *Basics* must be fulfilled for each time step, and the *Dynamics* link the time steps to each other. The storage variables

$$\left\{E^{t,0}_{\text{ESS1}}, P^{t,0}_{\text{ESS1,C}}, P^{t,0}_{\text{ESS1,D}}, Q^{t,0}_{\text{ESS1}}, E^{t,0}_{\text{ESS2}}, P^{t,0}_{\text{ESS2,C}}, P^{t,0}_{\text{ESS2,D}}, Q^{t,0}_{\text{ESS2}}\right\} \tag{6.4}$$

are added to $x^{t,0}$ for each time step t. The power balance of a node where a storage is connected must be augmented by the respective charging and discharging power set points. For example, the power balance of *Node 2* becomes

$$\begin{aligned}
P^{t,0}_{\text{G4}} + \mathrm{j}Q^{t,0}_{\text{G4}} + P^{t,0}_{\text{ESS2,D}} - P^{t,0}_{\text{ESS2,C}} + \mathrm{j}Q^{t,0}_{\text{ESS2}} + P^{t,0}_{\text{VSC3}} + \mathrm{j}Q^{t,0}_{\text{VSC3}} = \\
V^{t,0}_{\text{AC5}}\left((y^{t,0}_{\text{SP51}} + y^{t,0}_{\text{SP54}})V^{t,0}_{\text{AC5}} - y^{t,0}_{\text{S51}}V^{t,0}_{\text{AC1}} - y^{t,0}_{\text{S54}}V^{t,0}_{\text{AC4}}\right)^*
\end{aligned} \tag{6.5}$$

Furthermore, we add the following basic constraints which must be valid for any time step t:

$$\begin{aligned}
0.2 \le E^{t,0}_{\text{ESS1}}, E^{t,0}_{\text{ESS2}} \le 1.8 && \text{(6.6a)}\\
0 \le P^{t,0}_{\text{ESS1,C}}, P^{t,0}_{\text{ESS1,D}}, P^{t,0}_{\text{ESS2,C}}, P^{t,0}_{\text{ESS2,D}} \le 1 && \text{(6.6b)}\\
-1 \le Q^{t,0}_{\text{ESS1}}, Q^{t,0}_{\text{ESS2}} \le 1. && \text{(6.6c)}
\end{aligned}$$

The dynamic constraints connect the energy states of a storage over time by

adding (subtracting) the incremental charged (discharged) energy:

$$
\begin{aligned}
\mathit{Dynamics}(x^{1,0},..,x^{27,0}) \equiv \Bigg\{ & \\
E^{1,0}_{\mathrm{ESS}i} &= \underbrace{1}_{E^{0,0}_{\mathrm{ESS}i}} + (0.95 P^{1,0}_{\mathrm{ESS}i,\mathrm{C}} - 0.95^{-1} P^{1,0}_{\mathrm{ESS}i,\mathrm{D}}) \cdot \underbrace{0.25}_{\Delta t^{1,0}}, && \text{(6.7a)} \\
E^{2,0}_{\mathrm{ESS}i} &= E^{1,0}_{\mathrm{ESS}i} + (0.95 P^{2,0}_{\mathrm{ESS}i,\mathrm{C}} - 0.95^{-1} P^{2,0}_{\mathrm{ESS}i,\mathrm{D}}) \cdot 0.25, && \text{(6.7b)} \\
&\vdots & & \\
E^{16,0}_{\mathrm{ESS}i} &= E^{15,0}_{\mathrm{ESS}i} + (0.95 P^{16,0}_{\mathrm{ESS}i,\mathrm{C}} - 0.95^{-1} P^{16,0}_{\mathrm{ESS}i,\mathrm{D}}) \cdot 0.25, && \text{(6.7c)} \\
E^{17,0}_{\mathrm{ESS}i} &= E^{16,0}_{\mathrm{ESS}i} + (0.95 P^{17,0}_{\mathrm{ESS}i,\mathrm{C}} - 0.95^{-1} P^{17,0}_{\mathrm{ESS}i,\mathrm{D}}) \cdot 1, && \text{(6.7d)} \\
&\vdots & & \\
E^{24,0}_{\mathrm{ESS}i} &= E^{23,0}_{\mathrm{ESS}i} + (0.95 P^{24,0}_{\mathrm{ESS}i,\mathrm{C}} - 0.95^{-1} P^{24,0}_{\mathrm{ESS}i,\mathrm{D}}) \cdot 1, && \text{(6.7e)} \\
E^{25,0}_{\mathrm{ESS}i} &= E^{24,0}_{\mathrm{ESS}i} + (0.95 P^{25,0}_{\mathrm{ESS}i,\mathrm{C}} - 0.95^{-1} P^{25,0}_{\mathrm{ESS}i,\mathrm{D}}) \cdot 4, && \text{(6.7f)} \\
&\vdots & & \\
E^{27,0}_{\mathrm{ESS}i} &= E^{26,0}_{\mathrm{ESS}i} + (0.95 P^{27,0}_{\mathrm{ESS}i,\mathrm{C}} - 0.95^{-1} P^{27,0}_{\mathrm{ESS}i,\mathrm{D}}) \cdot 4, && \text{(6.7g)} \\
\forall i \in & \{1,2\} \Bigg\}.
\end{aligned}
$$

Note that $\Delta t^{t,0}$ varies between 0.25 and 4 due to the variable step sizes in receding horizon control. Furthermore, we assume an initially stored energy of 100 MWh, i.e. 1 pu, see (6.7a).

In Fig. 6.3a, we observe that wind power cannot fully be integrated between hours 5 to 15. This is due to fully exploited transmission capacities on both AC and DC network. Figure 6.3b shows that both constrained lines are fully loaded between hours 3 to 15. Meanwhile, it can be seen in Fig. 6.3c that the DC system is utilized to relieve the AC side as far as possible by transporting 200 MW from *VSC 3* to *VSC 2*. Energy storage dispatch is shown in Fig. 6.4b. During the first two hours, network constraints allow for a discharge of *ESS 2* to free some energy capacity for the anticipated wind peak. Notably, *ESS 2* is subsequently not charged at full power but rather shares its free energy capacity over hours 5 to 15, which leads to a grid-friendly peak-shaving of the wind power. On the other hand, *ESS 1* cannot absorb wind power due to the already fully loaded network.

On the second day, PV power is fully integrated. It is located in a network area with a large demand and thus does not need to be transported over the constrained lines. Nevertheless, it can be observed that the storages are actively discharged beforehand of the expected PV peak in order to absorb maximal possible PV

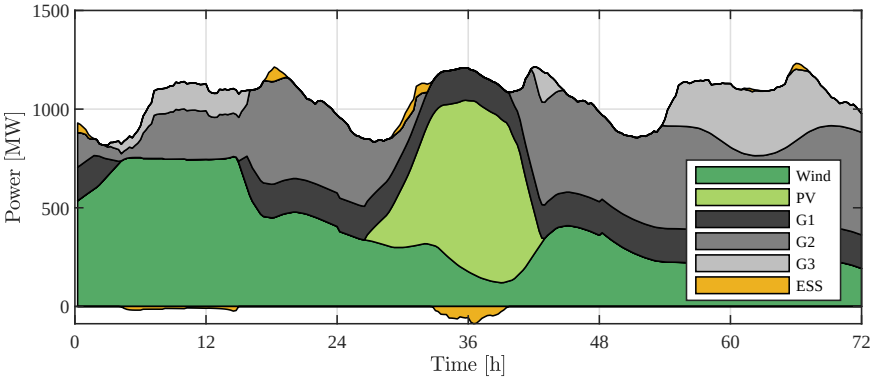

(a) Accumulated generator, RES and ESS dispatch.

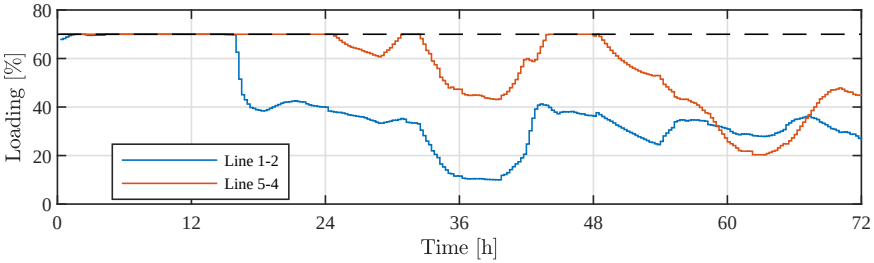

(b) Loading of the two constrained lines, where the limit is set to 70% during dispatch.

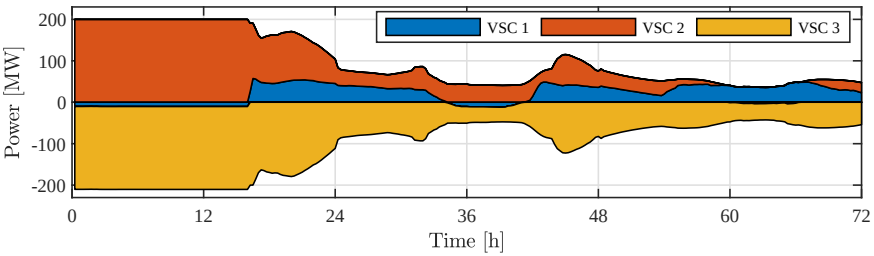

(c) Accumulated VSC power from DC to AC (positive value) and AC to DC (negative value).

Figure 6.3: D-OPF results in the 5-bus AC-DC system.

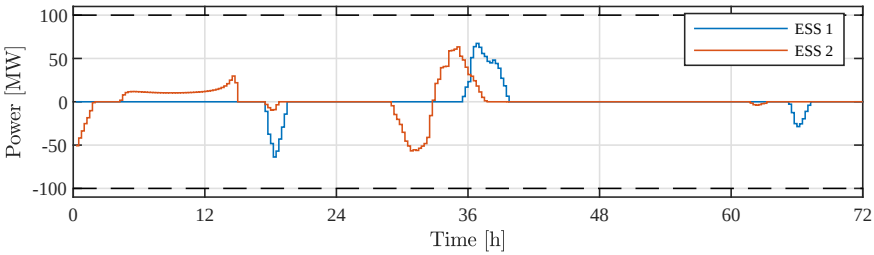

(a) Storage power. Positive value: charging, negative value: discharging.

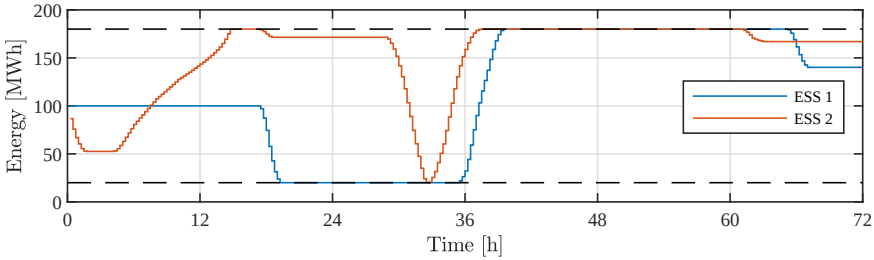

(b) Storage energy.

Figure 6.4: D-OPF results for energy storage in the 5-bus AC-DC system.

energy. This effect stems from fuel cost minimization. Instead of entirely ramping down the cheap conventional generator *G1*, an energy shift via the storage is used to replace more expensive generators at a later point in time. Lastly, due to the local consumption of PV power, the DC system is only marginally loaded during the PV peak and serves to minimize losses.

6.2.2 Redispatch with SC-D-OPF

An operational security analysis of a TSO will most importantly require N-1 security. Therefore, we extend the study by including the same outage as in Chapter 5.1.2, namely *Line 1-2*. Receding horizon control settings remain $RHC = [(4, 0.25), (8, 1), (12, 4)@2]$ and we have $(T_{\text{N-1}}, T) = (27, 27)$ per optimization, which leads to N-1 security for each time step. Recall from Chapter 3.4 that an SC-D-OPF with one contingency and T time steps is expressed with

$$\underset{x^{1,0},x^{1,1},\dots,x^{T,0},x^{T,1}}{\text{minimize}} \quad \sum_{t=1}^{T} \mathit{Costs}^{t,0}(x^{t,0}) + \sum_{t=1}^{T} p^{t,1} \cdot \mathit{Costs}^{t,1}(x^{t,1}) \tag{6.8a}$$

$$\text{subject to} \quad \mathit{Basics}^{1,0}(x^{1,0}) \tag{6.8b}$$

$$\mathit{Basics}^{1,1}(x^{1,1}) \tag{6.8c}$$

$$\mathit{N\text{-}1\ Coupling}^{1}(x^{1,0}, x^{1,1}) \tag{6.8d}$$

$$\vdots$$

$$\mathit{Basics}^{T,0}(x^{T,0}) \tag{6.8e}$$

$$\mathit{Basics}^{T,1}(x^{T,1}) \tag{6.8f}$$

$$\mathit{N\text{-}1\ Coupling}^{T}(x^{T,0}, x^{T,1}) \tag{6.8g}$$

$$\mathit{Dynamics}(x^{1,0}, .., x^{T,0}). \tag{6.8h}$$

The focus lies on the effects of 3 different ESS operation modes described in Chapter 4.2. Therefore, we use *Preventive-DC* throughout this subsection in order not to compound different effects. Independently from storage operation

mode, the following coupling constraints are added for each time step t:

$$
\begin{aligned}
&\textit{N-1 Coupling}^t(x^{t,0}, x^{t,1}) \equiv \Bigg\{ \\
&E^{t,1}_{\mathrm{ESS1}} = \underbrace{E^{t,0}_{\mathrm{ESS1}} - (1-\xi)(0.95 P^{t,0}_{\mathrm{ESS1,C}} - 0.95^{-1} P^{t,0}_{\mathrm{ESS1,D}}) \cdot \Delta^{t,0}}_{\overset{\xi=0}{=} E^{t-1,0}_{\mathrm{ESS1}}} \\
&\qquad\qquad + (0.95 P^{t,1}_{\mathrm{ESS2,C}} - 0.95^{-1} P^{t,1}_{\mathrm{ESS2,D}}) \cdot 0.5, && \text{(6.9a)} \\
&E^{t,1}_{\mathrm{ESS2}} = E^{t,0}_{\mathrm{ESS2}} - (0.95 P^{t,0}_{\mathrm{ESS2,C}} - 0.95^{-1} P^{t,0}_{\mathrm{ESS2,D}}) \cdot \Delta^{t,0} \\
&\qquad\qquad + (0.95 P^{t,1}_{\mathrm{ESS2,C}} - 0.95^{-1} P^{t,1}_{\mathrm{ESS2,D}}) \cdot 0.5, && \text{(6.9b)} \\
&-0.017 \leq (P^{t,0}_{\mathrm{G1,Up}} - P^{t,0}_{\mathrm{G1,Down}}) - (P^{t,1}_{\mathrm{G1,Up}} - P^{t,1}_{\mathrm{G1,Down}}) \leq 0.017, && \text{(6.9c)} \\
&\qquad\vdots \\
&-0.06 \leq (P^{t,0}_{\mathrm{G4,Up}} - P^{t,0}_{\mathrm{G4,Down}}) - (P^{t,1}_{\mathrm{G4,Up}} - P^{t,1}_{\mathrm{G4,Down}}) \leq 0.06, && \text{(6.9d)} \\
&0 \leq P^{t,0}_{\mathrm{VSC}i} - P^{t,1}_{\mathrm{VSC}i} \leq 0, \quad \forall i \in \{1,2,3\} \Bigg\}. && \text{(6.9e)}
\end{aligned}
$$

Here, (6.9a) and (6.9b) define the new energy states 0.5 hours after the contingency has occurred. We assume $\xi = 0$, which means that a contingency occurs at the beginning of a time step. Equations (6.9c)-(6.9d) describe the generator coupling ($\pm 1\,\%$ of installed capacity), and (6.9e) imposes preventive control on the HVDC system. Additional coupling constraints which depend on storage operation are presented in the course of the following studies.

Storage Operation

The differing storage operation depending on the control mode can be examined in Fig. 6.5 and Fig. 6.6. In Fig. 6.5, the stored energy in the base case is displayed. In Fig. 6.6, curative power set points are compared. Note that after the occurrence of an outage, the remaining optimal trajectory lacks N-1 security. We assume that a new optimization would be started with the new topology to bring the system back to an N-1 secure state. Therefore, an empty or full storage after a *hypothetical* outage does not affect the optimal normal operation in a consecutive time step, since we consider this time step only as a valid solution if the outage has *not* occurred. Post-outage set points in consecutive time steps should not be interpreted as a trajectory, but rather (practically) independent from each other.

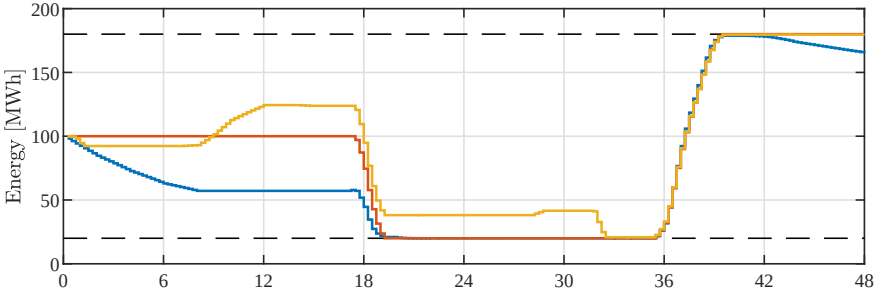

(a) Base case energy of *ESS 1*.

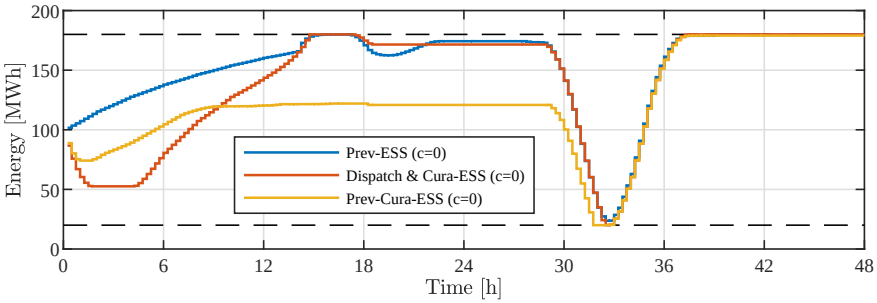

(b) Base case energy of *ESS 2*.

Figure 6.5: Storage energy levels with different control modes before ($c = 0$) the outage of *Line 1-2*.

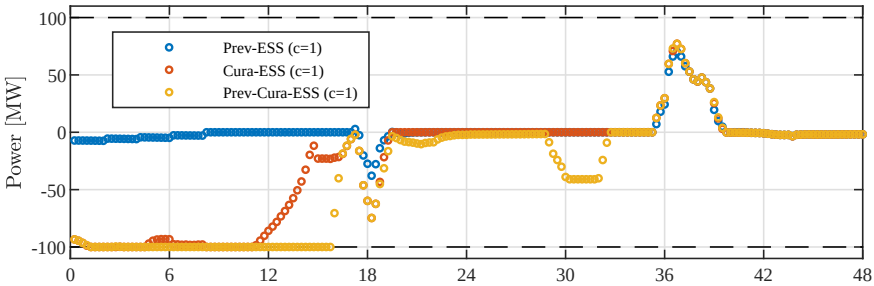

(a) Curative power set points *ESS 1*.

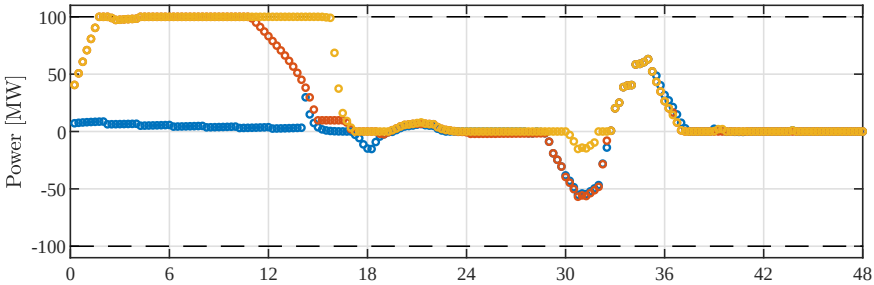

(b) Curative power set points *ESS 2*.

Figure 6.6: Storage power reserve with different control modes after ($c = 1$) the outage of *Line 1-2*. Positive value: charging, negative value: discharging.

- **Preventive-ESS**: the base case set points of the storage are controllable only. However, the state of charge must guarantee non-violated capacity limits after an outage, where the storage continues charging/discharging with the same set point. We have additional N-1 coupling constraints for each storage i and time step t:

$$0 \leq P^{t,0}_{\mathrm{ESS}i,\mathrm{C}} - P^{t,1}_{\mathrm{ESS}i,\mathrm{C}} \leq 0 \tag{6.10a}$$

$$0 \leq P^{t,0}_{\mathrm{ESS}i,\mathrm{D}} - P^{t,1}_{\mathrm{ESS}i,\mathrm{D}} \leq 0. \tag{6.10b}$$

  If a certain power is requested after a possible failure, the storage must adapt the set point already in the base case. Due to the limited energy capacity, this would quickly lead to full or empty storages. Subsequently, the ESSs are barely utilized during the critical first 18 hours. Both *ESS 1* and *ESS 2* are discharged and charged, respectively, over a longer time span at lower power than foreseen by the dispatch (Fig. 6.5). Later, when network stress is uncritical and no N-1 reserve is required, they participate in an energy shift of the cheap PV power. With no notable limitation, they use their full capacity to absorb as much PV energy as possible, see Fig. 6.5a hours 36 to 42 and Fig. 6.5b hours 32 to 38.

- **Curative-ESS:** each storage i has a fixed base case set point for each time step t from a previously determined dispatch ("*fix*"):

$$P^{t,0}_{\mathrm{ESS}i,\mathrm{C,fix}} \leq P^{t,0}_{\mathrm{ESS}i,\mathrm{C}} \leq P^{t,0}_{\mathrm{ESS}i,\mathrm{C,fix}} \tag{6.11a}$$

$$P^{t,0}_{\mathrm{ESS}i,\mathrm{D,fix}} \leq P^{t,0}_{\mathrm{ESS}i,\mathrm{D}} \leq P^{t,0}_{\mathrm{ESS}i,\mathrm{D,fix}}. \tag{6.11b}$$

  However, it is possible to react to an outage with a set point adaption if the state of charge allows it:

$$-\infty \leq P^{t,0}_{\mathrm{ESS}i,\mathrm{C}} - P^{t,1}_{\mathrm{ESS}i,\mathrm{C}} \leq \infty \tag{6.12a}$$

$$-\infty \leq P^{t,0}_{\mathrm{ESS}i,\mathrm{D}} - P^{t,1}_{\mathrm{ESS}i,\mathrm{D}} \leq \infty. \tag{6.12b}$$

  Increased flexibility is used to large extents during the first 15 hours. Located "ahead" of the contingency, *ESS 2* can be charged after the outage (see Fig. 6.6b) which means, from a grid perspective, the provision of negative power reserve. On the other hand, located "behind" the contingency, *ESS 1* can be discharged after the outage and provide positive power reserve, see Fig. 6.6a. This imitation of generator redispatch is only possible as long as the ESSs dispose over sufficient *energy* reserve. Between hour 4 and 15, *ESS 2* is charged during normal operation and comes closer to the upper energy limit, see Fig. 6.5b. Starting from hour 11, the energy reserve is so small that it reflects in a reduced post-outage power reserve in Fig. 6.6b, which vanishes completely in hour 15.

- **Preventive-Curative-ESS:** set points of storage i before *and* after an outage are optimized for each time step t:

$$-\infty \leq P^{t,0}_{\mathrm{ESS}i,\mathrm{C}} - P^{t,1}_{\mathrm{ESS}i,\mathrm{C}} \leq \infty \tag{6.13a}$$
$$-\infty \leq P^{t,0}_{\mathrm{ESS}i,\mathrm{D}} - P^{t,1}_{\mathrm{ESS}i,\mathrm{D}} \leq \infty. \tag{6.13b}$$

  Storages can be driven preventively towards energy states which allow for maximal power reserve at times where contingencies are expected to have the largest impact. In our case study, this can be observed during hours 11 to 18. While energy constraints on *ESS 2* prohibit full power reserve with *Curative-ESS* after hour 11, a security margin is observed with *Preventive-Curative-ESS*. That is, the base case energy level remains far below the upper energy limit, see Fig. 6.5b. This preventively maintains full power reserve after a possible outage and appears most desirable to avoid generator redispatch.

Preventive Generator and Storage Redispatch

In Fig. 6.7, accumulated generator and storage redispatch in the base case is compared for the ESS operation modes. With *Preventive-ESS* (see Fig. 6.7a), redispatch of about ±100 MW is necessary on both sides of the bottleneck during the first hours, since the identical power set points must be valid in case of reduced transmission capacity when *Line 1-2* fails. As stated above, the storages cannot hold up the necessary positive and negative power reserve for a time span of 15 hours due to the limited capacity. Subsequently, the largest portions of redispatch stem from wind power curtailment and an according power increase from generator *G2*.

With *Curative-ESS*, wind curtailment is avoided in large parts for the first 11 hours since power reserve by the storage is accessible in the case of an outage, see Fig. 6.7b. Then, however, the energy reserve of *ESS 2* vanishes and the network area ahead of the bottleneck must be relieved by triggering generator redispatch of about ±100 MW.

The largest storage flexibility is available with *Preventive-Curative-ESS*. Owing to preventive control, curative ESS power reserve is sufficient at all times to cope with a contingency. Subsequently, generator redispatch becomes negligible, see Fig. 6.7c. Note that between hours 28 and 33, storages are redispatched again in the opposite direction to correct the energy level and, as planned by the dispatch, have the full capacity available to absorb energy from PV production.

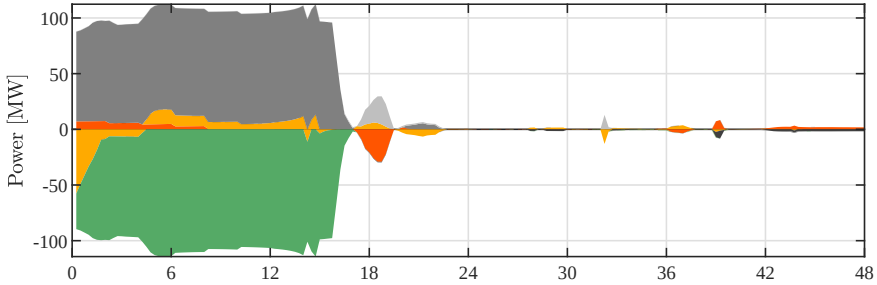

(a) Preventive-ESS. Generator redispatch of +1587/-1607 MWh.

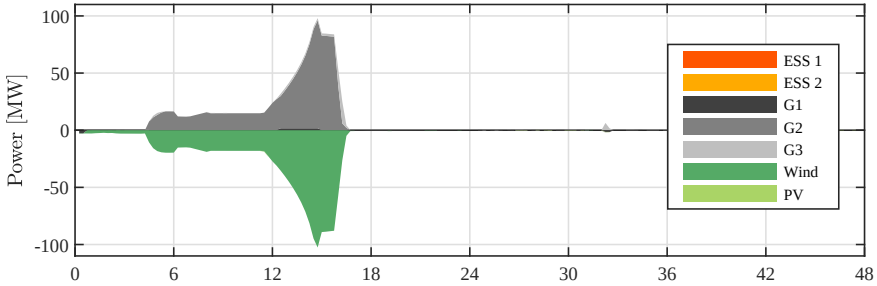

(b) Curative-ESS. Generator redispatch of +397/-402 MWh.

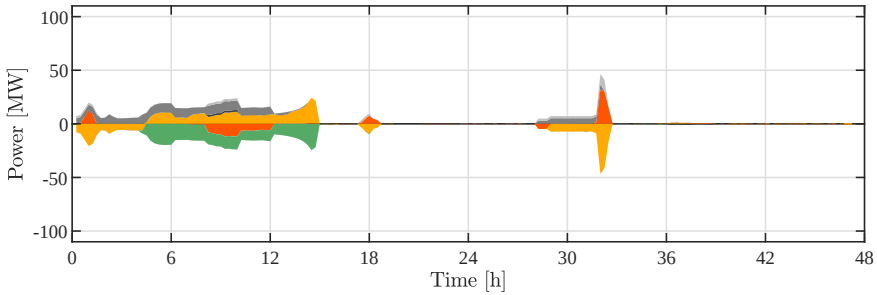

(c) Preventive-Curative-ESS. Generator redispatch of +134/-147 MWh.

Figure 6.7: Accumulated positive and negative preventive redispatch in the base case with different storage control modes.

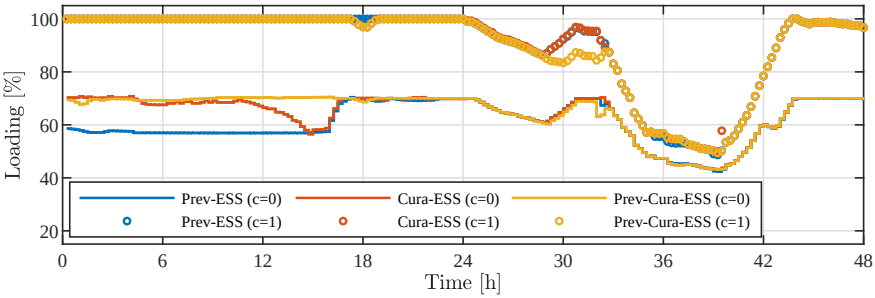

Figure 6.8: Loading of *Line 4-5* with different storage control modes before ($c = 0$) and after ($c = 1$) the outage of *Line 1-2*.

Line Loading

In Fig. 6.8, the loading of *Line 4-5* is depicted. The solid lines represent base case load, i.e. before an outage, and the loading after a contingency is indicated with markers 'o'. In the first 24 hours, the capacity of *Line 4-5* is fully exploited after an outage of *Line 1-2*, independently from the ESS control mode. In the base case, however, different security margins are notable. With *Preventive-ESS*, it is reserved over 40 % of line capacity for the possible outage. Introducing more storage flexibility, the allowed line loading is increased to over 70%. The security margins stem from a generator and storage redispatch, which relieves the line. Consequently, the points in time where the line load deviates among the control modes are the same points in time where preventive redispatch deviates among the control modes, see Fig. 6.7.

6.3 67-Bus System

We use the test system from Chapter 5.2 with *DC-Stage 1*. It is extended by 8 energy storage systems with characteristics from Table B.9. We connect 4 ESSs in *Region 1*, 3 ESSs in *Region 2*, and 1 ESS in *Region 3*. Furthermore, 4 additional wind parks are connected in *Region 1* and *2*. The enhanced topology is shown in Fig. 6.9. Again, forecast is provided by adapted profiles from the Belgian transmission system operator *Elia*. Original profiles are shown in Fig. C.1 and Fig. C.4; adapted profiles for usage in this case study are shown in Fig. C.3 and Fig. C.6. AC line flow limits are set to 2279 A, which equals 1500 MVA at 380 kV, and VSCs are limited to 1200 MVA.

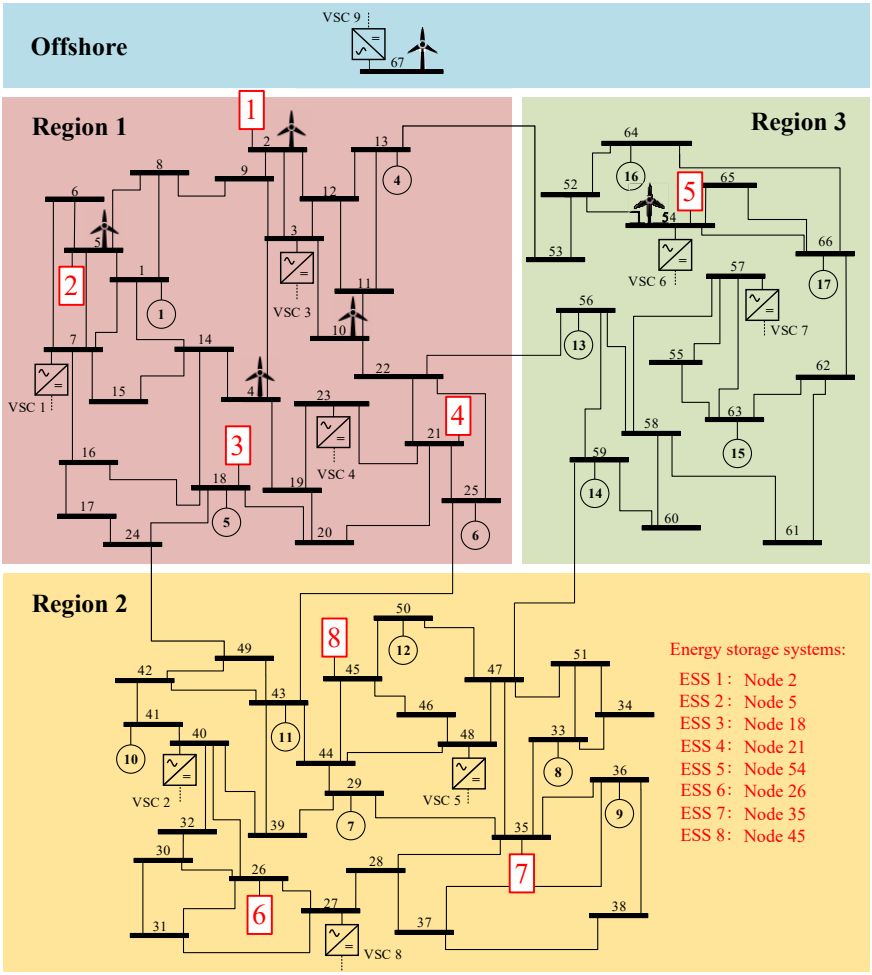

Figure 6.9: AC-Topology of 67-bus test system with 8 additional energy storage systems and 3 additional wind farms. Storage parameters from Table B.9.

6.3.1 Dispatch with D-OPF

A D-OPF with $RHC = [(4, 0.25), (8, 1), (12, 4)@2]$ and $(T_{\text{N-1}}, T) = (0, 27)$ is performed without line flow limits to obtain dispatch set points. We introduce generator ramping limits, such that each generator is able to change its power output at a rate of 100 % per hour. For example, for generator *G4* with an installed power of 887 MW, we add the constraints

$$-8.87 \cdot 0.25 \leq P_{\text{G4}}^{2,0} - P_{\text{G4}}^{1,0} \leq 8.87 \cdot 0.25 \tag{6.14a}$$

$$\vdots$$

$$-8.87 \cdot 1 \leq P_{\text{G4}}^{17,0} - P_{\text{G4}}^{16,0} \leq 8.87 \cdot 1 \tag{6.14b}$$

$$\vdots$$

$$-8.87 \cdot 4 \leq P_{\text{G4}}^{27,0} - P_{\text{G4}}^{26,0} \leq 8.87 \cdot 4. \tag{6.14c}$$

Generator, wind and summarized storage dispatch is shown in Fig. 6.10. Wind power sums up to a considerable portion of energy supply in the first 15 hours and, due to the price difference between regions, the remaining power is mainly produced in *Region 1* and *3*. Storage is charged either during the wind peak or during times of low demand in order to shift energy towards times of peak demand. The storage dispatch is shown in more detail in Fig. 6.11a, where it can be seen that the full accumulated energy capacity (dashed lines) is exploited. Furthermore, accumulated VSC power set points are shown in Fig. 6.11b. Up to 3.6 GW of power are collected in *Region 1* (grey) and *Region 3* (orange) in order to be transferred towards *Region 2* (green).

6.3.2 Redispatch with SC-D-OPF

Chapter 5.2.2 shows that a shrunk contingency list can be sufficient for N-1 security. Therefore, we use the reduced AC contingency set with $\mathcal{C} = \{3, 7, 8\}$. Furthermore, outages are included for the first 16 time steps of highest resolution only, leading to $(T_{\text{N-1}}, T) = (16, 27)$ per optimization. Settings for receding horizon control remain $RHC = [(4, 0.25), (8, 1), (12, 4)@2]$. In the previous sections, the effects of VSC and ESS control were investigated in detail. For the following case, a comparison of all possible combinations between different VSC and ESS control modes would go beyond the scope of this thesis. Instead, we highlight a reasonable selection by using *Preventive-Curative-DC* and a comparison between *Curative-ESS* and *Preventive-Curative-ESS*.

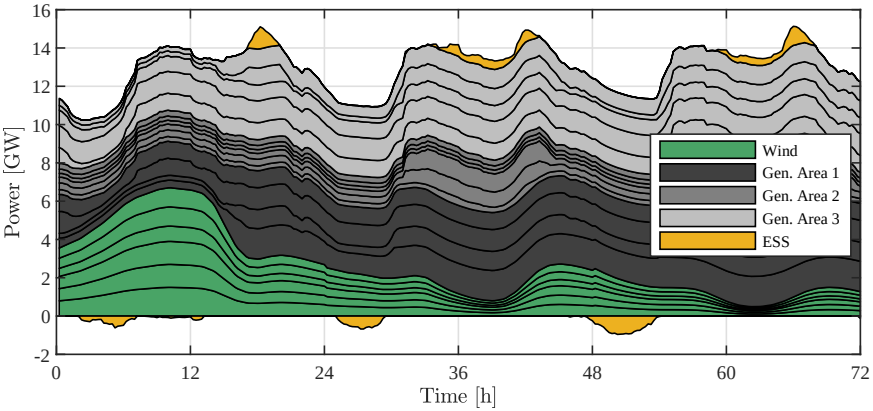

Figure 6.10: Accumulated generator, RES and ESS dispatch in the 67-bus system with D-OPF.

Storage operation

Storage energy levels during the base case are shown in Fig. 6.12a. It is notable that energy fluctuations are lower compared to the dispatch and that upper or lower limits are never met. These security margins lead to available N-1 reserves whenever necessary.

Curative storage actions after the occurrence of contingency $\#8^{\mathrm{AC}}$ are shown in Fig. 6.12b. Here, positive and negative power adaption from the base case to the contingency case is depicted. From grid-perspective, a positive value denotes an increase in power generation. As expected, ESSs in *Region 2* generate power in order to compensate for the lost transmission line. Storages in *Region 1* and *3* maintain power balance with an adequate negative power adaption, such as increased charging. Note that the power adaption of a 300 MW-storage can reach up to 600 MW, if it switches for example from charging in the base case to discharging after the outage.

Preventive Redispatch *Cura-ESS* vs. *Prev-Cura-ESS*

The preventive base case redispatch for generators and storages is shown in Fig. 6.13, where both generators and ESSs are clustered per area. With *Curative-ESS* (Fig. 6.13a), power production of up to 2 GW is shifted from generators in *Region 1* and *3* to generators in *Region 2*. This meets the expectation that *Region 2*, which is a load center with a power deficit, must ramp up generation if power supply over tie lines is endangered. With *Preventive-Curative-ESS*, storages

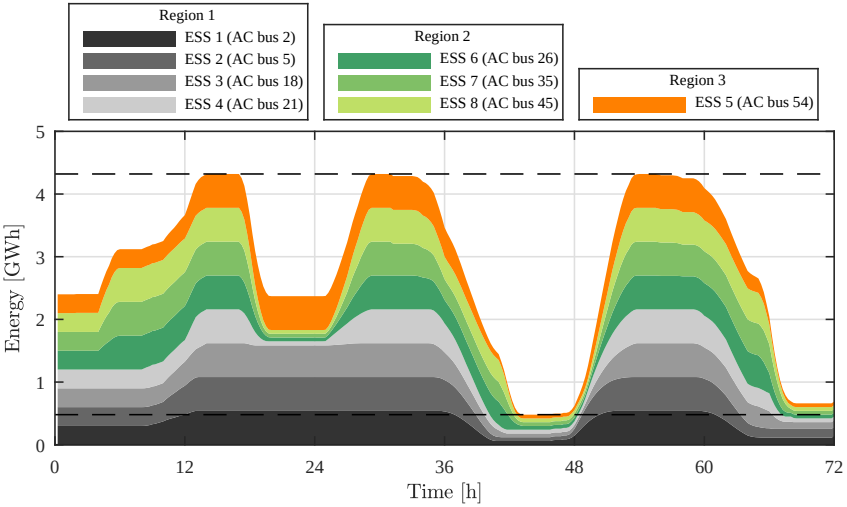

(a) Accumulated storage energy.

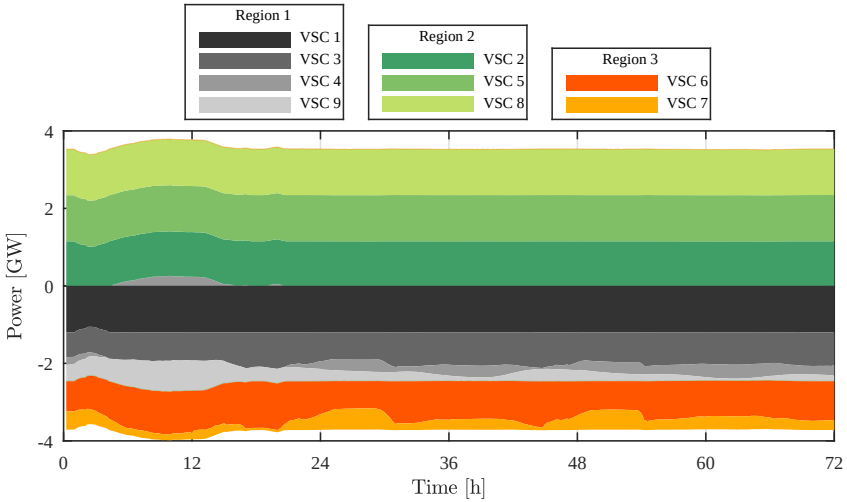

(b) Accumulated VSC set points. Positive value: power transfer from DC to AC.

Figure 6.11: Dispatch of VSCs and ESSs in the 67-bus system with D-OPF.

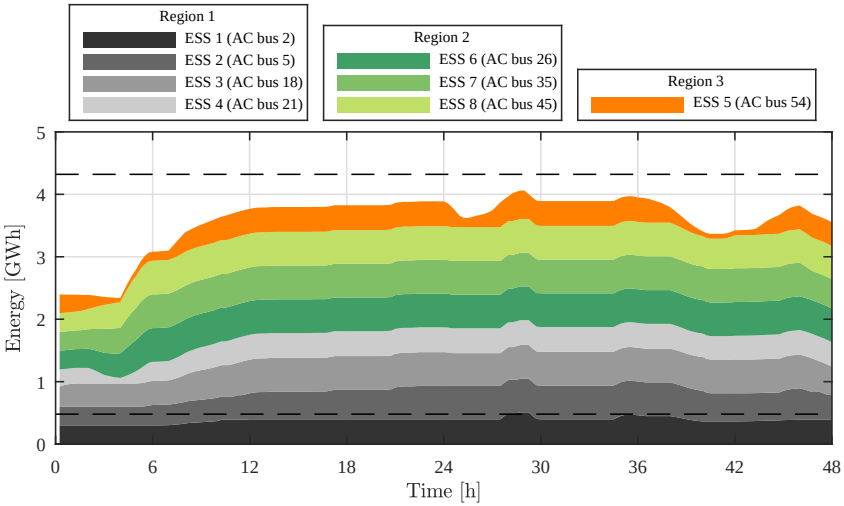

(a) Accumulated base case storage energy. Conservative operation compared to dispatch in order to maintain N-1 reserves.

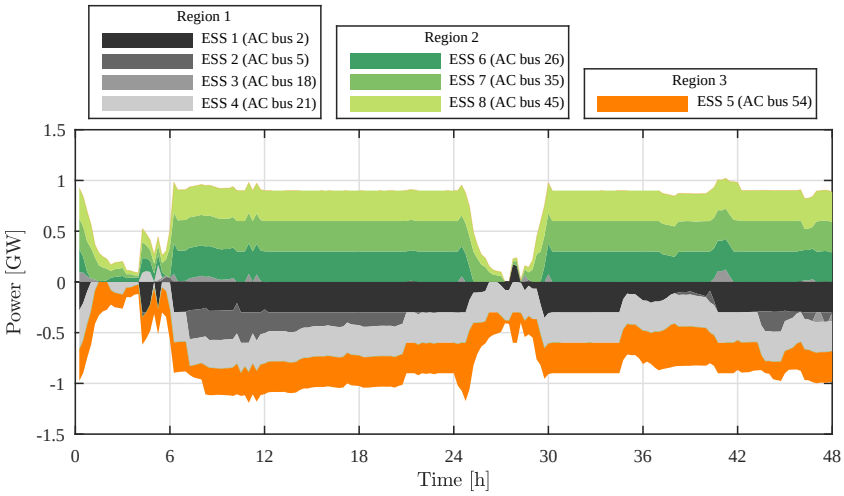

(b) Curative storage actions after contingency $\#8^{\mathrm{AC}}$. Positive value: increased power generation (from grid-perspective).

Figure 6.12: Storage operation in the 67-bus system with SC-D-OPF and *Preventive-Curative-ESS*.

are preventively kept in energy states which maintain the power reserve in case of a contingency. For example, between hours 12-15 and 32-36, storages are dispatched at almost full capacity. Therefore, with *Curative-ESS*, the reserve is small. During those hours, generator redispatch is reduced with *Preventive-Curative-ESS*, since storages are not fully charged in the base case and consequently provide a larger N-1 reserve. Although the 2 GW-peak around hour 18 cannot be avoided, the total positive redispatch is reduced from 47.4 GWh to 33.5 GWh (-29 %) over 48 hours.

Preventive Generator Redispatch

To understand the significance of the results, we compare the total required preventive generator redispatch with the potential worst and best case:

- ***No-ESS*:** No storage is connected in the grid at all. Dispatch and Redispatch are performed entirely without storage.
- ***Reserve-ESS*:** We use storage exclusively for N-1 curative actions. Therefore, dispatch and preventive redispatch are performed without storage. After the outage, each storage is assumed at 50 % state of charge and available for positive or negative power reserve.

Clearly, with a total amount of 129.4 GWh, the largest redispatch is required with no storage at all, see Fig. 6.14. On the contrary, the least redispatch (50.7 GWh) is achieved when storage is used exclusively for N-1 security. In that case, however, storages cannot be used at all during normal operation for an economic RES integration – they stand still for the whole time of normal operation without failure. It is notable, that with *Preventive-Curative-ESS*, the generator redispatch is only marginally larger (55.2 GWh). Thus, the N-1 benefit of the storage can almost fully be exploited, but storage is available to optimization during normal operation as well. In this case study, the cost of conventional generator dispatch during the first 48 hours comes to 16.68 M€ with storage (in average 26.8 €/MWh), and 17.14 M€ without storage (in average 27.5 €/MWh, in total +455,000 €). If the storage is available for an economic dispatch and N-1 curative actions, but not accessible for preventive redispatch (*Curative-ESS*), generator redispatch is substantially larger again (86.8 GWh).

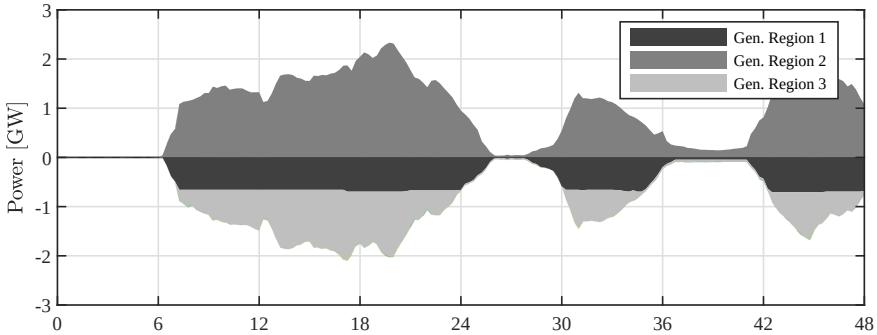

(a) *Curative-ESS*: no preventive actions by storage. Generator redispatch of +47.4/-40.3 GWh.

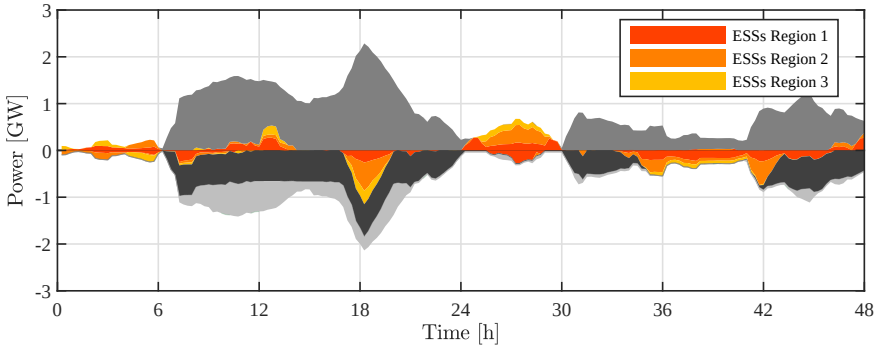

(b) *Preventive-Curative-ESS*: portions of generator redispatch are avoided or replaced by storage. Generator redispatch of +33.5/-21.8 GWh.

Figure 6.13: Preventive generator and storage redispatch for different storage control modes in the 67-bus system with SC-D-OPF. Generator and storage power is accumulated per area.

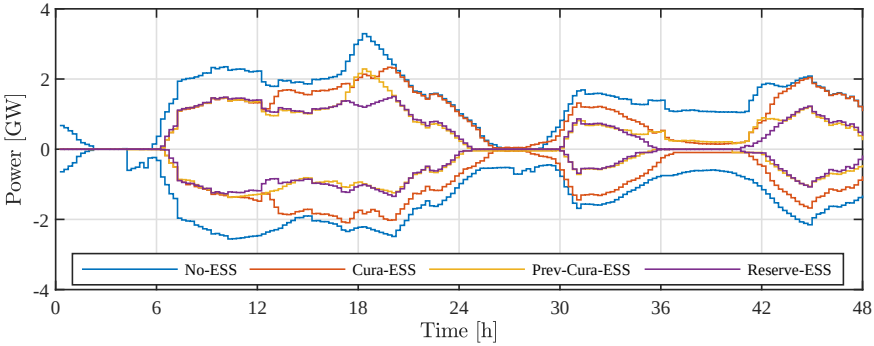

Figure 6.14: Total preventive generator redispatch in GWh: *No-ESS*: 129.4, *Cura-ESS*: 86.8, *Prev-Cura-ESS*: 55.2, *Reserve-ESS*: 50.7.

6.4 Summary

The case studies show that energy storage systems can reduce preventive generator redispatch. However, the operating mode is crucial.

- ***Preventive-ESS*** — as expected, only operating preventively has very little effect on post-contingency security. If power reserve is required over long periods of time, the storage is incapable of maintaining the power set point during normal operation due to energy limitations.
- ***Curative-ESS*** — this mode has the advantage, that no dynamic optimization over a forecast horizon is necessary; the curative set point is solely dependent on the actual load flow situation. However, that means the base case storage dispatch is controlled without knowledge of possible reserve needs and as a consequence, the storage might be unable to activate a needed reserve because it is full or empty.
- ***Preventive-Curative-ESS*** — this mode leads to the largest reduction of preventive generator redispatch. The storage systems are predictively driven into energy states which suffice post-contingency reserve needs. This leads to a more conservative base case storage operation when the network is stressed to hold up energy security margins. But, at times of no urgency for reserves, the storage capacity can be exploited to foster an economic RES integration. Preventive generator redispatch is reduced to an amount close to the minimum, which would be required if storage were installed exclusively for curative actions.

Chapter 7

Coordinated Multi-Area Optimization

Due to the increasing complexity of the power system and an operation closer to network limitations, central coordination in large scale networks comes with major computational burdens. Moreover, privacy, e.g. for each transmission system operator (TSO) controlling a certain region, is a concern. Subsequently, the interest in distributed optimization, also referred to as multi-area optimization, has substantially grown in recent years.

Parts of this chapter have been published in [93].

7.1 Literature Review

An early overview of distributed OPF algorithms can be found in [52] and the most recent developments are examined in detail in [61]. The most popular branches to tackle the non-convex AC OPF problem are Optimality Condition Decomposition (OCD) [19, 46, 69], Auxiliary Problem Principle (APP) [51, 5] and Alternating Direction of Multipliers Method (ADMM) [8, 32, 33, 44]. In OCD technique, primal and dual variables are assigned to a specific sub-problem. Each sub-problem then includes certain constraints which also involve variables from a foreign sub-problem. Those foreign variables are treated as constants, defined by the related neighbor after the previous iteration. By penalizing the coupling variables in the objective, convergence is achieved under certain assumptions (e.g. relatively weakly coupled sub-problems). Those assumptions cannot be guaranteed for any problem, however, the method is shown to work for certain networks up to a few hundred buses [69]. In contrast to OCD, in APP and ADMM each sub-problem uses variable duplicates from neighboring sub-problems and is solved to optimality. They are based on Augmented Lagrangian Relaxation, where penalty terms, calculated from the coupling variable deviation and their Lagrangian multipliers,

are added to the objective function. The improvement from APP to ADMM is a sequential update on internal and external variables, which reduces necessary information exchange and leads to communication between neighboring regions only. Convergence is achieved in a large-scale network [44], but again, convergence guarantees cannot be given for non-convex problems.

Most recently, further development of ADMM is presented in [45], which is called Augmented Lagrangian based Alternating Direction Inexact Newton (ALADIN) method. The agents solve similar local problems compared to ADMM, but it includes elements from the field of sequential quadratic programming to improve the central update step. Convergence rate is much faster than in ADMM and it can be extended using globalization strategies which guarantee convergence. ALADIN is applied to the conventional OPF problem in [25, 24] and shows an impressive improvement in terms of convergence speed and optimality gap. However, the communication is increased and as of now, the centralized update cannot yet be entirely distributed.

In [47], an AC-DC OPF is calculated in a distributed manner. However, the AC system is approximated with a linear DC approach, which is much easier in terms of local optimization as well as network decomposition and consensus between areas. Additionally, converter losses are neglected, which further simplifies the decoupling between AC and DC regions.

To the best of our knowledge, there have been no attempts to solve a multi-area SC-D-OPF.

7.2 Network Decomposition in AC-DC Grids

To allow for distributed algorithms, the optimization problem must be formulated in a separable way. Therefore, network partitioning and model decomposition methods are explained in detail, followed by a re-formulation of the original problem.

7.2.1 Network Partitioning

Network partitioning can be crucial for distributed algorithms to achieve good performance. That is why there exist methods to optimally divide networks into regions based on e.g. electrical distance [21], minimized number of tie lines [34] or spectral clustering [43]. However, we believe that network partitions are inherently given by structural responsibilities. For example, a region or control area could represent one TSO, multiple TSOs or a whole country. Thus, the number and dimension of AC regions are historically known. However, responsibilities in overlaying DC networks are yet to be defined. So far, existing DC links are subject to bilateral agreements if connecting different control areas. It is not clear how

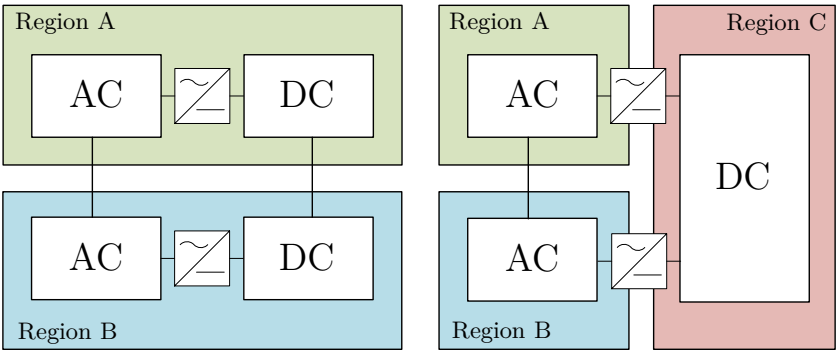

(a) *Shared-DC* approach: hybrid AC-DC regions are formed.

(b) *Joint-DC* approach: regions only contain either AC or DC nodes.

Figure 7.1: Network partitioning approaches in AC-DC networks.

authority is shared if multiple areas are involved in a truly meshed overlaying DC grid. Therefore, we identify two different approaches, which are explained in the following.

Let R non-overlapping regions be defined in $\mathcal{R} = \{1, ..., R\}$, and let $\mathcal{N}_k$ identify all nodes in *Region k*. Herewith, $\mathcal{N}_k^{\mathrm{AC}}$ collects all AC nodes and $\mathcal{N}_k^{\mathrm{DC}}$ all DC nodes in *Region k*. If there exist DC nodes ($\mathcal{N}^{\mathrm{DC}} \neq \emptyset$), we have the choice between two partitioning possibilities:

- ***Shared-DC***: We define $R = R^{\mathrm{AC}}$ hybrid AC-DC regions, where each AC region may also contain DC nodes. Thus, each existing TSO gains control over converters in its own control area, see Fig. 7.1a.
- ***Joint-DC***: We define R^{AC} regions containing only AC nodes and R^{DC} regions containing only DC nodes, leading to a total of $R = R^{\mathrm{AC}} + R^{\mathrm{DC}}$ regions. This approach follows the idea that there exist one or multiple independent entities which coordinate a pure DC network, see Fig. 7.1b.

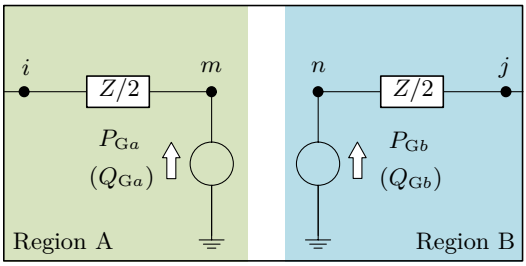

Figure 7.2: Decoupling model of a tie line (AC or DC) between nodes i and j. The line is opened in the middle; two auxiliary nodes (m and n) and two auxiliary generators (a and b) are connected to the open ends. Reactive power source Q_G is only added for an AC tie line.

7.2.2 Decoupling of Inter-Regional Connectors

The decoupling between two neighboring regions depends on the element which serves as inter-connector. In general, we distinguish between tie lines and converters. Let an inter-connector between nodes $i \in \mathcal{N}_A$ and $j \in \mathcal{N}_B$ link *Region A* and *Region B*. Depending on the region types (AC, DC or AC-DC) and the chosen DC decoupling approach, this could be an AC line, a DC line or an AC-DC VSC.

AC or DC Tie Line

In [51], the decomposition method for an AC tie line using dummy generators is described. Later, [32] only uses voltages for consensus. It is not clear why the generators are omitted, but convergence rates are rather poor and the authors then improve the decomposition method by including neighboring nodes from foreign regions, resulting in overlapping areas [33]. The weighted summation and difference of those two node voltages are then used for consensus and subsequently, convergence is improved. This is also adapted in [44]. However, possibly sensitive information of a neighboring region must be shared, such as connected loads, generators or cost functions. Therefore, we choose the dummy generator method of [51] for both AC and DC tie lines, see Fig. 7.2.

The original line is cut into two halves; auxiliary nodes (m, n) and auxiliary generators (a, b) are added at both open ends. Thus, node sets are augmented to $\mathcal{N}_A \leftarrow \{\mathcal{N}_A, m\}$, $\mathcal{N}_B \leftarrow \{\mathcal{N}_B, n\}$ and the generator set is augmented to $\mathcal{E}^{\mathrm{G}} \leftarrow \{\mathcal{E}^{\mathrm{G}}, a, b\}$. To guarantee a feasible power flow, the voltage must be equal at nodes m and n. Furthermore, the generators must produce the same amount of power of the opposite sign. In the case of an AC tie line ($i \in \mathcal{N}_A^{\mathrm{AC}}, j \in \mathcal{N}_B^{\mathrm{AC}}$), this leads to boundary conditions including complex voltage and both active and reactive

power:

$$|V_{\mathrm{AC}m}| = |V_{\mathrm{AC}n}| \tag{7.1a}$$
$$\angle V_{\mathrm{AC}m} = \angle V_{\mathrm{AC}n} \tag{7.1b}$$
$$P_{\mathrm{G}a} = -P_{\mathrm{G}b} \tag{7.1c}$$
$$Q_{\mathrm{G}a} = -Q_{\mathrm{G}b}. \tag{7.1d}$$

Note that if rectangular coordinates are used for AC voltage, the implementation involves real and imaginary part instead of magnitude and angle.
In the case of a DC tie line ($i \in \mathcal{N}_A^{\mathrm{DC}}, j \in \mathcal{N}_B^{\mathrm{DC}}$), only real voltage and active power must meet the constraints:

$$V_{\mathrm{DC}m} = V_{\mathrm{DC}n} \tag{7.2a}$$
$$P_{\mathrm{G}a} = -P_{\mathrm{G}b}. \tag{7.2b}$$

AC-DC Converter

Let *VSC a* connect $i \in \mathcal{N}_A^{\mathrm{AC}}$ with $j \in \mathcal{N}_B^{\mathrm{DC}}$, which separates *Region A* from *B*. This leads to $a \in \mathcal{E}_i^{\mathrm{VSC}}, \mathcal{E}_j^{\mathrm{VSC}}$, see also Fig. 4.1. A copy of the AC power source is created and connected at the DC side. This requires a new mapping since auxiliary *VSC b* instead of *VSC a* is connected to the DC side. *VSC a* remains on the AC side. Thus, the VSC set is augmented to $\mathcal{E}^{\mathrm{VSC}} \leftarrow \{\mathcal{E}^{\mathrm{VSC}}, b\}$, and, in turn, $a \in \mathcal{E}_i^{\mathrm{VSC}}, a \notin \mathcal{E}_j^{\mathrm{VSC}}$ and $b \in \mathcal{E}_j^{\mathrm{VSC}}, b \notin \mathcal{E}_i^{\mathrm{VSC}}$. Since the power sources both point in the direction of the AC grid, power variables on both sides must be equal:

$$P_{\mathrm{VSC}a} = P_{\mathrm{VSC}b} \tag{7.3a}$$
$$Q_{\mathrm{VSC}a} = Q_{\mathrm{VSC}b}. \tag{7.3b}$$

Equation system

We write consensus constraints (7.1)-(7.3) between *Region A* and *B* in a more compact form. With $x_{\mathcal{N}_A}$ and $x_{\mathcal{N}_B}$ the augmented optimization variables of *Region A* and *Region B*, respectively, we choose coupling matrices $\tilde{A}_A, \tilde{A}_B$ such that

$$\tilde{A}_A x_{\mathcal{N}_A} + \tilde{A}_B x_{\mathcal{N}_B} = 0. \tag{7.4}$$

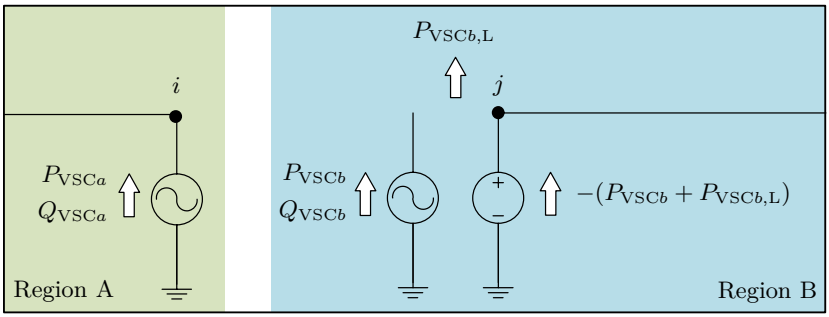

Figure 7.3: Decoupled converter model following the approach *Joint-DC*. Auxiliary AC power sources are added at the DC side to allow for an active power balance.

7.2.3 Problem Formulation

We use the central problem formulation (4.42) and adapt it to a shrunk node set $\mathcal{N}_k$ of *Region k*. We form variables, objective and constraints for *Region k* to

$$x_k \equiv \left\{ x^{t,c}_{\mathcal{N}_k},\ \forall (t,c) \in \mathcal{S} \right\} \tag{7.5a}$$

$$F_k(x_k) \equiv \sum_{(t,c)\in\mathcal{S}} p^{t,c} Costs^{t,c}_{\mathcal{N}_k}(x^{t,c}_{\mathcal{N}_k}) \tag{7.5b}$$

$$\begin{aligned} h_k(x_k) \leq 0 \equiv \Bigg\{ & Basics^{t,c}_{\mathcal{N}_k}(x^{t,c}_{\mathcal{N}_k}),\ \forall (t,c) \in \mathcal{S} \\ & N\text{-}1\ Coupling^{t}_{\mathcal{N}_k}(x^{t,0}_{\mathcal{N}_k}, .., x^{t,C}_{\mathcal{N}_k}),\ \forall t \in \mathcal{T}_{\text{N-1}} \\ & Dynamics_{\mathcal{N}_k}(x^{1,0}_{\mathcal{N}_k}, .., x^{T,0}_{\mathcal{N}_k}) \Bigg\}. \end{aligned} \tag{7.5c}$$

Note that we aggregate both equality and inequality constraints in $h_k(x_k) \leq 0$ for the sake of better readability. In the case of an SC-D-OPF, consensus constraints (7.4) must be fulfilled in every considered time or contingency scenario:

$$\tilde{A}^{t,c}_A x^{t,c}_{\mathcal{N}_A} + \tilde{A}^{t,c}_B x^{t,c}_{\mathcal{N}_B} = 0, \quad \forall (t,c) \in \mathcal{S}. \tag{7.6}$$

An exemplary problem decomposition for a two-area SC-D-OPF with 3 time steps and 2 contingencies is shown in Fig. 7.4. It results in two optimization problems (dashed boxes in Fig. 7.4b) with 9 scenarios each which must be coupled. Let N-1

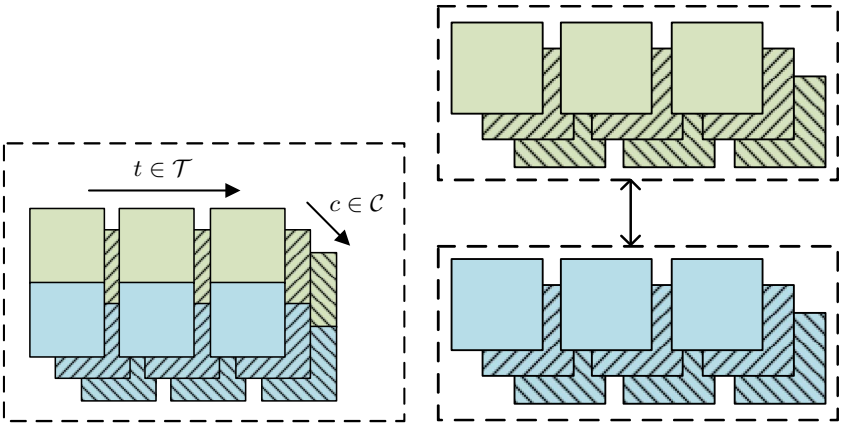

(a) Centralized SC-D-OPF. **(b)** Distributed SC-D-OPF.

Figure 7.4: Schematic problem decomposition for two areas (blue and green) under consideration of three time steps and two contingencies. A dashed box represents an optimization problem.

security be required over all time steps ($T_{\text{N-1}} = T$). Then we have

$$\begin{bmatrix} \tilde{A}_A^{1,0} & & & \tilde{A}_B^{1,0} & & \\ & \ddots & & & \ddots & \\ & & \tilde{A}_A^{T,C} & & & \tilde{A}_B^{T,C} \end{bmatrix} \begin{bmatrix} x_{\mathcal{N}_A}^{1,0} \\ \vdots \\ x_{\mathcal{N}_A}^{T,C} \\ x_{\mathcal{N}_B}^{1,0} \\ \vdots \\ x_{\mathcal{N}_B}^{T,C} \end{bmatrix} = 0. \tag{7.7}$$

Again, we improve readability of (7.7) by introducing matrices A_A, A_B such that

$$\underbrace{\begin{bmatrix} A_A & A_B \end{bmatrix}}_{A} \underbrace{\begin{bmatrix} x_A \\ x_B \end{bmatrix}}_{x} = 0 \tag{7.8}$$

or, in a more general form,

$$\sum_{k \in \{A,B\}} A_k x_k = 0. \tag{7.9}$$

7.3 Implemented Algorithms

Generally, a non-linear optimization problem can be described with

$$\underset{x}{\text{minimize}} \quad F(x) \tag{7.10a}$$

$$\text{subject to} \quad h(x) \leq 0, \tag{7.10b}$$

where $x \in \mathbb{R}^l$, $h : \mathbb{R}^l \to \mathbb{R}^m$ and $F : \mathbb{R}^l \to \mathbb{R}$ are optimization variables, constraints[1] and objective function, respectively.

Assume that due to inherent problem structures, x, h and F are separable. That is, each term can be assigned to a specific group or region and those regions are coupled to each other with linear constraints[2]. Thus, the problem can be written as

$$\underset{x}{\text{minimize}} \quad \sum_{k \in \mathcal{R}} F_k(x_k) \tag{7.11a}$$

$$\text{subject to} \quad h_k(x_k) \leq 0, \quad \forall k \in \mathcal{R} \tag{7.11b}$$

$$\sum_{k \in \mathcal{R}} A_k x_k = 0. \tag{7.11c}$$

Here, $x_k \in \mathbb{R}^{l_k}$, $h_k : \mathbb{R}^{l_k} \to \mathbb{R}^{m_k}$ and $F_k : \mathbb{R}^{l_k} \to \mathbb{R}$ are optimization variables, non-linear constraints and objective function, respectively, in *Region* $k \in \mathcal{R} = \{1, .., R\}$. Matrix $A_k \in \mathbb{R}^{n \times l_k}$ maps x_k onto the full set of n coupling constraints and enforces consensus between regions, i.e. guarantees cross-border feasibility.

In the following, two algorithms are presented, where the general idea to solve (7.11) is identical. Augmented regional OPFs are solved and the deviation of optimization variables from fixed auxiliary variables z, which are information stemming from neighboring regions, is penalized. The regions then exchange information and, depending on the algorithm, z is updated in a specific way. The update is re-distributed to the local agents for a new OPF calculation until consensus between regions is achieved.

7.3.1 ADMM

We construct an augmented Lagrangian of the form

$$\mathcal{L}(x, z, \lambda) = \sum_{k \in \mathcal{R}} \left\{ F_k(x_k) + \lambda_k^\top A_k(x_k - z_k) + \frac{\rho}{2} ||A_k(x_k - z_k)||_W^2 \right\} \tag{7.12}$$

[1] The constraints merge all linear and non-linear equality or inequality constraints.

[2] The described algorithms in this work are valid for affine coupling constraints as well. However, our problems only require linear coupling constraints.

with penalty parameter $\rho \in \mathbb{R}$ and

$$x = [x_1^\top \ ... \ x_R^\top]^\top \tag{7.13a}$$
$$z = [z_1^\top \ ... \ z_R^\top]^\top \tag{7.13b}$$
$$\lambda = [\lambda_1^\top \ ... \ \lambda_R^\top]^\top. \tag{7.13c}$$

Dual variables of the consensus constraints are denoted with $\lambda_k \in \mathbb{R}^{n\times 1}$ for each *Region k*, and $W \in \mathbb{R}^{n\times n}$ is a positive definite, diagonal weighting matrix[3], where each entry is related to one coupling constraint. The idea of using a scaling matrix W stems from the second algorithm, ALADIN. In ADMM literature, W is the identity matrix, which is referred to as *unscaled* ADMM in this work. The main steps during one iteration of the solving process are

1. $x = \text{argmin}_{x\in\mathcal{X}} \ \mathcal{L}(x, z, \lambda)$ (7.14a)
2. $z = \text{argmin}_{z\in\mathcal{Z}} \ \mathcal{L}(x, z, \lambda)$ (7.14b)
3. $\lambda \leftarrow \lambda + \rho W A(x - z)$ (7.14c)

with $A = [A_1 \ ... \ A_R]$. The first step (7.14a) minimizes a non-linear problem, where constraint region

$$\mathcal{X} = \{x | h_k(x_k) \leq 0, \forall k \in \mathcal{R}\} \tag{7.15}$$

enforces local constraints (7.11b). Since z is fixed, (7.14a) is in fact a series of R independent problems which can be calculated in parallel. Furthermore, since $\lambda_k^\top A_k z_k$ is independent of x, (7.14a) equals

$$x = \text{argmin}_{x\in\mathcal{X}} \ \sum_{k\in\mathcal{R}} \left\{ F_k(x_k) + \lambda_k^\top A_k x_k + \frac{\rho}{2} ||A_k(x_k - z_k)||_W^2 \right\}. \tag{7.16}$$

The second step minimizes a coupled quadratic problem, where

$$\mathcal{Z} = \left\{ z | \sum_{k\in\mathcal{R}} A_k z_k = 0 \right\} \tag{7.17}$$

enforces consensus of auxiliary variables z. In fact, (7.14b) calculates the average value between two consensus variables of neighboring regions [33, 8] and the problem can be reduced to

$$z = \text{argmin}_{z\in\mathcal{Z}} \ \sum_{k\in\mathcal{R}} \frac{\rho}{2} ||A_k(x_k - z_k)||_W^2. \tag{7.18}$$

[3] Note that a weighted norm is calculated to $||X||_W^2 = X^\top W X$, see also Appendix D.1 for matrix notation of augmentation terms.

The weighting factors ρ and W can be neglected in (7.18), if the same weight is assigned to two coupled variables, which is a reasonable choice. Once a region has gathered necessary neighbor information, this step can be calculated locally as well [32].

In the third step (7.14c), dual variables are updated based on a weighted distance between x and z. Again, with given local x_k and z_k, each region can calculate λ_k independently.

An overview of the implemented ADMM is given in Algorithm 1. Note that in ADMM, an update rule on ρ can be useful to enforce consensus. Parameter $\rho_k \in \mathbb{R}$ is assigned to *Region k*, and it can be increased depending on the local residual, see (7.22b). If the residual has not decreased sufficiently compared to the previous iteration (indicator $0 < \Theta \in \mathbb{R} < 1$), the penalty is increased by a constant factor of $\tau \in \mathbb{R} > 1$. In this work, the penalty update is only used for unscaled ADMM and SC-D-OPF, otherwise step 6 and 7 in Algorithm 1 can be skipped. In any case, the penalty parameter must be chosen carefully since it is widely known to be crucial for good convergence behavior [60].

7.3.2 ALADIN

We construct an augmented Lagrangian of the form

$$\mathcal{L}(x, z, \lambda) = \sum_{k \in \mathcal{R}} \left\{ F_k(x_k) + \lambda^\top A_k(x_k - z_k) + \frac{\rho}{2} ||(x_k - z_k)||^2_{W_k} \right\}. \tag{7.23}$$

In contrast to ADMM, the weighting matrix W_k is a diagonal matrix with entries related to each variable instead of consensus constraint. Thus, $W_k \in \mathbb{R}^{l_k \times l_k}$ is defined for each *Region k*.

As stated before, the main difference between ALADIN and ADMM is the update of z. While (7.20) is a simple averaging step, the idea for the coordination step in ALADIN stems from sequential quadratic programming [7], where the Lagrangian is approximated with a second-order Taylor expansion. Furthermore, nonlinear equality and active inequality constraints are approximated with an active set[4] (7.26c), which ensures for example that linearized node balance equations are still fulfilled with an updated z. It results a quadratic problem (7.26) which relies on gradients (7.25b) and Hessians (7.25c) of the local problems. For numerical reasons, a slack variable s is introduced to replace consensus constraints in the Lagrangian. The dual variables λ_{QP} of the consensus constraints (7.26b) are used for the update of λ. An overview of ALADIN is shown in Algorithm 2.

Note that the Hessians are required to be positive definite to ensure convergence [45, 7]. Where necessary, this is enforced with a modified $LDL^\top$ Cholesky

[4] An active set is a method to treat inequality constraints. If a condition meets or exceeds a certain limit, it is transformed into an equality constraint setting the condition equal to the potentially violated limit.

Algorithm 1 ADMM

1: **Initialization:** Weighting matrix W, tolerance ϵ; for all $k \in \mathcal{R}$: initial guesses z_k, penalty parameters $\rho_k = \rho$, dual variables $\lambda_k = \mathbf{0}$, local solutions $x_k = \boldsymbol{\infty}$, local residues $\Gamma_k = \infty$.

2: **while** $||Ax||_\infty > \epsilon$ and $||x - z||_\infty > \epsilon$ **do**

3: Solve for all $k \in \mathcal{R}$ the decoupled NLPs

$$\min_{x_k} \; F_k(x_k) + \lambda_k^\top A_k x_k + \frac{\rho_k}{2} ||A_k(x_k - z_k)||_W^2 \tag{7.19a}$$

$$\text{s.t. } h_k(x_k) \leq 0 \quad | \; \kappa_k \tag{7.19b}$$

4: Solve the coupled averaging step

$$\min_{z} \; \sum_{k \in \mathcal{R}} ||A_k(x_k - z_k)||_2^2 \tag{7.20a}$$

$$\text{s.t. } \sum_{k \in \mathcal{R}} A_k z_k = 0 \tag{7.20b}$$

5: Update dual variables for all $k \in \mathcal{R}$

$$\lambda_k \leftarrow \lambda_k + \rho_k W A_k(x_k - z_k) \tag{7.21}$$

6: Calculate local residues and penalty parameter updates for all $k \in \mathcal{R}$

$$\Gamma_k^+ = ||A_k(x_k - z_k)||_\infty \tag{7.22a}$$

$$\rho_k \leftarrow \begin{cases} \rho_k & \text{if } \Gamma_k^+ \leq \Theta \Gamma_k \\ \tau \rho_k & \text{otherwise} \end{cases} \tag{7.22b}$$

7: Update $\Gamma_k \leftarrow \Gamma_k^+$ for all $k \in \mathcal{R}$

8: **end while**

factorization [41]. Furthermore, large values of $\mu \in \mathbb{R}$ may lead to numerical instability at the beginning of the algorithm. Therefore, as proposed in [24], a factor $r_\mu \in \mathbb{R} \geq 1$ can be used to ramp up μ to the desired value during the first iterations. Deeper insights on similarities and differences between ALADIN and ADMM are found in [45]. Moreover, the authors present convergence guarantees for non-convex problems with a globalization strategy, which is not used in this work.

Algorithm 2 ALADIN

1: **Initialization:** Penalty parameters ρ and $\mu = \underline{\mu}$, dual variables $\lambda = \mathbf{0}$, tolerance ϵ; for all $k \in \mathcal{R}$: initial guesses z_k, weighting matrices W_k, local solutions $x_k = \boldsymbol{\infty}$.
2: **while** $||Ax||_\infty > \epsilon$ and $||x - z||_\infty > \epsilon$ **do**
3: Solve for all $k \in \mathcal{R}$ the decoupled NLPs

$$\min_{x_k} \; F_k(x_k) + \lambda^\top A_k x_k + \frac{\rho}{2}||x_k - z_k||^2_{W_k} \tag{7.24a}$$

$$\text{s.t. } h_k(x_k) \leq 0 \quad | \; \kappa_k \tag{7.24b}$$

4: Compute for all $k \in \mathcal{R}$ Jacobians, gradients and Hessians

$$C_{k,j} = \begin{cases} \frac{\partial}{\partial y}(h_k(y))_j|_{y=x_k} & \text{if } (h_k(x_k))_j = 0 \\ 0 & \text{otherwise} \end{cases} \tag{7.25a}$$

$$g_k = \nabla F_k(x_k) \tag{7.25b}$$

$$H_k = \nabla^2\{F_k(x_k) + \kappa_k^\top h_k(x_k)\} \tag{7.25c}$$

5: Solve coupled quadratic problem

$$\min_{\Delta x, s} \; \sum_{k\in\mathcal{R}} \left\{ \frac{1}{2}\Delta x_k^\top H_k \Delta x_k + g_k^\top \Delta x_k \right\} + \lambda^\top s + \frac{\mu}{2}||s||_2^2 \tag{7.26a}$$

$$\text{s.t. } \sum_{k\in\mathcal{R}} A_k(x_k + \Delta x_k) = s \quad | \; \lambda_{\text{QP}} \tag{7.26b}$$

$$C_k \Delta x_k = 0, \quad \forall k \in \mathcal{R} \tag{7.26c}$$

6: Update $z \leftarrow x + \Delta x$, $\lambda \leftarrow \lambda_{\text{QP}}$, $\mu \leftarrow \min(\overline{\mu}, r_\mu \mu)$
7: **end while**

7.4 Simple 2-Bus Example

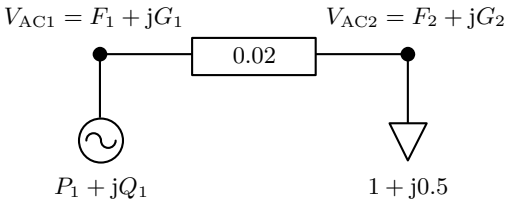

Figure 7.5: Simple 2-bus system with a generator and a load connected by a pure resistance.

For a comprehensive understanding of the algorithms, we describe the distributed optimization of a minimal 2-bus system, which is depicted in Fig. 7.5. State variables are two complex bus voltages in rectangular coordinates and a complex power source:

$$x = \begin{bmatrix} F_1 & F_2 & G_1 & G_2 & P_1 & Q_1 \end{bmatrix}^\top . \tag{7.27}$$

We neglect generator, voltage and branch flow limits and thus only have the power balance and a reference voltage as constraints. Assuming a base power of 100 MVA, a minimization of P_1 at costs of 1 €/MWh leads to an optimization problem of the form

$$\begin{aligned}
\underset{x}{\text{minimize}} \quad & 0.01 P_1 \cdot \text{€/h} && \text{(7.28a)}\\
\text{subject to} \quad & P_1 = \Re\left((F_1 + \mathrm{j}G_1) \frac{(F_1 + \mathrm{j}G_1)^* - (F_2 + \mathrm{j}G_2)^*}{0.02} \right) \\
& \quad = 50(F_1(F_1 - F_2) + G_1(G_1 - G_2)) && \text{(7.28b)}\\
& Q_1 = 50(G_1(F_1 - F_2) - F_1(G_1 - G_2)) && \text{(7.28c)}\\
& -1 = \Re\left((F_2 + \mathrm{j}G_2) \frac{(F_2 + \mathrm{j}G_2)^* - (F_1 + \mathrm{j}G_1)^*}{0.02} \right) \\
& \quad = 50(F_2(F_2 - F_1) + G_2(G_2 - G_1)) && \text{(7.28d)}\\
& -0.5 = 50(G_2(F_2 - F_1) - F_2(G_2 - G_1)) && \text{(7.28e)}\\
& F_1 = 1 && \text{(7.28f)}\\
& G_1 = 0, && \text{(7.28g)}
\end{aligned}$$

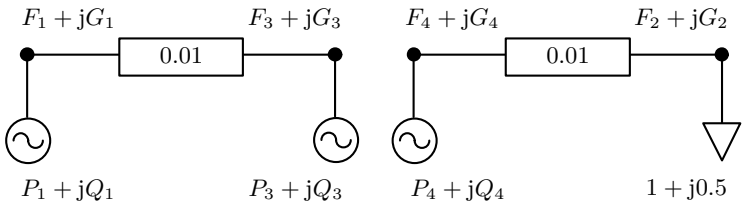

Figure 7.6: Decoupled 2-bus system with two auxiliary buses and two auxiliary generators. The two resistances are half the original one.

where the optimal solution[5] is

$$x = \begin{bmatrix} F_1 \\ F_2 \\ G_1 \\ G_2 \\ P_1 \\ Q_1 \end{bmatrix} = \begin{bmatrix} 1 \\ 0.9795 \\ 0 \\ 0.0100 \\ 1.0261 \\ 0.5000 \end{bmatrix}, \tag{7.29}$$

which signifies an active power production of 102.61 MW at costs of 102.61 €/h. Note that due to the low complexity, the quadratic equation system (7.28b)-(7.28g) is solvable analytically, which returns $(P_1, F_2) = (1.026056, 0.979479)$ and $(P_1, F_2) = (48.974, 0.0205)$ besides the remaining unique variable solutions.

7.4.1 Preparation

Preparation of the central problem to allow for distributed optimization is equal for both ADMM and ALADIN. Following the decomposition approach from section 7.2.2, two separate networks are created, see Fig. 7.6. The state variables of both areas are extended to

$$x_1 = \begin{bmatrix} F_1 & F_3 & G_1 & G_3 & P_1 & P_3 & Q_1 & Q_3 \end{bmatrix}^\top \tag{7.30a}$$

$$x_2 = \begin{bmatrix} F_2 & F_4 & G_2 & G_4 & P_4 & Q_4 \end{bmatrix}^\top, \tag{7.30b}$$

and the coupling constraints to enforce a feasible overall power flow are

$$F_3 = F_4 \tag{7.31a}$$

$$G_3 = G_4 \tag{7.31b}$$

$$P_3 = -P_4 \tag{7.31c}$$

$$Q_3 = -Q_4. \tag{7.31d}$$

[5] computed with IPOPT [80]

The constraints in area 1 and 2 are collected in $Y_1(x_1)$ and $Y_2(x_2)$, respectively:

$$Y_1(x_1) = 0 \equiv \begin{cases} P_1 = 100(F_1(F_1 - F_3) - G_1(G_1 - G_3)) \\ Q_1 = 100(G_1(F_1 - F_3) + F_1(G_1 - G_3)) \\ P_3 = 100(F_3(F_3 - F_1) - G_3(G_3 - G_1)) \\ Q_3 = 100(G_3(F_3 - F_1) + F_3(G_3 - G_1)) \\ F_1 = 1 \\ G_1 = 0 \end{cases} \tag{7.32a}$$

$$Y_2(x_2) = 0 \equiv \begin{cases} -1 = 100(F_2(F_2 - F_4) - G_2(G_2 - G_4)) \\ -0.5 = 100(G_2(F_2 - F_4) + F_2(G_2 - G_4)) \\ P_4 = 100(F_4(F_4 - F_2) - G_4(G_4 - G_2)) \\ Q_4 = 100(G_4(F_4 - F_2) + F_4(G_4 - G_2)) \end{cases} . \tag{7.32b}$$

7.4.2 ADMM

Variable results for each iteration are shown in Table 7.1.

1. Initialization

$$z_1 = \begin{bmatrix} z_{\mathrm{F3}} \\ z_{\mathrm{G3}} \\ z_{\mathrm{P3}} \\ z_{\mathrm{Q3}} \end{bmatrix} = \begin{bmatrix} 1 \\ 0 \\ 0 \\ 0 \end{bmatrix}, z_2 = \begin{bmatrix} z_{\mathrm{F4}} \\ z_{\mathrm{G4}} \\ z_{\mathrm{P4}} \\ z_{\mathrm{Q4}} \end{bmatrix} = \begin{bmatrix} 1 \\ 0 \\ 0 \\ 0 \end{bmatrix}, \lambda_1 = \lambda_2 = \begin{bmatrix} \lambda_{\mathrm{F}} \\ \lambda_{\mathrm{G}} \\ \lambda_{\mathrm{P}} \\ \lambda_{\mathrm{Q}} \end{bmatrix} = \begin{bmatrix} 0 \\ 0 \\ 0 \\ 0 \end{bmatrix} \tag{7.33}$$

Weighting factors $W_1(V) = W_2(V) = 10^4$ and $W_1(S) = W_2(S) = 10^2$. Parameter $\rho_1 = \rho_2 = 10^2$. Tolerance $\epsilon = 10^{-4}$.

2. Get local solutions x_1 and x_2

$$\begin{aligned} \min_{x_1} \quad & 100P_1 + \lambda_{\mathrm{F}}F_3 + \lambda_{\mathrm{G}}G_3 + \lambda_{\mathrm{P}}P_3 + \lambda_{\mathrm{Q}}Q_3 \\ & + \frac{1}{2}10^6\left((F_3 - z_{\mathrm{F3}})^2 + (G_3 - z_{\mathrm{G3}})^2\right) \\ & + \frac{1}{2}10^4\left((P_3 - z_{\mathrm{P3}})^2 + (Q_3 - z_{\mathrm{Q3}})^2\right) && (7.34a) \\ \text{s.t.} \quad & Y_1(x_1) = 0 && (7.34b) \end{aligned}$$

$$\begin{aligned}\min_{x_2} \quad & -\lambda_{\mathrm{F}}F_4 - \lambda_{\mathrm{G}}G_4 + \lambda_{\mathrm{P}}P_4 + \lambda_{\mathrm{Q}}Q_4 \\ & + \frac{1}{2}10^6\big((F_4 - z_{\mathrm{F4}})^2 + (G_4 - z_{\mathrm{G4}})^2\big) \\ & + \frac{1}{2}10^4\big((P_4 - z_{\mathrm{P4}})^2 + (Q_4 - z_{\mathrm{Q4}})^2\big) \qquad (7.35a) \\ \text{s.t.} \quad & Y_2(x_2) = 0 \qquad (7.35b)\end{aligned}$$

3. Average consensus variables and compute new z's

$$z_{\mathrm{F3}} = z_{\mathrm{F4}} = \frac{1}{2}(F_3 + F_4) \qquad (7.36a)$$
$$z_{\mathrm{G3}} = z_{\mathrm{G4}} = \frac{1}{2}(G_3 + G_4) \qquad (7.36b)$$
$$z_{\mathrm{P3}} = -z_{\mathrm{P4}} = \frac{1}{2}(P_3 - P_4) \qquad (7.36c)$$
$$z_{\mathrm{Q3}} = -z_{\mathrm{Q4}} = \frac{1}{2}(Q_3 - Q_4) \qquad (7.36d)$$

4. Update λ's.

$$\lambda_{\mathrm{F}} \leftarrow \lambda_{\mathrm{F}} + 10^6(F_3 - z_{\mathrm{F3}}) \qquad (= \lambda_{\mathrm{F}} - 10^6(F_4 - z_{\mathrm{F4}})) \qquad (7.37a)$$
$$\lambda_{\mathrm{G}} \leftarrow \lambda_{\mathrm{G}} + 10^6(G_3 - z_{\mathrm{G3}}) \qquad (= \lambda_{\mathrm{G}} - 10^6(G_4 - z_{\mathrm{G4}})) \qquad (7.37b)$$
$$\lambda_{\mathrm{P}} \leftarrow \lambda_{\mathrm{P}} + 10^4(P_3 - z_{\mathrm{P3}}) \qquad (= \lambda_{\mathrm{P}} + 10^4(P_4 - z_{\mathrm{P4}})) \qquad (7.37c)$$
$$\lambda_{\mathrm{Q}} \leftarrow \lambda_{\mathrm{Q}} + 10^4(Q_3 - z_{\mathrm{Q3}}) \qquad (= \lambda_{\mathrm{Q}} + 10^4(Q_4 - z_{\mathrm{Q4}})) \qquad (7.37d)$$

5. Skipped: update penalty parameter and local residues

6. Check convergence

Go to step 2 if any of the following conditions is violated, otherwise quit and return (x_1, x_2) as solutions to the controllers.

$$|F_3 - F_4| < \epsilon \qquad (7.38a)$$
$$|G_3 - G_4| < \epsilon \qquad (7.38b)$$
$$|P_3 + P_4| < \epsilon \qquad (7.38c)$$
$$|Q_3 + Q_4| < \epsilon \qquad (7.38d)$$

Table 7.1: Variable convergence in 2-bus example with ADMM.

Iteration	0	1	2	3	4	5	6	...	27	28	29
F_1	1	1.0000	1.0000	1.0000	1.0000	1.0000	1.0000	F_1	1.0000	1.0000	1.0000
F_3	1	1.0096	0.9999	0.9902	0.9852	0.9849	0.9870	F_3	0.9897	0.9897	0.9897
G_1	0	0.0000	0.0000	0.0000	0.0000	0.0000	0.0000	G_1	0.0000	0.0000	0.0000
G_3	0	0.0000	0.0049	0.0073	0.0074	0.0063	0.0052	G_3	0.0050	0.0050	0.0050
P_1	0	-0.9624	0.0144	0.9840	1.4810	1.5093	1.2992	P_1	1.0257	1.0258	1.0260
P_3	0	0.9717	-0.0121	-0.9690	-1.4536	-1.4826	-1.2796	P_3	-1.0126	-1.0128	-1.0130
Q_1	0	0.0000	0.4854	0.7277	0.7369	0.6301	0.5178	Q_1	0.4999	0.5000	0.5000
Q_3	0	0.0000	-0.4854	-0.7277	-0.7369	-0.6301	-0.5178	Q_3	-0.4999	-0.5000	-0.5000
F_2	1	0.9901	1.0001	0.9949	0.9798	0.9672	0.9643	F_2	0.9795	0.9795	0.9795
F_4	1	1.0003	1.0101	1.0050	0.9901	0.9776	0.9748	F_4	0.9898	0.9898	0.9897
G_2	0	0.0050	0.0049	0.0098	0.0147	0.0160	0.0138	G_2	0.0100	0.0100	0.0100
G_4	0	0.0000	0.0000	0.0049	0.0097	0.0110	0.0088	G_4	0.0050	0.0050	0.0050
P_4	0	1.0127	1.0125	1.0126	1.0130	1.0134	1.0134	P_4	1.0130	1.0130	1.0130
Q_4	0	0.5000	0.5000	0.5000	0.5000	0.5000	0.5000	Q_4	0.5000	0.5000	0.5000
z_{F3}	1	1.0049	1.0050	0.9976	0.9877	0.9812	0.9809	z_{F3}	0.9898	0.9898	0.9897
z_{G3}	0	0.0000	0.0024	0.0061	0.0085	0.0087	0.0070	z_{G3}	0.0050	0.0050	0.0050
z_{P3}	0	-0.0205	-0.5123	-0.9908	-1.2333	-1.2480	-1.1465	z_{P3}	-1.0128	-1.0129	-1.0130
z_{Q3}	0	-0.2500	-0.4927	-0.6138	-0.6184	-0.5650	-0.5089	z_{Q3}	-0.5000	-0.5000	-0.5000
z_{F4}	1	1.0049	1.0050	0.9976	0.9877	0.9812	0.9809	z_{F4}	0.9898	0.9898	0.9897
z_{G4}	0	0.0000	0.0024	0.0061	0.0085	0.0087	0.0070	z_{G4}	0.0050	0.0050	0.0050
z_{P4}	0	0.0205	0.5123	0.9908	1.2333	1.2480	1.1465	z_{P4}	1.0128	1.0129	1.0130
z_{Q4}	0	0.2500	0.4927	0.6138	0.6184	0.5650	0.5089	z_{Q4}	0.5000	0.5000	0.5000
λ_{F}	0	46.8031	-4.5424	-78.9786	-103.6168	-67.0455	-5.8910	λ_{F}	-2.7470	-2.8502	-2.8572
λ_{G}	0	0.0000	24.2716	36.3704	24.6745	1.1332	-16.8299	λ_{G}	0.0410	0.0395	0.0150
λ_{P}	0	99.2211	149.2433	151.4225	129.3931	105.9312	92.6210	λ_{P}	102.1219	102.1329	102.1346
λ_{Q}	0	25.0000	25.7285	14.3459	2.5034	-3.9999	-4.8877	λ_{Q}	1.0260	1.0263	1.0242
$\lvert F_3 - F_4 \rvert$	0	9.36E-03	1.03E-02	1.49E-02	4.93E-03	7.31E-03	1.22E-02	$\lvert F_3 - F_4 \rvert$	3.90E-05	2.07E-05	1.39E-06
$\lvert G_3 - G_4 \rvert$	0	7.94E-17	4.85E-03	2.42E-03	2.34E-03	4.71E-03	3.59E-03	$\lvert G_3 - G_4 \rvert$	8.48E-06	2.40E-07	4.89E-06
$\lvert P_3 + P_4 \rvert$	0	1.98E+00	1.00E+00	4.36E-02	4.41E-01	4.69E-01	2.66E-01	$\lvert P_3 + P_4 \rvert$	3.79E-04	2.19E-04	3.50E-05
$\lvert Q_3 + Q_4 \rvert$	0	5.00E-01	1.46E-02	2.28E-01	2.37E-01	1.30E-01	1.78E-02	$\lvert Q_3 + Q_4 \rvert$	8.92E-05	6.26E-06	4.22E-05

7.4.3 ALADIN

Variable results for each iteration are shown in Table 7.2.

1. Initialization

$$z_1 = \begin{bmatrix} z_{\mathrm{F1}} \\ z_{\mathrm{F3}} \\ z_{\mathrm{G1}} \\ z_{\mathrm{G3}} \\ z_{\mathrm{P1}} \\ z_{\mathrm{P3}} \\ z_{\mathrm{Q1}} \\ z_{\mathrm{Q3}} \end{bmatrix} = \begin{bmatrix} 1 \\ 1 \\ 0 \\ 0 \\ 0 \\ 0 \\ 0 \\ 0 \end{bmatrix}, z_2 = \begin{bmatrix} z_{\mathrm{F2}} \\ z_{\mathrm{F4}} \\ z_{\mathrm{G2}} \\ z_{\mathrm{G4}} \\ z_{\mathrm{P4}} \\ z_{\mathrm{Q4}} \end{bmatrix} = \begin{bmatrix} 1 \\ 1 \\ 0 \\ 0 \\ 0 \\ 0 \\ 0 \\ 0 \end{bmatrix}, \lambda = \begin{bmatrix} \lambda_{\mathrm{F}} \\ \lambda_{\mathrm{G}} \\ \lambda_{\mathrm{P}} \\ \lambda_{\mathrm{Q}} \end{bmatrix} = \begin{bmatrix} 0 \\ 0 \\ 0 \\ 0 \end{bmatrix} \tag{7.39}$$

Weighting factors $W_1(V) = W_2(V) = 10^4$ and $W_1(S) = W_2(S) = 10^2$. Parameters $\rho = 10^2$, $\mu = 10^4$ and $r_\mu = 1$. Tolerance $\epsilon = 10^{-4}$.

2. Get local solutions x_1 and x_2 with dual multipliers κ and σ

$$\begin{aligned} \min_{x_1} \quad & 100P_1 + \lambda_{\mathrm{F}} F_3 + \lambda_{\mathrm{G}} G_3 + \lambda_{\mathrm{P}} P_3 + \lambda_{\mathrm{Q}} Q_3 \\ & + \frac{1}{2}10^6\big((F_1 - z_{\mathrm{F1}})^2 + (F_3 - z_{\mathrm{F3}})^2 + (G_1 - z_{\mathrm{G1}})^2 + (G_3 - z_{\mathrm{G3}})^2\big) \\ & + \frac{1}{2}10^4\big((P_1 - z_{\mathrm{P1}})^2 + (P_3 - z_{\mathrm{P3}})^2 + (Q_1 - z_{\mathrm{Q1}})^2 + (Q_3 - z_{\mathrm{Q3}})^2\big) \end{aligned} \tag{7.40a}$$

$$\text{s.t.} \quad Y_1(x_1) = 0 \quad |\kappa, \tag{7.40b}$$

where $\kappa = [\kappa_1, \kappa_2, \kappa_3, \kappa_4, \kappa_5, \kappa_6]^\top$,

$$\begin{aligned} \min_{x_2} \quad & -\lambda_{\mathrm{F}} F_4 - \lambda_{\mathrm{G}} G_4 + \lambda_{\mathrm{P}} P_4 + \lambda_{\mathrm{Q}} Q_4 \\ & + \frac{1}{2}10^6\big((F_2 - z_{\mathrm{F2}})^2 + (F_4 - z_{\mathrm{F4}})^2 + (G_2 - z_{\mathrm{G2}})^2 + (G_4 - z_{\mathrm{G4}})^2\big) \\ & + \frac{1}{2}10^4\big((P_4 - z_{\mathrm{P4}})^2 + (Q_4 - z_{\mathrm{Q4}})^2\big) \end{aligned} \tag{7.41a}$$

$$\text{s.t.} \quad Y_2(x_2) = 0 \quad |\sigma, \tag{7.41b}$$

where $\sigma = [\sigma_1, \sigma_2, \sigma_3, \sigma_4]^\top$.

3. Compute matrices

Since the constraints only contain equalities, the active sets become

$$C_1 = \nabla_{x_1} Y_1(x_1) \tag{7.42a}$$
$$C_2 = \nabla_{x_2} Y_2(x_2). \tag{7.42b}$$

Furthermore, the objective does not contain quadratic terms (or higher), therefore, second derivatives of $F_k(x_k)$ are zero and the Hessians become

$$H_1 = \nabla^2_{x_1}(\kappa^\top Y_1(x_1)) \tag{7.43a}$$
$$H_2 = \nabla^2_{x_2}(\sigma^\top Y_2(x_2)). \tag{7.43b}$$

Matrices (details in Appendix D.3.2) are formed to

$$L = \begin{bmatrix} H_1 & 0 & 0 \\ 0 & H_2 & 0 \\ 0 & 0 & 10^4 \cdot \mathbf{1} \end{bmatrix} \tag{7.44a}$$
$$B = \begin{bmatrix} A_1 & A_2 & -\mathbf{1} \\ C_1 & 0 & 0 \\ 0 & C_2 & 0 \end{bmatrix} \tag{7.44b}$$
$$f = \begin{bmatrix} g_1^\top & g_2^\top & \lambda^\top \end{bmatrix} \tag{7.44c}$$
$$b = \begin{bmatrix} -A_1 x_1 - A_2 x_2 \\ 0 \end{bmatrix}, \tag{7.44d}$$

with $\mathbf{1}$ the unity matrix of appropriate size.

4. Solve quadratic problem

The update step is solved with

$$\begin{bmatrix} \Delta x_1 \\ \Delta x_2 \\ s \\ \lambda_{\mathrm{QP}} \\ \zeta \end{bmatrix} = \begin{bmatrix} L & B^\top \\ B & 0 \end{bmatrix}^{-1} \begin{bmatrix} -f^\top \\ b \end{bmatrix}, \tag{7.45}$$

where ζ are dual variables of the active sets C_1, C_2; s includes slack variables for each consensus constraint of (7.31); Newton step directions are

$$\Delta x_1 = \begin{bmatrix} \Delta F_1 & \Delta F_3 & \Delta G_1 & \Delta G_3 & \Delta P_1 & \Delta P_3 & \Delta Q_1 & \Delta Q_3 \end{bmatrix}^\top \tag{7.46a}$$
$$\Delta x_2 = \begin{bmatrix} \Delta F_2 & \Delta F_4 & \Delta G_2 & \Delta G_4 & \Delta P_4 & \Delta Q_4 \end{bmatrix}^\top; \tag{7.46b}$$

and dual variables of the consensus constraints are collected in

$$\lambda_{\mathrm{QP}} = \begin{bmatrix} \lambda_{\mathrm{QP,F}} & \lambda_{\mathrm{QP,G}} & \lambda_{\mathrm{QP,P}} & \lambda_{\mathrm{QP,Q}} \end{bmatrix}^\top. \tag{7.47}$$

5. Update

$$z_1 \leftarrow x_1 + \Delta x_1 \tag{7.48a}$$
$$z_2 \leftarrow x_2 + \Delta x_2 \tag{7.48b}$$
$$\lambda \leftarrow \lambda_{\mathrm{QP}} \tag{7.48c}$$

6. Check convergence

Go to step 2 if any of the following conditions is violated, otherwise quit and return (x_1, x_2) as solutions to the controllers.

$$||\Delta x_1||_\infty < \epsilon \tag{7.49a}$$
$$||\Delta x_2||_\infty < \epsilon \tag{7.49b}$$
$$|F_3 - F_4| < \epsilon \tag{7.49c}$$
$$|G_3 - G_4| < \epsilon \tag{7.49d}$$
$$|P_3 + P_4| < \epsilon \tag{7.49e}$$
$$|Q_3 + Q_4| < \epsilon \tag{7.49f}$$

7.4.4 Summary

Both algorithms approach optimality at $P_1 = 102.602\,\mathrm{MW}$ with ADMM and $P_1 = 102.605\,\mathrm{MW}$ with ALADIN. ALADIN converges after 4 iterations, while ADMM requires 29 iterations.

Table 7.2: Variable convergence in 2-bus example with ALADIN.

Iteration	0	1	2	3	4
F_1	1	1.0000	1.0000	1.0000	1.0000
F_3	1	1.0049	0.9910	0.9898	0.9897
G_1	0	0.0000	0.0000	0.0000	0.0000
G_3	0	0.0000	0.0050	0.0050	0.0050
P_1	0	-0.4939	0.9049	1.0242	1.0261
P_3	0	0.4963	-0.8942	-1.0113	-1.0130
Q_1	0	0.0000	0.4969	0.4995	0.5000
Q_3	0	0.0000	-0.4969	-0.4995	-0.5000
κ_1	-	-50.6140	-100.3692	-100.0072	-100.0000
κ_2	-	-49.6299	-102.2501	-102.1267	-102.1231
κ_3	-	0.0000	0.2589	0.0000	0.0000
κ_4	-	0.0000	-0.7545	-1.0200	-1.0211
κ_5	-	0.0000	0.2633	0.0000	0.0000
κ_6	-	-48.9000	5.2548	5.4312	5.4342
F_2	1	0.9951	0.9834	0.9796	0.9795
F_4	1	1.0052	0.9937	0.9898	0.9897
G_2	0	0.0025	0.0100	0.0100	0.0100
G_4	0	-0.0025	0.0050	0.0050	0.0050
P_4	0	1.0126	1.0129	1.0130	1.0130
Q_4	0	0.5000	0.5000	0.5000	0.5000
σ_1	-	-103.8284	-102.5237	-104.2759	-104.2799
σ_2	-	-101.2623	-100.4201	-102.1196	-102.1231
σ_3	-	-51.2750	-1.5338	-2.0843	-2.0856
σ_4	-	-50.0000	-0.4956	-1.0200	-1.0211
z_{F1}	1	1.0000	1.0000	1.0000	1.0000
z_{F3}	1	0.9910	0.9898	0.9897	0.9897
z_{G1}	0	0.0000	0.0000	0.0000	0.0000
z_{G3}	0	0.0050	0.0050	0.0050	0.0050
z_{P1}	0	0.9012	1.0242	1.0261	1.0261
z_{P3}	0	-0.9125	-1.0113	-1.0130	-1.0130
z_{Q1}	0	0.4995	0.4995	0.5000	0.5000
z_{Q3}	0	-0.4995	-0.4995	-0.5000	-0.5000
z_{F2}	1	0.9835	0.9796	0.9795	0.9795
z_{F4}	1	0.9937	0.9898	0.9897	0.9897
z_{G2}	0	0.0100	0.0100	0.0100	0.0100
z_{G4}	0	0.0050	0.0050	0.0050	0.0050
z_{P4}	0	1.0129	1.0130	1.0130	1.0130
z_{Q4}	0	0.5000	0.5000	0.5000	0.5000
λ_{F}	0	-2.6801	-2.7436	-2.7452	-2.7452
λ_{G}	0	-0.0221	-0.0138	-0.0139	-0.0139
λ_{P}	0	100.4196	102.1195	102.1231	102.1231
λ_{Q}	0	0.4956	1.0200	1.0211	1.0211
$\lvert F_3 - F_4 \rvert$	0	2.53E-04	2.72E-03	6.43E-05	1.59E-06
$\lvert G_3 - G_4 \rvert$	0	2.50E-03	4.83E-05	8.35E-06	4.73E-08
$\lvert P_3 + P_4 \rvert$	0	1.51E+00	1.19E-01	1.77E-03	3.65E-06
$\lvert Q_3 + Q_4 \rvert$	0	5.00E-01	3.08E-03	5.25E-04	1.10E-06

7.5 Algorithm Comparison

7.5.1 Computational Effort

The NLPs (7.19) and (7.24) require the same amount of computational effort. The main difference between the two algorithms lies in the calculation of the update step (7.20) and (7.26), respectively. In ADMM, each controller calculates simple voltage and power averages for each inter-connector. In ALADIN, the update step is a large-scale problem. However, since it is a quadratic problem, it is essentially a linear system to solve, see Appendix D.2. Even at large scale, this can be done efficiently nowadays. It is thus favorable to solve such large-scale linear system rather than a centralized large-scale nonlinear and non-convex problem, especially against the background that realistic problem sizes grow very large due to network size or additional constraints (N-1 security, multiple time steps, ...). Furthermore, due to the much more sophisticated update step, a strong decrease is expected in terms of iteration numbers. Thus, the total computation time is expected to decline.

7.5.2 Communication

In ADMM, only local boundary variables must be exchanged after each iteration. In the 2-bus example from above, TSO 1 sends the result of (F_3, G_3, P_3, Q_3) to TSO 2, and TSO 2 sends (F_4, G_4, P_4, Q_4) to TSO 1. Then, each TSO computes the average step, the update, and a new NLP solution. No central entity is required, see Fig. 7.7a. Due to the relatively large number of expected iterations, communication run times should be considered as well. In ALADIN, a central coordinator is required to collect large amounts of data, see Fig. 7.7b. Apart from the full local solution x_k, the objective derivative g_k, Hessian H_k and active set C_k must be requested from each control area k, see (D.15)-(D.17) for the 2-bus example. The amount of exchanged data rapidly grows in large systems. For example, in a 300-bus test case, the number of floats reaches almost 130,000 (compared to 244 with ADMM) [24]. New methods are presented in [24] to avoid the exchange of full Hessian matrices by means of estimation and pre-calculation. Nevertheless, future communication systems could be able to cope with the necessary traffic for a real power grid. Still, the question remains valid whether or not the information itself is subject to privacy concerns. Each control area must reveal possibly delicate cost sensitivities, shadow prices and generator information to the central coordinator.

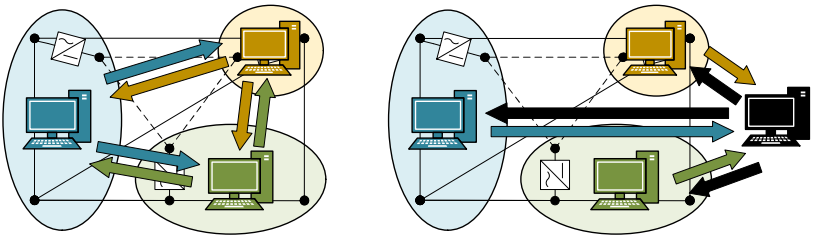

(a) ADMM. **(b)** ALADIN.

Figure 7.7: Necessary communication links between control areas and a possible central coordinator (black) for different algorithms.

N-1 Security

If N-1 security shall be included, additional information must be shared among the areas prior to the coordinated optimization with both ADMM and ALADIN. Since the power flow must be feasible for all considered scenarios, a controller will need to guarantee operational security in his area for scenarios where the topology remains unchanged, but the power flow is altered due to contingencies in foreign areas. There is no further information necessary about the nature of the contingency except the fact that it is not situated in the own control area. Thus, a full-size contingency list of unique order must be shared among the controllers, where each participant knows at which positions of the list own contingencies are located.

7.6 Summary

The main findings of this chapter are:

- **Partitioning** — hybrid AC-DC grids can be partitioned in two different ways. Either each AC region gains control over certain parts of the DC system, or a DC region is created which has its own controller. The decision is expected to be a political one.
- **ADMM vs. ALADIN** — the computational effort for the centralized step is much higher with ALADIN. Furthermore, much more (possibly delicate) information is required from each region. On the other hand, faster convergence is expected with ALADIN.
- **Tutorial** — a 2-bus system is optimized for a comprehensive understanding of both algorithms.

Chapter 8

Case Studies: Multi-Area Optimization

8.1 Test Systems

The test systems are adapted from previous chapters with small modifications.

8.1.1 5-Bus System

We use the identical network from Chapter 5.1. We assume quadratic generator cost functions as in [25] (see Table A.5) and one cost coefficient for all reactive power injections ($a_{\mathrm{q}i} = 0.001\left[€/(\mathrm{Mvar}^2 \cdot \mathrm{h})\right], i \in \mathcal{N}$). A schematic overview of possible network partitions is shown in Fig. 8.1: we form either 3 hybrid AC-DC regions with *Shared-DC* (Fig. 8.1a) or 3 AC regions plus one DC region with *Joint-DC* (Fig. 8.1b). The centralized solution to the AC-DC OPF gives a total generated power of 1,009.81 MW at costs of 21,373.41 €/h.

8.1.2 66-Bus System

We use the network from Chapter 5.2, except that *Node 67*, which is a supplementary offshore wind park, is neglected (and consequently *VSC 9* as well). We assume generator cost functions, where the coefficients are in the range of the 5-bus system with a small random deviation (see Table B.7), and we further use one cost coefficient for all reactive power injections ($a_{\mathrm{q}i} = 0.001\left[€/(\mathrm{Mvar}^2 \cdot \mathrm{h})\right], i \in \mathcal{N}$). We choose *DC-Stage 2* (see Fig. 5.10b), which is a grid extension to include all VSCs in one meshed DC system. Partitioning is straightforward, since we do not alter the 3 designated AC control areas from [75], see Fig. 5.9. Wind farms are treated

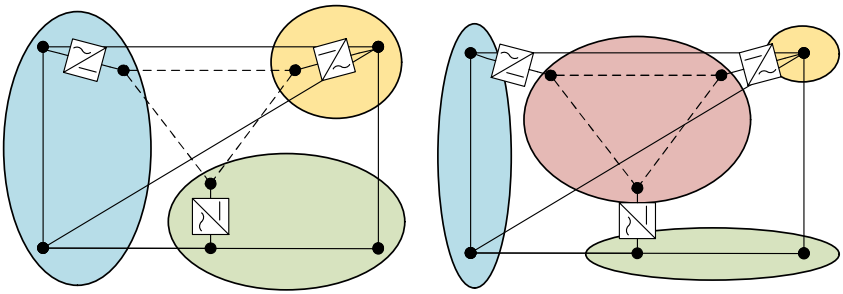

(a) *Shared-DC*: AC regions are extended. **(b)** *Joint-DC*: Additional DC region.

Figure 8.1: Region partitioning of 5-bus system with different approaches.

as negative demand and non-controllable. The centralized solution to the AC-DC OPF gives a total generated power of 9,497.07 MW at costs of 214,561.99 €/h.

8.2 Computation and Performance Indices

Algorithm parameter settings are shown in Table 8.1. Base power for all per unit values is 100 MVA and the error criterion is $\epsilon = 10^{-4}$. Inspired by [24], we use the following quantities in order to depict convergence behavior. All of them are desired to approach zero:

- The deviation of full optimization variable vector x from the optimal values x^*, i.e. $||x - x^*||_\infty$, shows the similarity between distributed solution and centralized solution[1].

- The norm of consensus constraints, i.e. $||Ax||_\infty$, describes to which extent boundary conditions are fulfilled. It illustrates the feasibility of the distributed solution.

- The algorithm step size for the z-update $||d||_\infty$, with $d = A(x - z)$ (ADMM) or $d = x - z$ (ALADIN). [2]

- The cost suboptimality $\tilde{f} = |1 - f/f^*|$ depicts the relative difference between the total distributed cost f and the centralized cost f^*.

[1] The centralized solution is obtained by solving (4.42).
[2] Note that in ADMM, due to the averaging properties, $||d||_\infty = \frac{1}{2}||Ax||_\infty$.

Table 8.1: Parameter settings for ADMM and ALADIN throughout Section 8.3. Weighting matrix entries related to power are denoted with $W_k(S)$, and entries related to voltage are denoted with $W_k(V)$.

Parameter	unscaled ADMM		scaled ADMM		ALADIN	
	5-bus	66-bus	5-bus	66-bus	5-bus	66-bus
$\rho_{(k)}$	10000	1000	1000	100	1000	100
$W_{(k)}(S)$	1	1	1	1	1	1
$W_{(k)}(V)$	1	1	100	100	100	100
τ	1.02	1.02	1	1	-	-
Θ	0.99	0.99	1	1	-	-
$\underline{\mu}$	-	-	-	-	10^3	10^3
$\overline{\mu}$	-	-	-	-	10^6	10^6
r_μ	-	-	-	-	2	2

8.3 Multi-Area AC-DC Optimal Power Flow

Performance of ADMM and ALADIN is tested on both systems for traditional AC-DC OPF without N-1 security or dynamics. In this section, branch flow limits are neglected. Parameter settings are given in Table 8.1. Parts of this chapter have been published in [93].

Scaled vs. Unscaled ADMM

First, a short comparison between scaled and unscaled ADMM is shown. Recall that with unscaled ADMM, weighting matrix W is the unity matrix. That is, all matrix entries $W_k(S) = W_k(V) = 1$. With scaled ADMM, we increase all entries related to voltages to $W_k(V) = 100$, see Table 8.1. To foster a fair comparison, parameters were tuned for both algorithms and penalty updates are allowed in the traditional unscaled ADMM, which is not always necessary with scaled ADMM. Performance indices for both test systems without HVDC extensions are shown in Fig. 8.2. With scaled ADMM, it can be observed how fewer iterations are necessary until consensus ($||Ax||_\infty$) is satisfactory to allow for a feasible power flow. Also, the distance from solution x to the centrally computed minimizer x^* is smaller. Nevertheless, the optimality gap is acceptable with both versions. This general convergence behavior was observed in a broader range of test cases and the scaled ADMM version, simply referred to as ADMM from now on, is chosen for the remainder.

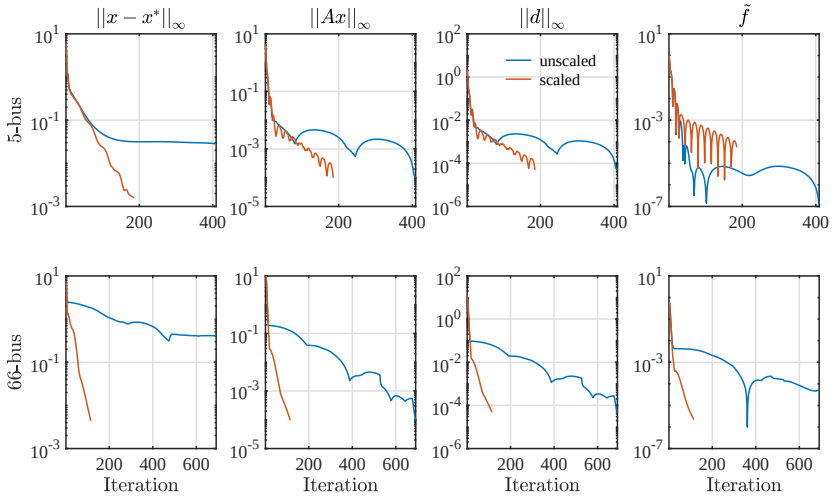

Figure 8.2: Convergence behavior of unscaled ADMM (blue) and scaled ADMM (red) for both test systems without HVDC extensions.

8.3.1 ADMM vs. ALADIN in 5-Bus System

The general convergence behavior for the quantities stated at the beginning of the chapter is shown in Fig. 8.3. For comparison, the results of the original AC test system without HVDC extensions (*"AC"*) is added. It is notable that in both ADMM and ALADIN, convergence properties are similar across all 3 grid configurations. The difference between ADMM and ALADIN however, is substantial. In ADMM, index improvement is faster in the first iterations and then continues less steep after around 20-30 iterations. Especially in the cost function, a ripple is observable. This stems from oscillating around and "overshooting" the targeted solution. In ALADIN, the first 4-5 iterations show a rather slow progression but then the target solution is approached very quickly. The consensus error falls below the criteria after 10-11 iterations in ALADIN and after 185-189 iterations in ADMM, while the objective error is in the range of 0.00005 % for ALADIN and 0.005 % for ADMM. Moreover, the variable suboptimality is considerably smaller in ALADIN.

Next, variable convergence toward the centrally computed value ($||x - x^*||_\infty$) is depicted in more detail for different variable types. In Fig. 8.4, the iterative evolution of generator and VSC power output as well as AC and DC voltages is shown for the *Joint-DC* approach. All variables eventually converge to the centrally computed value with both ADMM (top) and ALADIN (bottom). In

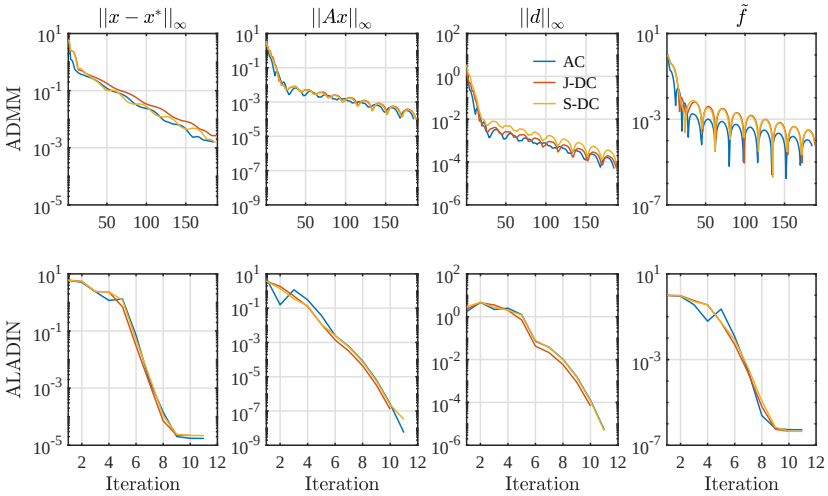

Figure 8.3: Convergence of ADMM and ALADIN in the 5-bus system. Blue: *AC*, red: *Joint-DC*, yellow: *Shared-DC*. All values per unit.

ADMM, generator power, which has the largest impact on objective function, reaches near-optimality after 50 iterations. The remaining variables, i.e. converter power and voltages, require more iterations. In ALADIN, all variables reach near-optimality after 5-6 iterations. With *Shared-DC*, the results are generally similar, see Fig. 8.5, especially with regard to generator power and AC voltages. However, due to the different partitioning approach, the progression differs for variables directly related to the DC side. That is, $P_{\text{VSC}}, Q_{\text{VSC}}$ and V_{DC} show larger deviations from the optimal solution during the first iterations.

Lastly, an excerpt of the consensus constraints ($||Ax||_\infty$), namely AC voltage constraint (7.1a)-(7.1b), is examined in detail. To enforce a feasible load flow, voltages in the middle of four AC tie lines must converge toward an identical value for both neighboring control areas. Voltage magnitude and angle are shown in Fig. 8.6 for the *Shared-DC* approach in ADMM. For each tie line, the variable results from both related areas are depicted. It can be observed that the results from both areas oscillate around each other and eventually converge toward the same value. Voltage angles show a marginally more stable behavior, which can be explained by the slower convergence of generator reactive power outputs. With ALADIN, deviations are larger in the first iterations, see Fig. 8.7. Voltage magnitude differs up to 0.02 pu between the two neighboring areas, see for example *Line 1-2* after the second iteration. Nevertheless, deviations are quickly compensated and the areas reach consensus.

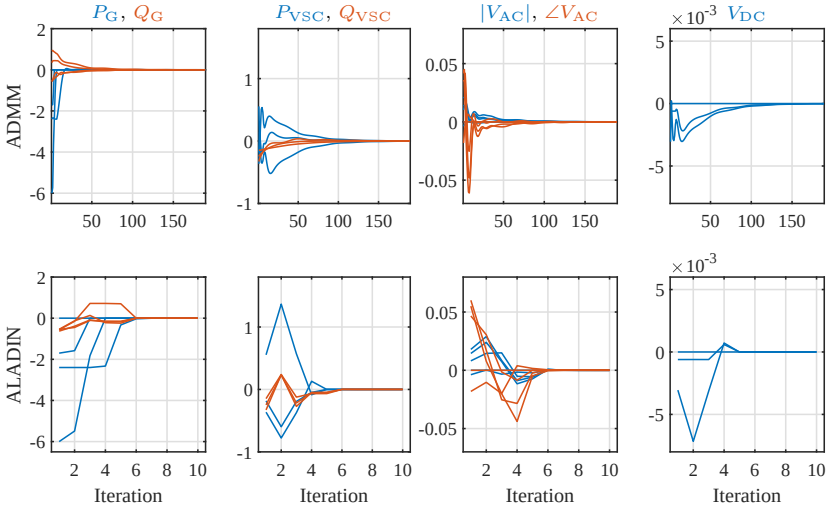

Figure 8.4: Variable difference $X - X^*$ between distributed solution X and central solution X^* with ADMM (top) and ALADIN (bottom) in 5-bus system using *Joint-DC*. All values per unit.

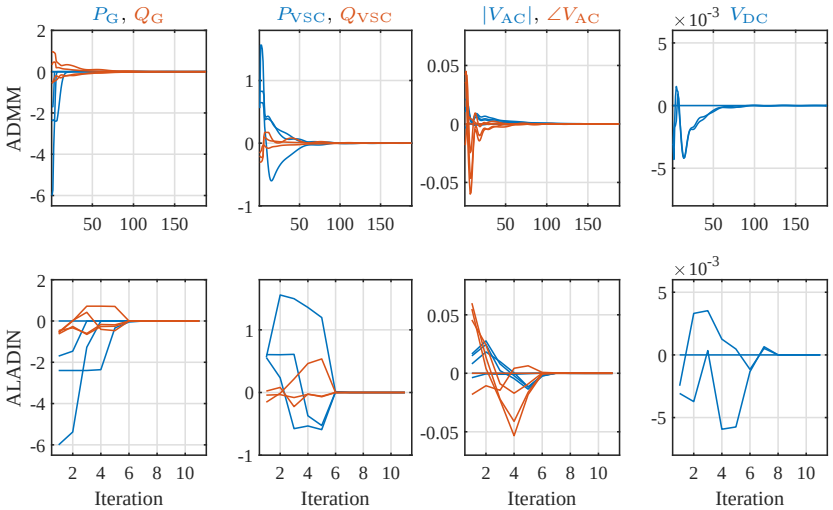

Figure 8.5: Variable difference $X - X^*$ between distributed solution X and central solution X^* with ADMM (top) and ALADIN (bottom) in 5-bus system using *Shared-DC*. All values per unit.

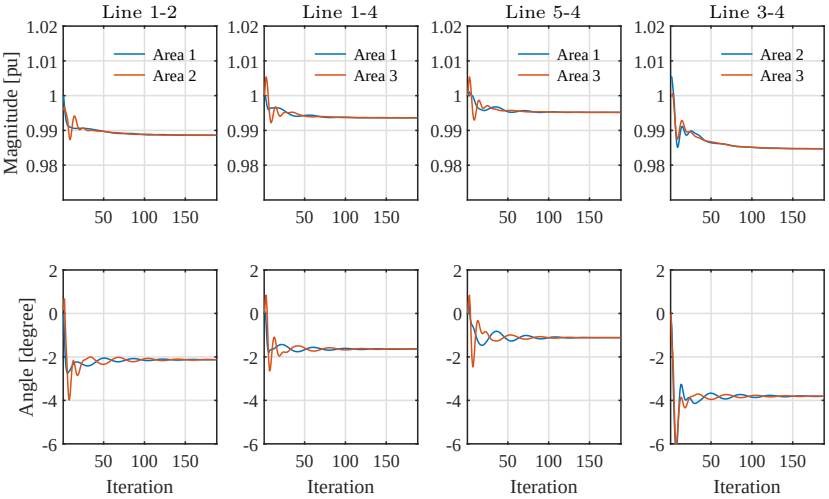

Figure 8.6: Voltage results from two neighboring areas in the center of an AC tie line using ADMM in 5-bus system with *Shared-DC*.

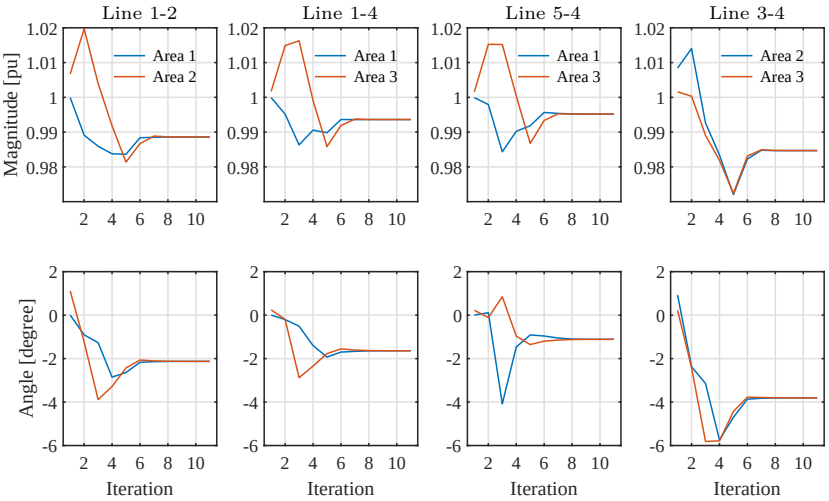

Figure 8.7: Voltage results from two neighboring areas in the center of an AC tie line using ALADIN in 5-bus system with *Shared-DC*.

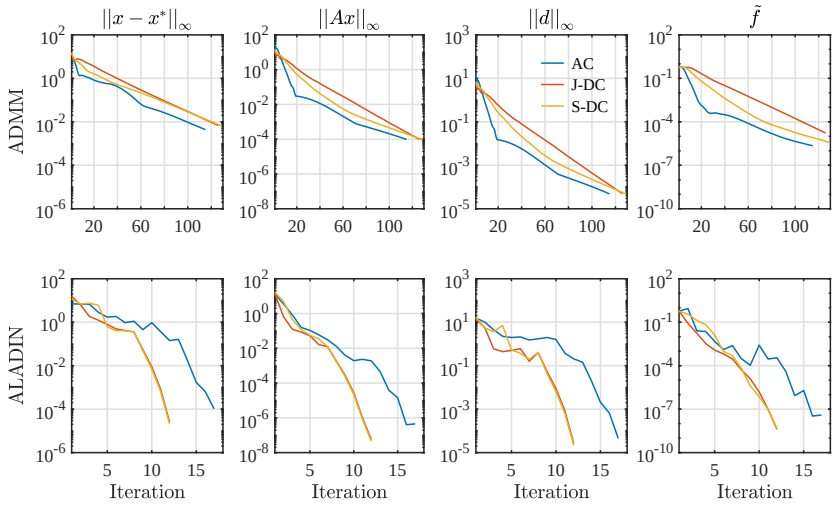

Figure 8.8: Convergence of ADMM and ALADIN in the 66-bus system. Blue: *AC*, red: *Joint-DC*, yellow: *Shared-DC*. All values per unit.

8.3.2 ADMM vs. ALADIN in 66-Bus System

Convergence behavior for the 66-bus case is shown in Fig. 8.8. ADMM shows similar exponential convergence behavior (linear in a logarithmic scale) for all 3 topologies. However, the *AC* case converges slightly faster in 115 iterations compared to 126-129 iterations for the *DC* cases. Contrarily, ALADIN struggles longer with the *AC* case compared to both *DC* cases. Similar to the 5-bus case, convergence speed appears marginally slower during the first iterations. Nevertheless, the centrally computed objective value is again reached with high accuracy for all ADMM and ALADIN cases (error falls below 0.002 % and 0.000004 %, respectively).

Finally, it is shown variable convergence towards the centrally computed value for both *Joint-DC* (Fig. 8.9) and *Shared-DC* (Fig. 8.10) approaches. All variables converge toward the desired operating point. However, the difference between the two decomposition approaches becomes apparent: variables related to the DC system are subject to much larger oscillations during the first iterations with the *Shared-DC* approach. This is especially the case for DC voltages, which are explicitly part of coupling constraints within the DC network.

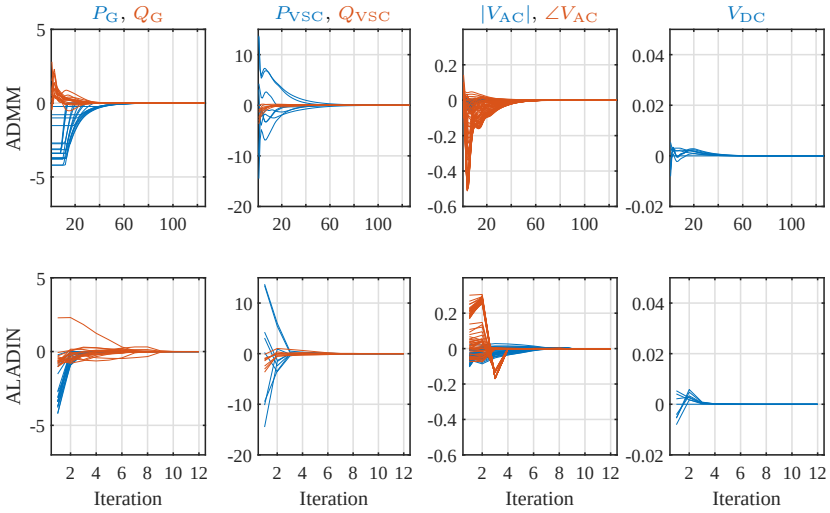

Figure 8.9: Variable difference $X - X^*$ between distributed solution X and central solution X^* with ADMM (top) and ALADIN (bottom) in 66-bus system using *Joint-DC*. All values per unit.

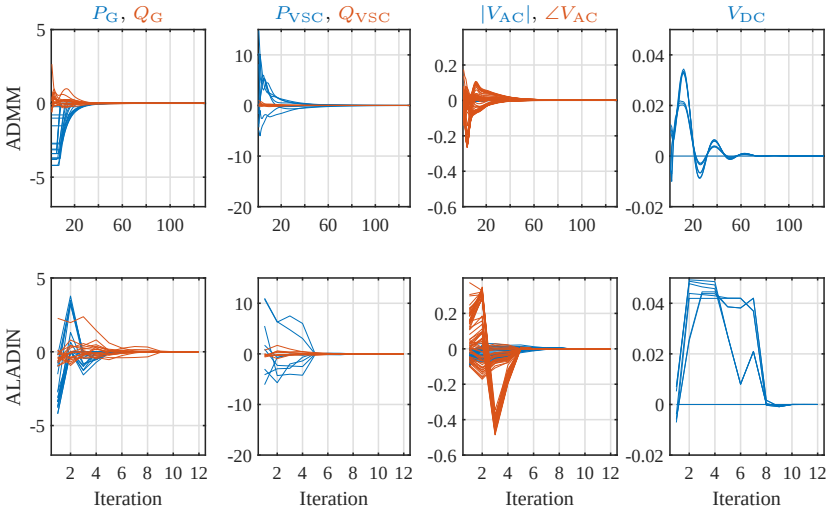

Figure 8.10: Variable difference $X - X^*$ between distributed solution X and central solution X^* with ADMM (top) and ALADIN (bottom) in 66-bus system using *Shared-DC*. All values per unit.

Table 8.2: Iteration numbers, wall clock time t and cost suboptimality under varied test systems and partitioning approaches

Case		ADMM			ALADIN		
		# it.	t [s]	$\tilde{f}$	# it.	t [s]	$\tilde{f}$
5-bus	*AC*	185	17.7	5.5e−5	11	1.2	5.3e−7
	J-DC	189	25.6	5.5e−5	10	1.6	4.5e−7
	S-DC	188	21.3	8.5e−5	11	1.5	4.5e−7
66-bus	*AC*	115	14.6	2.2e−6	17	2.9	3.9e−8
	J-DC	126	17.6	1.7e−5	12	2.4	4.0e−9
	S-DC	129	18.1	3.8e−6	12	2.8	4.5e−9

8.3.3 Comparison

Results for both systems are summarized in Table 8.2. It is notable that even though ten times larger in terms of number of nodes and system load, fewer ADMM iterations are required in the 66-bus case compared to the 5-bus case. ALADIN iterations are in the same range, except for the *AC* case. Since only 5 out of 66 AC buses are boundary buses compared to 4 out of 5 AC buses in the smaller case, one could presume the larger case to be more weakly coupled and thus less challenging for distributed optimization. Wall clock times are given for calculations on an Intel(R) Core(TM) i7-3630QM CPU at 2.40 GHz with 16 GB RAM. The computational costs per iteration are only slightly higher for ALADIN in our test systems, which leads to a strong wall clock time decrease. A total speedup factor between 14-16 is achieved for the 5-bus cases and a factor between 5-8 is achieved for the 66-bus cases.

8.4 Multi-Area SC-D-OPF

To show applicability of the distributed approach to N-1 secure and dynamic OPF problems, a small example is presented in the following. The system setup is taken from Chapter 6.2 and an SC-D-OPF dispatch optimization is performed for the described contingency (*Line 1-2*) and the first 4 time steps ($T_{\text{N-1}} = T = 4$) with *Preventive-Curative-ESS* and *Preventive-Curative-DC*. We use ADMM with $\rho = 500$, $\tau = 1.02$, $\Theta = 0.99$, $W(S) = 1$ and $W(V) = 100$. Parts of this chapter have been published in [94].

General convergence behavior is shown in Fig. 8.11. Consensus error and objective suboptimality show similar behavior compared to previous OPF cases. Consensus error falls below the required threshold after 344 iterations with an objective value

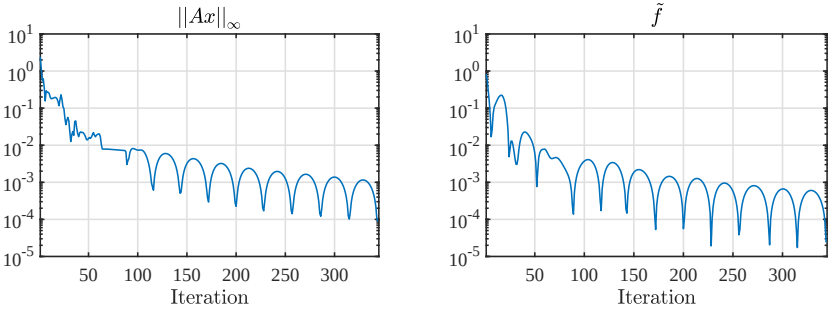

Figure 8.11: Convergence behavior for a distributed SC-D-OPF in the 5-bus system with 4 time steps and 1 contingency.

error below 0.01 %.

The iterative progress of all variables is clustered into all included scenarios and shown in Fig. 8.12 by means of subtracting the distributed result from the centralized result. It can be seen that generally, the centralized solution is approached, i.e. the difference approaches zero. However, some variables do not converge exactly toward the target values. For example, there remain small offsets for P_{VSC} and $\angle V_{\mathrm{AC}}$ in the outage cases with $c = 1$ (every second row). This indicates that after an outage, two converters marginally shift set points from the centralized to the distributed solution. In other words, *VSC 2* delivers a few MW too much, and *VSC 3* delivers a few MW too little. This change in power injection and thus in power flow is in line with altered voltage angles for those cases. However, Fig. 8.11 shows that the final objective value is not affected. Therefore, the impact on the cost function is too small for the algorithm to sense.

The progress of storage variables is shown in Fig. 8.13 for all time steps after the outage. Dashed lines denote results from the centralized solution. To provide the appropriate power reserve after the outage, *ES 2* is charged and *ESS 1* is discharged. The amount of reserve is increased with time for a growing network stress level, but energy levels remain within limits. The distributed solution is represented by solid lines. Those oscillate around and, as desired, eventually approach the target levels.

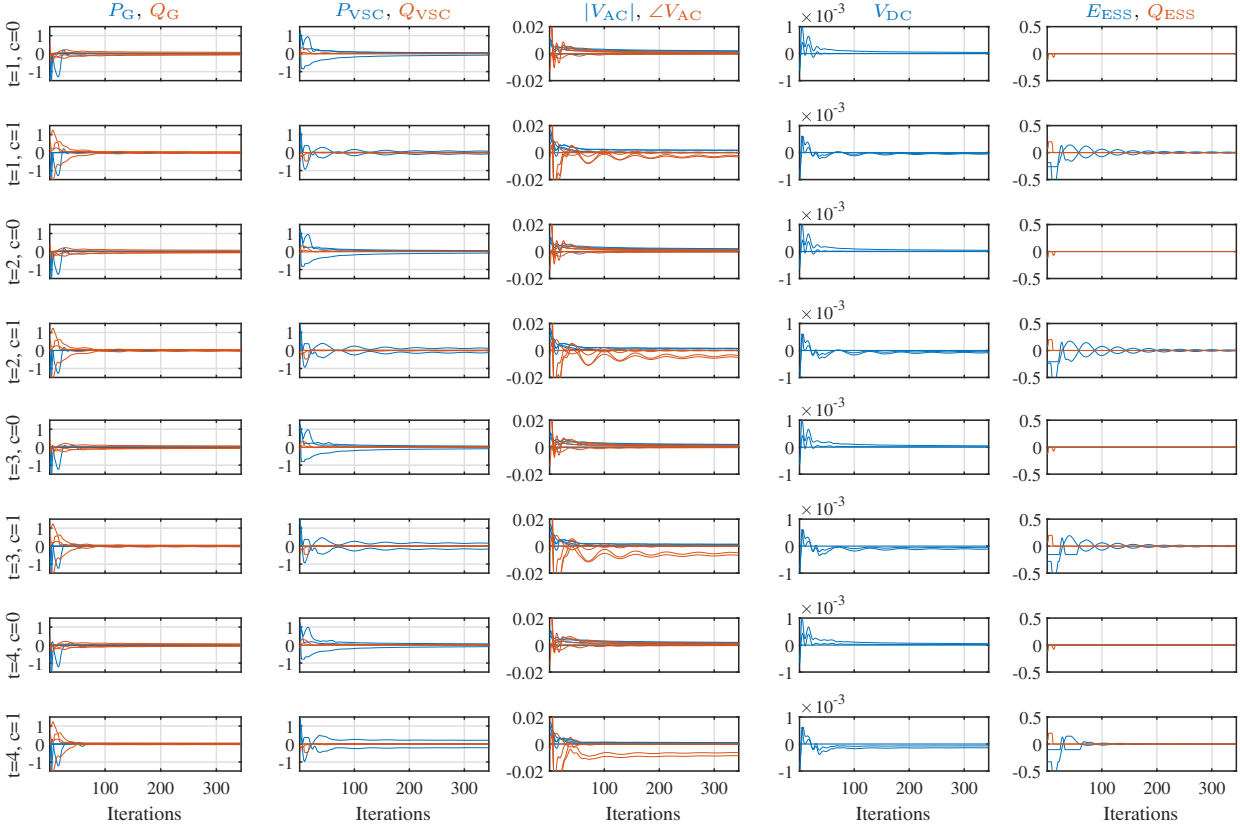

Figure 8.12: Variable difference $X - X^*$ between distributed solution X and central solution X^* for all scenarios in SC-D-OPF.

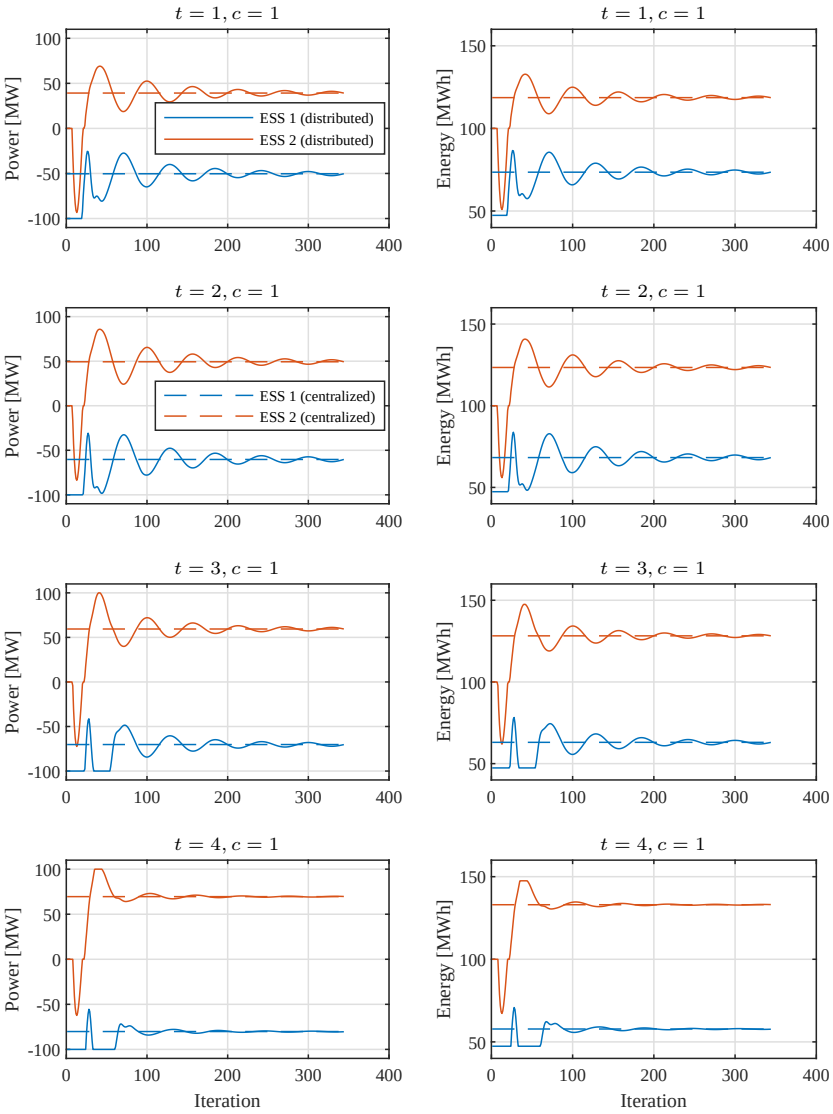

Figure 8.13: Convergence of storage power and energy levels compared to central solution with distributed SC-D-OPF after the outage.

8.5 Summary

The main findings of this chapter are:

- **AC-DC grid partitioning** — the results of two different partitioning methods for hybrid AC-DC grids show that convergence and optimality are comparable. From a computational perspective, there is no reasonable tendency to favor one approach.
- **ADMM vs. ALADIN (I)** — ALADIN converges substantially faster with iteration numbers of 10-17 against 115-189. Optimality of the distributed solutions is excellent with both algorithms, i.e. below 0.005 % cost function error for any case. The computational effort for the update step is substantially larger in ALADIN.
- **ADMM vs. ALADIN (II)** — ALADIN requires a lot of data from the local system operators, such as cost sensitivities of each generator or physical states of the whole network area. Contrarily, ADMM only requires the sharing of information concerning the boundary buses.
- **Multi-area SC-D-OPF** — a proof of concept and functionality is presented in a small system with consideration of N-1 security and dynamics. An acceptable objective error below 0.01 % is achieved, however, the centralized solution is not approached as closely as in the OPF studies.

Chapter 9

Conclusion

9.1 Summary

A versatile optimal power flow framework is presented in Chapter 4. Beside standard OPF network restrictions, a multitude of available constraints is provided to include phase shifting transformers, embedded HVDC and energy storage systems. Multiple time steps can be considered to respect generator ramping and storage energy limits. Various topologies can be included to guarantee feasible load flows after contingencies and to cope with N-1 security. Furthermore, different operating modes are available which allow units to be optimized preventively, curatively or in combination of both. In Chapters 5 and 6 we show extensively the advantages of above-stated assets at hands of a system operator in a stressed power grid. In Chapter 5 we focus on PST and HVDC which introduce distinct degrees of freedom to flexibly re-route power flows in order to relieve network overloads. While a converter simply draws power from a certain node, a PST manipulates the node voltage angle which can be more effective in case of unevenly loaded parallel lines. But clearly, the additional transmission capacity of an embedded DC grid has a great impact on AC side load flow. This is especially the case if it is enabled to be operated in a curative way to reduce preventive generator redispatch. However, in the case of a DC link parallel to an AC contingency, redispatch is only prevented with a restricted HVDC dispatch in the first place, or by the installation of an additional terminal. That terminal does not contribute to transmission capacity – as an additional line would – but provides the flexibility to shift power injections between two converters where one is located close and the other one far from the contingency. We show further that DC-side grid meshing substantially increases flexibility and N-1 reserves, especially under consideration of DC contingencies. In Chapter 6 we focus on the integration of energy storage. ESS *power reserve* after an outage is comparable to a converter, given that the DC

side power flow is not restrictive and that positive and negative curative actions of the storage are complementary to maintain power balance. But, in contrast to a converter, *energy reserve* and herewith the operation strategy before an outage play a role in determining N-1 effectiveness of storage. Clearly, a constant reserve is available if the storage is permanently operated at 50 % state of charge – in that case, large storage potential would be given up. Therefore, we show that the inter-play of predictive control and curative activity is essential to exploit storage capacity during normal operation, but nonetheless reserve sufficient positive or negative capacity in due time before a stressed situation.

Approaches to multi-area optimization are presented in Chapter 7. A detailed description of network decomposition and comprehensive tutorial examples contribute to a profound algorithm understanding of the reader. Advantages and disadvantages in terms of computational effort and necessary information exchange are discussed. Depending on the algorithm, necessary data exchange can reduce to a few variables per boundary bus, which protects the privacy of each control area. The application in two AC-DC case studies follow in Chapter 8. Promising results show good convergence and, more importantly, very small errors in the cost function compared to a centrally computed solution. We point out that we mainly investigate distributed optimization of generator dispatch – however, the simpler case of only optimizing HVDC set points where generator set points are considered non-controllable, is possible as well. Lastly, ADMM is successfully applied to an N-1 secure and dynamic OPF problem.

9.2 Discussion

The considered devices do not require any fuel supply and subsequently, operating costs are comparatively small. Of course, this does not imply that flexibilities and reserves are inexpensive – on the contrary, the installations come with massive investments. Undoubtedly, investment costs for HVDC systems cannot be motivated by additional flexibility only. Transmission capacity is the main driver to avoid different price regions and renewable energy curtailment. Point-to-point connections could possibly do large portions of the transmission job – but effective flexibility is created with multiple terminals, which might be redundant during normal operation. Clearly, such a “reserve” terminal can be expected out of operation for many hours of the year. On the other hand, it should be investigated how many expenses could be saved over the years by avoiding generator redispatch.

Similarly, installing large-scale energy storage systems *only* for the provision of flexible power reserve does not seem economical. Instead, multiple objectives should be aimed for, N-1 security reserve as one of them. However, as of today, additional objectives are hard to realize since not all markets are accessible to a transmission system operator.

This thesis does not claim to have an answer to above-mentioned issues – however, the presented methods can be used supportively to make investment decisions once applied to the respective use cases in order to estimate the benefit of a specific installation.

All of the above assumptions on system optimization and consequently cost minimization have one important requirement in common: reliable communication. Not only must the network be well observed and detailed measurements regularly be sent to the operator. Additionally, the communication and implementation of new optimal set points must be ensured within minutes, if not seconds. Especially after a contingency, the detection of a specific failure and the implementation of related curative measures must be executed in a short time to avoid equipment overloads. Those measures should be pre-calculated and could be sent regularly to the device as a lookup table requiring only a specific trigger, or the set points themselves are sent to the device after an outage has occurred. In any case, communication will be the backbone for an *intelligent* system operation.

9.3 Outlook

The presented optimization framework is highly versatile and covers a wide range of constraints. Nevertheless, model improvements can be done in the following fields:

- We only consider fast curative actions and neglect the time to activate them, which leads to a single new power flow situation. This implies for example, that slower units have enough time to replace power reserve from storage which is inherently limited in time. Those slower units could be modeled explicitly, which would require a **second time frame after the outage has occurred**.
- Iterative prediction updates reduce the error in forecast profiles. Nevertheless, there will remain **uncertainty** which must be dealt with via secondary control. However, the consideration of uncertainty during the optimization could lead to a more robust solution which is near-optimal for a broader range of possible load and RES trajectories.
- In general, explicit incorporation of a large contingency list requires heavy computational effort for realistic grid sizes – even more, if multiple time steps are considered. However, the description of the full problem and simulated case studies must contribute to a thorough understanding of complex interplays. Furthermore, computing power increases every year. Nevertheless, research effort could be put into the **reduction of problem complexity**. Many contingencies are subject to a week coupling to the base case – for example if the provision of reserve after an outage is not restricting

the base case operation. In that case, the two topologies could be treated independently and calculated in parallel.

- **Outages of generators** are not considered in this work, but are straightforward to implement. The violated power balance must then be established by sharing the missing power among the other generators.

Distributed optimization is only starting to evolve. The following aspects should be further investigated:

- We test our methods on two different systems, but **additional case studies** are necessary to better understand convergence properties and dependencies on parameter settings. This includes variations of the cost coefficients and larger grid sizes since realistic transmission systems have hundreds or thousands of buses.

- The application of ADMM to SC-D-OPF is successfully shown for a small problem. The **use of ALADIN for SC-D-OPF** problems is readily implemented but requires further parameter tests. Larger SC-D-OPF problems must be tested.

- With increasing system sizes, the computational costs for the central step are expected to grow faster for ALADIN compared to ADMM. Thus, the **interplay of iteration numbers and computational costs per iteration** in large-scale systems will be of interest.

- While ADMM is fully distributable, i.e. there is no central entity mandatory for coordination, ALADIN still relies on a centralized update step. Additionally, each TSO must provide sensitive information such as generator cost functions or shadow prices of each node, which could be a privacy concern. These issues require further investigations on how to **minimize the necessary information exchange**.

Appendix A

5-Bus Case Data

Table A.1: Line parameters 5-bus AC case/ 3-bus DC case with base power 100 MVA.

Line	Resistance [pu]	Reactance [pu]	Total susceptance [pu]
1-2	0.00281	0.0281	0.00712
1-4	0.00304	0.0304	0.00658
1-5	0.00064	0.0064	0.03126
2-3	0.00108	0.0108	0.01852
4-3	0.00297	0.0297	0.00674
5-4	0.00297	0.0297	0.00674
DC	0.002	0	0

Table A.2: Power demand 5-bus case in Chapter 5.

Node	P_{D} [MW]	Q_{D} [Mvar]
2	300	98.61
3	300	98.61
4	400	131.47

Table A.3: Generator parameters 5-bus case.

Generator	Node	$\underline{P_G}$ [MW]	$\overline{P_G}$ [MW]	$\underline{Q_G}$ [Mvar]	$\overline{Q_G}$ [Mvar]
G1	1	0	170	-127.5	127.5
G2	3	0	520	-390	390
G3	4	0	200	-150	150
G4 (Wind)[1]	5	0	600	-450	450
G5 (PV)[1][2]	3	0	600	-450	450

[1]In Chapter 6, $\overline{P_G}$ is replaced by a time-variant profile from Fig. C.5
[2]Only active in Chapter 6

Table A.4: Generator dispatch and redispatch cost coefficients 5-bus case in Chapters 5 and 6. All other coefficients are zero.

Generator	Cost coefficients		
	$b_G \left[\frac{1}{\text{MW}} \frac{€}{\text{h}}\right]$	$b_{G,Up} \left[\frac{1}{\text{MW}} \frac{€}{\text{h}}\right]$	$b_{G,Down} \left[\frac{1}{\text{MW}} \frac{€}{\text{h}}\right]$
G1	15	100	-2
G2	30	100	-2
G3	40	100	-2
G4 (Wind)	5	100	-1
G5 (PV)[1]	5	100	-1

[1]Only active in Chapter 6

Table A.5: Quadratic generator cost coefficients 5-bus case in Chapter 8.

Generator	Cost coefficients		
	$a_G \left[\frac{1}{\text{MW}^2} \frac{€}{\text{h}}\right]$	$b_G \left[\frac{1}{\text{MW}} \frac{€}{\text{h}}\right]$	$a_q \left[\frac{1}{\text{Mvar}^2} \frac{€}{\text{h}}\right]$
G1	0.010	15	0.001
G2	0.011	30	0.001
G3	0.012	40	0.001
G4	0.013	10	0.001

Table A.6: Energy storage systems in 5-bus case.

Nodes	3, 5
Capacity	200 MWh
Maximal power	100 MW
Minimal energy	20 MWh
Maximal energy	180 MWh
Efficiency	95%
Costs	
– discharge	10 €/MWh
– charge	0 €/MWh

Appendix B

67-Bus Case Data

Table B.1: Generator parameters 67-bus case in Chapters 5.2.1, 5.2.2 and 6.

Generator	Node	$\underline{P_G}$ [MW]	$\overline{P_G}$ [MW]	$\underline{Q_G}$ [Mvar]	$\overline{Q_G}$ [Mvar]
G1	1	0	1000	-500	1,000
G2	4	0	560	-350	350
G3	10	0	560	-350	350
G4	13	0	630	-300	300
G5	18	0	720	-400	400
G6	25	0	560	-250	250
G7	29	0	630	-350	350
G8	33	0	850	-500	500
G9	36	0	720	-400	400
G10	41	0	850	-450	450
G11	43	0	720	-250	500
G12	50	0	720	-400	400
G13	56	0	560	-250	250
G14	59	0	720	-350	350
G15	63	0	520	-300	250
G16	64	0	560	-400	250
G17	66	0	630	-400	300
Wind 1[1]	2	0	1500	-100	100
Wind 2[1]	5	0	1200	-100	100
Wind 3[1]	67	0	800	-100	100
Wind 4[1,2]	54	0	1200	-100	100
Wind 5[1,2]	4	0	1000	-100	100
Wind 6[1,2]	10	0	1000	-100	100

[1] In Chapter 6, $\overline{P_G}$ is replaced by a time-variant profile from Fig. C.6

[2] Only active in Chapter 6

Table B.2: Generator parameters 67-bus case in Chapter 5.2.3 ($\overline{P_{\mathrm{G}}}$ is increased by 10 %).

Generator	Node	$\underline{P_{\mathrm{G}}}$ [MW]	$\overline{P_{\mathrm{G}}}$ [MW]	$\underline{Q_{\mathrm{G}}}$ [Mvar]	$\overline{Q_{\mathrm{G}}}$ [Mvar]
G1	1	0	1100	-500	1.000
G2	4	0	616	-350	350
G3	10	0	616	-350	350
G4	13	0	693	-300	300
G5	18	0	792	-400	400
G6	25	0	616	-250	250
G7	29	0	693	-350	350
G8	33	0	935	-500	500
G9	36	0	792	-400	400
G10	41	0	935	-450	450
G11	43	0	792	-250	500
G12	50	0	792	-400	400
G13	56	0	616	-250	250
G14	59	0	792	-350	350
G15	63	0	572	-300	250
G16	64	0	616	-400	250
G17	66	0	693	-400	300
Wind 1	2	0	1500	-100	100
Wind 2	5	0	1200	-100	100
Wind 3	67	0	800	-100	100

Table B.3: Generator parameters 67-bus case in Chapter 8.3.

Generator	Node	$\underline{P_G}$ [MW]	$\overline{P_G}$ [MW]	$\underline{Q_G}$ [Mvar]	$\overline{Q_G}$ [Mvar]
G1	1	400	1584.0	-500	1,320
G2	4	220	887.0	-350	739.2
G3	10	220	887.0	-350	739.2
G4	13	250	997.9	-300	831.6
G5	18	300	1140.5	-400	950.4
G6	25	220	887.0	-250	739.2
G7	29	250	997.9	-350	831.6
G8	33	350	1346.4	-500	1122
G9	36	300	1140.5	-400	950.4
G10	41	200	1346.4	-450	1122
G11	43	220	1140.5	-250	950.4
G12	50	300	1140.5	-400	950.4
G13	56	220	887.0	-250	739.2
G14	59	300	1140.5	-350	950.4
G15	63	250	823.7	-300	686.4
G16	64	250	887.0	-400	739.2
G17	66	250	997.9	-400	831.6

Table B.4: Line parameters 67-bus case with base power 100 MVA.

Line	Resistance [pu]	Reactance [pu]	Total susceptance [pu]
All AC lines	0.002077562	0.01731302	0
All DC lines	0.0006	0.0348	0.0000144

Table B.5: Power demand 67-bus case.

Node	Chapters 5.2.1, 8.3		Chapters 5.2.2, 5.2.3,	
	P_D [MW]	Q_D [Mvar]	P_D [MW]	Q_D [Mvar]
2	0	-100	0	-100
5	0	-100	0	-100
6	191	76	191	76
8	287	73	287	73
9	186	74	186	74
11	271	55	271	55
12	171	87	171	87
14	199	60	199	60
15	113	52.5	113	52.5
16	38	7	38	7
17	275	106	275	106
19	165	46	165	46
20	178	82.5	178	82.5
22	30	7	30	7
24	32	7	32	7
26	395	89	466.42	89
28	665	99	785.23	99
30	266	100	314.09	100
31	845	119	997.78	119
32	332	137	392.03	137
34	540	158	637.63	158
35	460	97	543.17	97
37	451	190	532.54	190
38	150	0	177.12	0
39	629	87	742.72	87
42	709	180	837.19	180
44	474	92	559.70	92
45	668	109	788.77	109
46	614	95	725.01	95
47	81	-50	95.64	-50
51	430	123	507.74	123
52	309	102	364.87	102
53	100	30	118.08	30
55	303	110	357.78	110
58	324	157	382.58	157
60	115	42	135.79	42
61	187	75	220.81	75
62	319	95	376.68	95
65	315	97	371.95	97

Table B.6: Generator dispatch and redispatch cost coefficients 67-bus case in Chapters 5 and 6. All other coefficients are zero.

Generator	Cost coefficients		
	$b_{\mathrm{G}}\left[\frac{1}{\mathrm{MW}}\frac{€}{\mathrm{h}}\right]$	$b_{\mathrm{G,Up}}\left[\frac{1}{\mathrm{MW}}\frac{€}{\mathrm{h}}\right]$	$b_{\mathrm{G,Down}}\left[\frac{1}{\mathrm{MW}}\frac{€}{\mathrm{h}}\right]$
Area 1	20	100	-2
Area 2	100	100	-2
Area 3	20	100	-2
Wind	5	100	-2

Table B.7: Quadratic generator cost coefficients for 66-bus case in Chapter 8.

Generator	Cost coefficients		
	$a_{\mathrm{G}}\left[\frac{1}{\mathrm{MW}^2}\frac{€}{\mathrm{h}}\right]$	$b_{\mathrm{G}}\left[\frac{1}{\mathrm{MW}}\frac{€}{\mathrm{h}}\right]$	$a_{\mathrm{q}}\left[\frac{1}{\mathrm{Mvar}^2}\frac{€}{\mathrm{h}}\right]$
G1	0.0141	14.1	0.001
G2	0.0145	14.5	0.001
G3	0.0106	10.6	0.001
G4	0.0146	14.6	0.001
G5	0.0132	13.2	0.001
G6	0.0105	10.5	0.001
G7	0.0164	16.4	0.001
G8	0.0177	17.7	0.001
G9	0.0198	19.8	0.001
G10	0.0198	19.8	0.001
G11	0.0158	15.8	0.001
G12	0.0199	19.9	0.001
G13	0.0148	14.8	0.001
G14	0.0124	12.4	0.001
G15	0.0140	14.0	0.001
G16	0.0107	10.7	0.001
G17	0.0121	12.1	0.001

Table B.8: Generator dispatch set points (OPF results) for various redispatch studies in the 67-bus case. All values in [MW].

Generator	Section 5.2.1	Section 5.2.2	Section 5.2.3	
			DC-Stage 1	DC-Stage 2
G1	700	1000	1100	1100
G2	523	560	616	616
G3	436	560	616	616
G4	541	630	693	693
G5	681	720	792	792
G6	469	560	616	616
G7	500	630	621.3	609.7
G8	496	850	935	935
G9	512	720	792	792
G10	350	561.8	87.1	155.2
G11	574	0	0	0
G12	581	720	386.1	296.6
G13	496	560	616	616
G14	431	720	792	792
G15	488	520	572	572
G16	300	560	616	616
G17	537	630	693	693
Wind 1	1500	1500	1500	1500
Wind 2	1200	1200	1200	1200
Wind 3	800	800	800	800

Table B.9: Energy storage systems in 67-bus case.

Nodes	2, 5, 18, 21, 26, 35, 45, 54
Capacity	600 MWh
Maximal power	300 MW
Minimal energy	60 MWh
Maximal energy	540 MWh
Efficiency	95%
Costs	
– discharge	10 €/MWh
– charge	-5 €/MWh

Appendix C

Power Profiles for Multi-Time Step Calculations

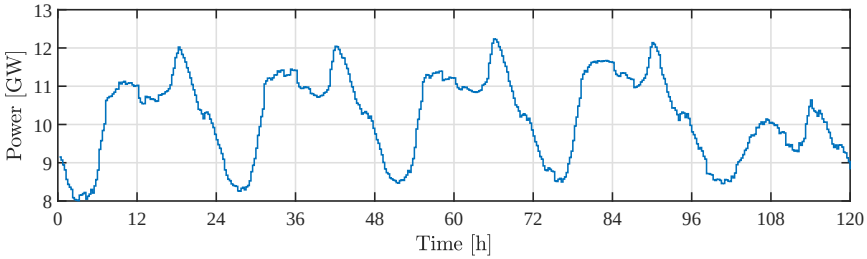

Figure C.1: Load forecast "most recent" from *Elia* for 13.11.2018 to 17.11.2018.

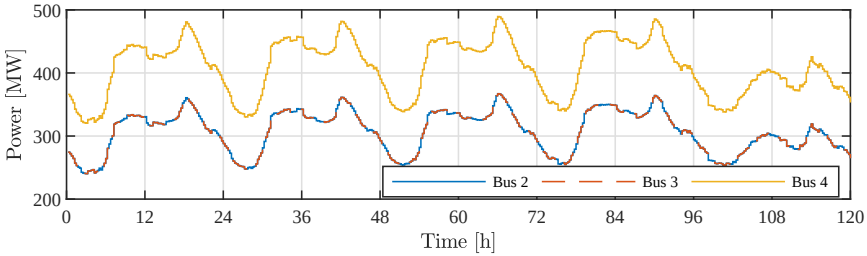

Figure C.2: Load profiles adapted for multi-period calculations in the 5-bus case.

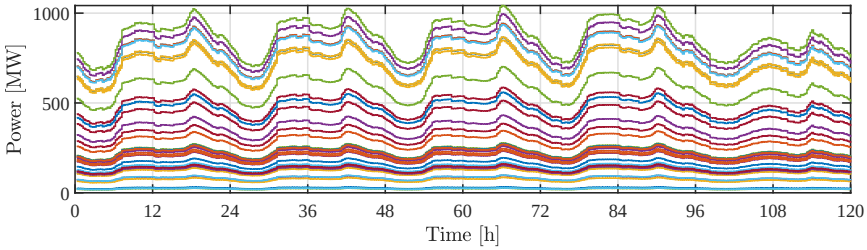

Figure C.3: Load profiles adapted for multi-period calculations in the 67-bus case.

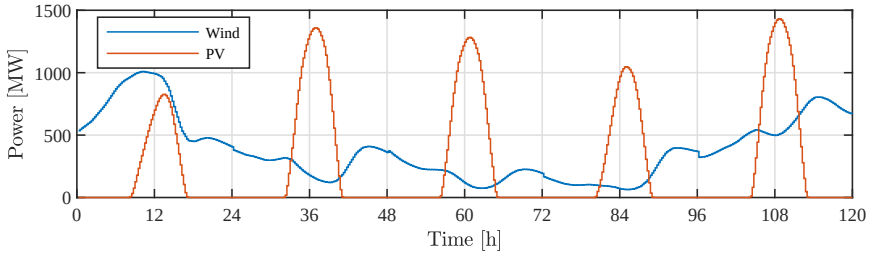

Figure C.4: RES forecast "day-ahead" from *Elia* for 13.11.2018 to 17.11.2018. Wind data is filtered to "Belgian onshore wind farms".

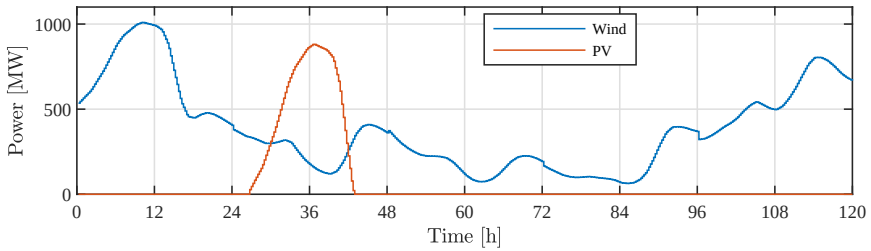

Figure C.5: RES profiles adapted for multi-period calculations in the 5-bus case.

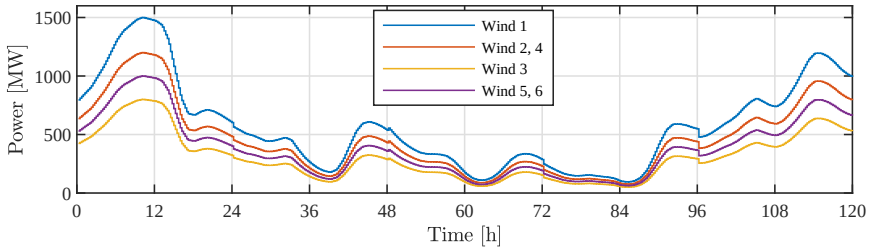

Figure C.6: RES profiles adapted for multi-period calculations in the 67-bus case.

Appendix D

Implementation of Distributed Algorithms

D.1 Augmentation of the Objective

D.1.1 ADMM

The augmented Lagrangian for region k (7.19) is expressed by

$$\mathcal{L}_k(x_k, z_k, \lambda_k) = F_k(x_k) + \underbrace{\lambda_k^\top A_k x_k + \frac{\rho_k}{2}||A_k(x_k - z_k)||_W^2}_{\tilde{F}_k}. \tag{D.1}$$

The augmenting part $\tilde{F}_k$, its derivate $\nabla\tilde{F}_k$ and Hessian $\nabla^2\tilde{F}_k$ (all with respect to x_k), respectively, are written in matrix notation as

$$\tilde{F}_k = \lambda_k^\top A_k x_k + \frac{1}{2}(A_k(x_k - z_k))^\top \rho_k W_k A_k(x_k - z_k) \tag{D.2}$$

$$\nabla\tilde{F}_k = A_k^\top \lambda_k + A_k^\top \rho_k W_k A_k(x_k - z_k) \tag{D.3}$$

$$\nabla^2\tilde{F}_k = A_k^\top \rho_k W_k A_k. \tag{D.4}$$

D.1.2 ALADIN

The augmented Lagrangian for region k (7.24) is expressed by

$$\mathcal{L}_k(x_k, z_k, \lambda) = F_k(x_k) + \underbrace{\lambda^\top A_k x_k + \frac{\rho}{2}||x_k - z_k||_{W_k}^2}_{\tilde{F}_k}. \tag{D.5}$$

The augmenting part $\tilde{F}$, its derivate $\nabla\tilde{F}$ and Hessian $\nabla^2\tilde{F}$ (all with respect to x_k), respectively, are written in matrix notation as

$$\tilde{F}_k = \lambda^\top A_k x_k + \frac{1}{2}(x_k - z_k)^\top \rho W_k (x_k - z_k) \tag{D.6}$$

$$\nabla\tilde{F}_k = A_k^\top \lambda + \rho W_k (x_k - z_k) \tag{D.7}$$

$$\nabla^2\tilde{F}_k = \rho W_k. \tag{D.8}$$

D.2 Quadratic Problem in ALADIN

The original problem (7.26) is

$$\underset{\Delta x, s}{\text{minimize}} \quad \sum_{k\in\mathcal{R}} \left\{ \frac{1}{2}\Delta x_k^\top H_k \Delta x_k + g_k^\top \Delta x_k \right\} + \lambda^\top s + \frac{\mu}{2}||s||_2^2 \tag{D.9a}$$

$$\text{subject to} \quad \sum_{k\in\mathcal{R}} A_k(x_k + \Delta x_k) = s \quad | \ \lambda_{\text{QP}} \tag{D.9b}$$

$$C_k \Delta x_k = 0, \quad \forall k \in \mathcal{R}. \tag{D.9c}$$

In matrix notation it becomes

$$\underset{\Delta x, s}{\text{minimize}} \quad \frac{1}{2}\begin{bmatrix}\Delta x^\top & s^\top\end{bmatrix} \underbrace{\begin{bmatrix} H & 0 \\ 0 & \mu\cdot\mathbf{1}\end{bmatrix}}_{L} \begin{bmatrix}\Delta x \\ s\end{bmatrix} + \underbrace{\begin{bmatrix} g^\top & \lambda^\top\end{bmatrix}}_{f} \underbrace{\begin{bmatrix}\Delta x \\ s\end{bmatrix}}_{x} \tag{D.10a}$$

$$\text{subject to} \quad \underbrace{\begin{bmatrix} A & -\mathbf{1} \\ C & 0\end{bmatrix}}_{B} \begin{bmatrix}\Delta x \\ s\end{bmatrix} = \underbrace{\begin{bmatrix} -Ax \\ 0\end{bmatrix}}_{b} \tag{D.10b}$$

with $H = \text{diag}(H_1, .., H_R)$, $C = \text{diag}(C_1, .., C_R)$, $g = [g_1^\top, .., g_R^\top]^\top$ and $\mathbf{1}$ the identity matrix. The equivalent linear equation system is

$$\begin{bmatrix} L & B^\top \\ B & 0\end{bmatrix} \begin{bmatrix}\Delta x \\ s \\ \lambda_{\text{QP}} \\ \zeta\end{bmatrix} = \begin{bmatrix} -f^\top \\ b\end{bmatrix}. \tag{D.11}$$

D.3 Simple 2-Bus Example

Consensus matrices:

$$A_1 = \begin{bmatrix} 0 & 1 & 0 & 0 & 0 & 0 & 0 & 0 \\ 0 & 0 & 0 & 1 & 0 & 0 & 0 & 0 \\ 0 & 0 & 0 & 0 & 0 & 1 & 0 & 0 \\ 0 & 0 & 0 & 0 & 0 & 0 & 0 & 1 \end{bmatrix} \tag{D.12a}$$

$$A_2 = \begin{bmatrix} 0 & -1 & 0 & 0 & 0 & 0 \\ 0 & 0 & 0 & -1 & 0 & 0 \\ 0 & 0 & 0 & 0 & 1 & 0 \\ 0 & 0 & 0 & 0 & 0 & 1 \end{bmatrix} \tag{D.12b}$$

D.3.1 ADMM

Weighting matrix:

$$W = \begin{bmatrix} 100 & 0 & 0 & 0 \\ 0 & 100 & 0 & 0 \\ 0 & 0 & 1 & 0 \\ 0 & 0 & 0 & 1 \end{bmatrix} \tag{D.13}$$

D.3.2 ALADIN

Weighting matrices:

$$W_1 = \begin{bmatrix} 100 & 0 & 0 & 0 & 0 & 0 & 0 & 0 \\ 0 & 100 & 0 & 0 & 0 & 0 & 0 & 0 \\ 0 & 0 & 100 & 0 & 0 & 0 & 0 & 0 \\ 0 & 0 & 0 & 100 & 0 & 0 & 0 & 0 \\ 0 & 0 & 0 & 0 & 1 & 0 & 0 & 0 \\ 0 & 0 & 0 & 0 & 0 & 1 & 0 & 0 \\ 0 & 0 & 0 & 0 & 0 & 0 & 1 & 0 \\ 0 & 0 & 0 & 0 & 0 & 0 & 0 & 1 \end{bmatrix} \tag{D.14a}$$

$$W_2 = \begin{bmatrix} 100 & 0 & 0 & 0 & 0 & 0 \\ 0 & 100 & 0 & 0 & 0 & 0 \\ 0 & 0 & 100 & 0 & 0 & 0 \\ 0 & 0 & 0 & 100 & 0 & 0 \\ 0 & 0 & 0 & 0 & 1 & 0 \\ 0 & 0 & 0 & 0 & 0 & 1 \end{bmatrix} \tag{D.14b}$$

Objective gradients:

$$g_1 = \begin{bmatrix} 0 & 0 & 0 & 0 & 100 & 0 & 0 & 0 \end{bmatrix}^\mathsf{T} \tag{D.15a}$$

$$g_2 = \begin{bmatrix} 0 & 0 & 0 & 0 & 0 & 0 \end{bmatrix}^\mathsf{T} \tag{D.15b}$$

Active set matrices:

$$C_1 = 100 \begin{bmatrix} 2F_1 - F_3 & G_3 & -F_3 & -G_3 & 1 & 0 \\ -F_1 & -G_1 & 2F_3 - F_1 & G_1 & 0 & 0 \\ 2G_1 - G_3 & -F_3 & -G_3 & F_3 & 0 & 1 \\ -G_1 & F_1 & 2G_3 - G_1 & -F_1 & 0 & 0 \\ -1 & 0 & 0 & 0 & 0 & 0 \\ 0 & 0 & -1 & 0 & 0 & 0 \\ 0 & -1 & 0 & 0 & 0 & 0 \\ 0 & 0 & 0 & -1 & 0 & 0 \end{bmatrix} \tag{D.16a}$$

$$C_2 = 100 \begin{bmatrix} 2F_2 - F_4 & G_4 & -F_4 & -G_4 \\ -F_2 & -G_2 & 2F_4 - F_2 & G_4 \\ 2G_2 - G_4 & -F_4 & -G_4 & 0 \\ -G_2 & F_2 & 2G_4 - G_2 & F_4 - F_2 \\ 0 & 0 & -1 & 0 \\ 0 & 0 & 0 & -1 \end{bmatrix} \tag{D.16b}$$

Hessian matrices:

$$H_1 = 100 \begin{bmatrix} 2\kappa_1 & -\kappa_1 - \kappa_3 & 0 & \kappa_2 - \kappa_4 & 0 & 0 & 0 & 0 \\ -\kappa_1 - \kappa_3 & 2\kappa_3 & \kappa_4 - \kappa_2 & 0 & 0 & 0 & 0 & 0 \\ 0 & \kappa_4 - \kappa_2 & 2\kappa_1 & -\kappa_1 - \kappa_3 & 0 & 0 & 0 & 0 \\ \kappa_2 - \kappa_4 & 0 & -\kappa_1 - \kappa_3 & 2\kappa_3 & 0 & 0 & 0 & 0 \\ 0 & 0 & 0 & 0 & 0 & 0 & 0 & 0 \\ 0 & 0 & 0 & 0 & 0 & 0 & 0 & 0 \\ 0 & 0 & 0 & 0 & 0 & 0 & 0 & 0 \\ 0 & 0 & 0 & 0 & 0 & 0 & 0 & 0 \end{bmatrix} \tag{D.17a}$$

$$H_2 = 100 \begin{bmatrix} 2\sigma_1 & -\sigma_1 - \sigma_3 & 0 & \sigma_2 - \sigma_4 & 0 & 0 \\ -\sigma_1 - \sigma_3 & 2\sigma_3 & -\sigma_2 & \sigma_4 & 0 & 0 \\ 0 & -\sigma_2 & 2\sigma_1 & -\sigma_1 - \sigma_3 & 0 & 0 \\ \sigma_2 - \sigma_4 & \sigma_4 & -\sigma_1 - \sigma_3 & 2\sigma_3 & 0 & 0 \\ 0 & 0 & 0 & 0 & 0 & 0 \\ 0 & 0 & 0 & 0 & 0 & 0 \end{bmatrix} \tag{D.17b}$$

Appendix E

Bibliography

E.1 References

[1] 50Hertz, Amprion, TenneT, TransnetBW. Netzentwicklungsplan Strom 2030, Version 2019. Erster Entwurf der Übertragungsnetzbetreiber.

[2] O. Alsac and B. Stott. Optimal load flow with steady-state security. *IEEE Transactions on Power Apparatus and Systems*, PAS-93(3):745–751, May 1974.

[3] S. An, J. Condren, and T. W. Gedra. An ideal transformer UPFC model, OPF first-order sensitivities, and application to screening for optimal UPFC locations. *IEEE Transactions on Power Systems*, 22(1):68–75, February 2007.

[4] M. Aragüés-Peñalba, A. Egea Alvarez, S. Galceran Arellano, and O. Gomis-Bellmunt. Optimal power flow tool for mixed high-voltage alternating current and high-voltage direct current systems for grid integration of large wind power plants. *IET Renewable Power Generation*, 9(8):876–881, 2015.

[5] R. Baldick, B. H. Kim, C. Chase, and Yufeng Luo. A fast distributed implementation of optimal power flow. *IEEE Transactions on Power Systems*, 14(3):858–864, August 1999.

[6] M. Baradar, M. R. Hesamzadeh, and M. Ghandhari. Second-order cone programming for optimal power flow in VSC-type AC-DC grids. *IEEE Transactions on Power Systems*, 28(4):4282–4291, November 2013.

[7] P. Boggs and J. W. Tolle. Sequential quadratic programming. *Acta Numerica*, 4:1–51, January 1995.

[8] S. Boyd, N. Parikh, E. Chu, B. Peleato, and J. Eckstein. Distributed optimization and statistical learning via the alternating direction method of multipliers. *Found. Trends Mach. Learn.*, 3(1):1–122, January 2011.

[9] Bundesnetzagentur. Monitoring report 2014.

[10] Bundesnetzagentur. Quartalsbericht zu Netz- und Systemsicherheitsmaßnahmen. Erstes Quartal 2018.

[11] J. Cao, W. Du, and H. Wang. An improved corrective security constrained OPF with distributed energy storage. *IEEE Transactions on Power Systems*, 31(2):1537–1545, March 2016.

[12] J. Cao, W. Du, and H. F. Wang. An improved corrective security constrained OPF for meshed AC/DC grids with multi-terminal VSC-HVDC. *IEEE Transactions on Power Systems*, 31(1):485–495, January 2016.

[13] J. Cao, W. Du, H. F. Wang, and S. Q. Bu. Minimization of transmission loss in meshed AC/DC grids with VSC-MTDC networks. *IEEE Transactions on Power Systems*, 28(3):3047–3055, August 2013.

[14] F. Capitanescu. Enhanced risk-based SCOPF formulation balancing operation cost and expected voluntary load shedding. *Electric Power Systems Research*, 128:151–155, November 2015.

[15] F. Capitanescu. Critical review of recent advances and further developments needed in AC optimal power flow. *Electric Power Systems Research*, 136:57–68, July 2016.

[16] F. Capitanescu, J.L. Martinez Ramos, P. Panciatici, D. Kirschen, A. Marano Marcolini, L. Platbrood, and L. Wehenkel. State-of-the-art, challenges, and future trends in security constrained optimal power flow. *Electric Power Systems Research*, 81(8):1731–1741, August 2011.

[17] J. Carpentier. Contribution a l'etude du dispatching economique. *Bulletin de la Societe Francaise des Electriciens*, 3:431–447, August 1962.

[18] D. Chattopadhyay. Daily generation scheduling: quest for new models. *IEEE Transactions on Power Systems*, 13(2):624–629, May 1998.

[19] A. J. Conejo, F. J. Nogales, and F. J. Prieto. A decomposition procedure based on approximate Newton directions. *Mathematical Programming*, 93(3):495–515, December 2002.

[20] A.S. Costa, W. Uturbey, S. Nakanishi, A. de Marco, and S.S. Pacheco. An OPF based tool for demand relief programs. In *IEEE/PES Transmision and Distribution Conference and Exposition: Latin America (IEEE Cat. No. 04EX956)*. IEEE, 2004.

[21] E. Cotilla-Sanchez, P. D. H. Hines, C. Barrows, S. Blumsack, and M. Patel. Multi-attribute partitioning of power networks based on electrical distance. *IEEE Transactions on Power Systems*, 28(4):4979–4987, November 2013.

[22] H. Dommel and W. Tinney. Optimal power flow solutions. *IEEE Transactions on Power Apparatus and Systems*, PAS-87(10):1866–1876, October 1968.

[23] J. Eickmann, C. Bredtmann, and A. Moser. Security-constrained optimization framework for large-scale power systems including post-contingency remedial actions and inter-temporal constraints. In *Trends in Mathematics*, pages 47–63. Springer International Publishing, 2017.

[24] A. Engelmann, Y. Jiang, T. Mühlpfordt, B. Houska, and T. Faulwasser. Toward distributed OPF using ALADIN. *IEEE Transactions on Power Systems*, 34(1):584–594, January 2019.

[25] A. Engelmann, T. Mühlpfordt, Y. Jiang, B. Houska, and T. Faulwasser. Distributed AC optimal power flow using ALADIN. In *IFAC-PapersOnLine*, volume 50, pages 5536–5541. 20th IFAC World Congress, July 2017.

[26] ENTSO-E. Operation Handbook.

[27] ENTSO-E. Operation Handbook - Appendix 3: Operational Security.

[28] ENTSO-E. Operation Handbook - Policy 3: Operational Security.

[29] ENTSO-E. Operation Handbook - Policy 5: Emergency Operations.

[30] ENTSO-E. Research, Development & Innovation roadmap 2017 – 2026.

[31] ENTSO-E. First joint report on the progress and potential problems with the implementation of intraday and day-ahead coupling as well as forward capacity allocation, August 2018.

[32] T. Erseghe. Distributed optimal power flow using ADMM. *IEEE Transactions on Power Systems*, 29(5):2370–2380, September 2014.

[33] T. Erseghe. A distributed approach to the OPF problem. *EURASIP Journal on Advances in Signal Processing*, 2015(1):45, May 2015.

[34] G. A. Ezhilarasi and S. Swarup. Network partitioning using harmony search and equivalencing for distributed computing. *Journal of Parallel and Distributed Computing*, 72:936–943, August 2012.

[35] W. Feng, L. A. Tuan, L. B. Tjernberg, A. Mannikoff, and A. Bergman. A new approach for benefit evaluation of multiterminal VSC-HVDC using a proposed mixed AC/DC optimal power flow. *IEEE Transactions on Power Delivery*, 29(1):432–443, February 2014.

[36] E.B. Fisher, R.P. O. Neill, and M.C. Ferris. Optimal transmission switching. *IEEE Transactions on Power Systems*, 23(3):1346–1355, August 2008.

[37] A. Fuchs, J. Garrison, and T. Demiray. A security-constrained multi-period OPF for the locational allocation of automatic reserves. In *2017 IEEE Manchester PowerTech*, pages 1–6, June 2017.

[38] A. Gabash and P. Li. Active-reactive optimal power flow in distribution networks with embedded generation and battery storage. *IEEE Transactions on Power Systems*, 27(4):2026–2035, November 2012.

[39] L. L. Garver. Power generation scheduling by integer programming-development of theory. *Transactions of the American Institute of Electrical Engineers. Part III: Power Apparatus and Systems*, 81(3):730–734, April 1962.

[40] S.Y. Ge and T.S. Chung. Optimal active power flow incorporating power flow control needs in flexible AC transmission systems. *IEEE Transactions on Power Systems*, 14(2):738–744, May 1999.

[41] P. Gill, W. Murray, and M. Wright. *Practical optimization*. Academic Press, London, 1981.

[42] S. Gill, I. Kockar, and G.W. Ault. Dynamic optimal power flow for active distribution networks. *Power Systems, IEEE Transactions on*, 29(1):121–131, January 2014.

[43] J. Guo, G. Hug, and O. K. Tonguz. Intelligent partitioning in distributed optimization of electric power systems. *IEEE Transactions on Smart Grid*, 7(3):1249–1258, May 2016.

[44] J. Guo, G. Hug, and O. K. Tonguz. A case for nonconvex distributed optimization in large-scale power systems. *IEEE Transactions on Power Systems*, 32(5):3842–3851, September 2017.

[45] B. Houska, J. Frasch, and M. Diehl. An augmented lagrangian based algorithm for distributed nonconvex optimization. *SIAM Journal on Optimization*, 26, April 2016.

[46] G. Hug-Glanzmann and G. Andersson. Decentralized optimal power flow control for overlapping areas in power systems. *IEEE Transactions on Power Systems*, 24(1):327–336, February 2009.

[47] E. Iggland, R. Wiget, S. Chatzivasileiadis, and G. Anderson. Multi-area DC-OPF for HVAC and HVDC grids. *IEEE Transactions on Power Systems*, 30(5):2450–2459, September 2015.

[48] R. A. Jabr, S. Karaki, and J. A. Korbane. Robust multi-period OPF with storage and renewables. *IEEE Transactions on Power Systems*, 30(5):2790–2799, September 2015.

[49] P. Javanbakht and S. Mohagheghi. A risk-averse security-constrained optimal power flow for a power grid subject to hurricanes. *Electric Power Systems Research*, 116:408–418, November 2014.

[50] K. Karoui, L. Platbrood, H. Crisciu, and R. A. Waltz. New large-scale security constrained optimal power flow program using a new interior point algorithm. In *2008 5th International Conference on the European Electricity Market*. IEEE, May 2008.

[51] B. H. Kim and R. Baldick. Coarse-grained distributed optimal power flow. *IEEE Transactions on Power Systems*, 12(2):932–939, May 1997.

[52] B. H. Kim and R. Baldick. A comparison of distributed optimal power flow algorithms. *IEEE Transactions on Power Systems*, 15(2):599–604, May 2000.

[53] H. W. Kuhn and A. W. Tucker. Nonlinear programming. In *Proceedings of the Second Berkeley Symposium on Mathematical Statistics and Probability*, pages 481–492, Berkeley, Calif., 1951. University of California Press.

[54] A. J. Lamadrid, T. D. Mount, and R. J. Thomas. Scheduling of energy storage systems with geographically distributed renewables. In *IEEE Ninth International Symposium on Parallel and Distributed Processing with Applications Workshops*. IEEE, May 2011.

[55] A. J. Lamadrid, D. L. Shawhan, C. E. Murillo-S á nchez, R. D. Zimmerman, Y. Zhu, D. J. Tylavsky, A. G. Kindle, and Z. Dar. Stochastically optimized, carbon-reducing dispatch of storage, generation, and loads. *IEEE Transactions on Power Systems*, 30(2):1064–1075, March 2015.

[56] C. Lehmkoster. Security constrained optimal power flow for an economical operation of FACTS-devices in liberalized energy markets. *IEEE Transactions on Power Delivery*, 17(2):603–608, April 2002.

[57] F. Li and R. Bo. Small test systems for power system economic studies. In *IEEE PES General Meeting*, pages 1–4, July 2010.

[58] A. K. Marten and D. Westermann. Schedule for converters of a meshed HVDC grid and a contingency schedule for adaption to unscheduled power flow changes. In *IEEE PES General Meeting*, pages 1–5, July 2013.

[59] A. Mesanovic, U. Munz, and C. Ebenbauer. Robust optimal power flow for mixed AC/DC transmission systems with volatile renewables. *IEEE Transactions on Power Systems*, 33(5):5171–5182, September 2018.

[60] S. Mhanna, G. Verbic, and A. C. Chapman. A component-based dual decomposition method for the OPF problem. *CoRR*, abs/1704.03647, 2017.

[61] D. K. Molzahn, F. Dörfler, H. Sandberg, S. H. Low, S. Chakrabarti, R. Baldick, and J. Lavaei. A survey of distributed optimization and control algorithms for electric power systems. *IEEE Transactions on Smart Grid*, 8(6):2941–2962, November 2017.

[62] J.A. Momoh, R. Adapa, and M.E. El-Hawary. A review of selected optimal power flow literature to 1993. I. nonlinear and quadratic programming approaches. *IEEE Transactions on Power Systems*, 14(1):96–104, February 1999.

[63] J.A. Momoh, M.E. El-Hawary, and R. Adapa. A review of selected optimal power flow literature to 1993. II. Newton, linear programming and interior point methods. *IEEE Transactions on Power Systems*, 14(1):105–111, February 1999.

[64] J.A. Momoh and J.Z. Zhu. A new approach to optimal power flow with phase shifter. In *IEEE International Conference on Systems, Man, and Cybernetics (Cat. No.98CH36218)*. IEEE, 1998.

[65] A. Monticelli, M. V. F. Pereira, and S. Granville. Security-constrained optimal power flow with post-contingency corrective rescheduling. *IEEE Transactions on Power Systems*, 2(1):175–180, February 1987.

[66] C. E. Murillo-Sanchez, R. D. Zimmerman, C. L. Anderson, and R. J. Thomas. Secure planning and operations of systems with stochastic sources, energy storage, and active demand. *IEEE Transactions on Smart Grid*, 4(4):2220–2229, December 2013.

[67] C. E. Murillo-Sanchez, R. D. Zimmerman, C. L. Anderson, and R. J. Thomas. A stochastic, contingency-based security-constrained optimal power flow for the procurement of energy and distributed reserve. *Decision Support Systems*, 56:1–10, December 2013.

[68] I.M. Nejdawi, K.A. Clements, L.M. Kimball, and P.W. Davis. Nonlinear optimal power flow with intertemporal constraints. *IEEE Power Engineering Review*, 20(5):74–75, May 2000.

[69] F. J. Nogales, F. J. Prieto, and A. J. Conejo. A decomposition methodology applied to the multi-area optimal power flow problem. *Annals of Operations Research*, 120(1):99–116, April 2003.

[70] D. E. Olivares, C. A. Canizares, and M. Kazerani. A centralized energy management system for isolated microgrids. *IEEE Transactions on Smart Grid*, 5(4):1864–1875, July 2014.

[71] A.D. Papalexopoulos, C.F. Imparato, and F.F. Wu. Large-scale optimal power flow: effects of initialization, decoupling and discretization. *IEEE Transactions on Power Systems*, 4(2):748–759, May 1989.

[72] A. Pizano-Martinez, C. R. Fuerte-Esquivel, H. Ambriz-PÉrez, and E. Acha. Modeling of VSC-based HVDC systems for a Newton-Raphson OPF algorithm. *IEEE Transactions on Power Systems*, 22(4):1794–1803, November 2007.

[73] J. Rimez and R. Belmans. A combined AC/DC optimal power flow algorithm for meshed AC and DC networks linked by VSC converters. *International Transactions on Electrical Energy Systems*, 25(10):2024–2035, June 2014.

[74] V. Saplamidis, R. Wiget, and G. Andersson. Security constrained optimal power flow for mixed AC and multi-terminal HVDC grids. In *2015 IEEE Eindhoven PowerTech*, pages 1–6, June 2015.

[75] F. Sass, T. Sennewald, A. K. Marten, and D. Westermann. Mixed AC high-voltage direct current benchmark test system for security constrained optimal power flow calculation. *IET Generation, Transmission Distribution*, 11(2):447–455, 2017.

[76] H. Sharifzadeh, N. Amjady, and H. Zareipour. Multi-period stochastic security-constrained OPF considering the uncertainty sources of wind power, load demand and equipment unavailability. *Electric Power Systems Research*, 146:33–42, May 2017.

[77] G.L. Torres and V.H. Quintana. An interior-point method for nonlinear optimal power flow using voltage rectangular coordinates. *IEEE Transactions on Power Systems*, 13(4):1211–1218, 1998.

[78] W. Uturbey and A. S. Costa. Dynamic optimal power flow approach to account for consumer response in short term hydrothermal coordination studies. *IET Generation, Transmission & Distribution*, 1(3):414, 2007.

[79] J. Verboomen. *Optimisation of Transmission Systems by use of Phase Shifting Transformers*. PhD thesis, TU Delft, 2008.

[80] A. Wächter and L. T. Biegler. On the implementation of an interior-point filter line-search algorithm for large-scale nonlinear programming. *Mathematical Programming*, 106(1):25–57, March 2006.

[81] Q. Wang, J. D. McCalley, T. Zheng, and E. Litvinov. A computational strategy to solve preventive risk-based security-constrained OPF. *IEEE Transactions on Power Systems*, 28(2):1666–1675, May 2013.

[82] Q. Wang, J. D. McCalley, T. Zheng, and E. Litvinovv. Solving corrective risk-based security-constrained optimal power flow with lagrangian relaxation and benders decomposition. *International Journal of Electrical Power & Energy Systems*, 75:255–264, February 2016.

[83] H. Wei, H. Sasaki, J. Kubokawa, and R. Yokoyama. An interior point nonlinear programming for optimal power flow problems with a novel data structure. *IEEE Transactions on Power Systems*, 13(3):870–877, 1998.

[84] H. Wei, H. Sasaki, J. Kubokawa, and R. Yokoyama. Large scale hydrothermal optimal power flow problems based on interior point nonlinear programming. *IEEE Transactions on Power Systems*, 15(1):396–403, 2000.

[85] Y. Wen, C. Guo, D. S. Kirschen, and S. Dong. Enhanced security-constrained OPF with distributed battery energy storage. *IEEE Transactions on Power Systems*, 30(1):98–108, January 2015.

[86] Y. Wen, C. Guo, H. Pandzic, and D. S. Kirschen. Enhanced security-constrained unit commitment with emerging utility-scale energy storage. *IEEE Transactions on Power Systems*, 31(1):652–662, January 2016.

[87] R. Wiget and G. Andersson. Optimal power flow for combined AC and multi-terminal HVDC grids based on VSC converters. In *IEEE PES General Meeting*, pages 1–8, July 2012.

[88] R. Wiget, E. Iggland, and G. Andersson. Security constrained optimal power flow for HVAC and HVDC grids. In *2014 Power Systems Computation Conference*. IEEE, August 2014.

[89] Y.-C. Wu, A.S. Debs, and R.E. Marsten. A direct nonlinear predictor-corrector primal-dual interior point algorithm for optimal power flows. *IEEE Transactions on Power Systems*, 9(2):876–883, May 1994.

[90] K. Xie and Y.H. Song. Optimal power flow with time-related constraints by a nonlinear interior point method. In *IEEE Power Engineering Society Winter Meeting. Conference Proceedings (Cat. No.00CH37077)*. IEEE, 2000.

[91] R. Yang and G. Hug. Potential and efficient computation of corrective power flow control in cost vs. risk trade-off. *IEEE Transactions on Smart Grid*, 5(4):2033–2043, July 2014.

[92] A. Zerrahn, W. Schill, and C. Kemfert. On the economics of electrical storage for variable renewable energy sources. *European Economic Review*, 108:259–279, September 2018.

E.2 Related work

E.2.1 Peer-reviewed journal articles

[93] N. Meyer-Hübner, M. Suriyah, and T. Leibfried. Distributed Optimal Power Flow in Hybrid AC–DC Grids. *IEEE Transactions on Power Systems*, 34(4):2937–2946, July 2019.

E.2.2 Conference articles

[94] N. Hübner, N. Schween, M. Suriyah, V. Heuveline, and T. Leibfried. Multi-area coordination of security-constrained dynamic optimal power flow in AC-DC grids with energy storage. In Valentin Bertsch, Wolf Fichtner, Vincent Heuveline, and Thomas Leibfried, editors, *Trends in Mathematics*. Springer International Publishing, 2019.

[95] N. Meyer-Hübner, F. Gielnik, M. Suriyah, and T. Leibfried. Dynamic optimal power flow in AC networks with multi-terminal HVDC and energy storage. In *2016 IEEE Innovative Smart Grid Technologies - Asia (ISGT-Asia)*. IEEE, November 2016.

[96] N. Meyer-Hübner, M. Haas, M. Uhrig, M. Suriyah, and T. Leibfried. Dynamic optimal power flow for dimensioning and operating quarter based storage in low voltage grids. In *2017 IEEE PES Innovative Smart Grid Technologies Conference Europe (ISGT-Europe)*. IEEE, September 2017.

[97] N. Meyer-Hübner, A. Mosaddeg, M. Suriyah, T. Leibfried, C. A. Canizares, and K. Bhattacharya. Large-scale dynamic optimal power flow problems with energy storage systems. In *2018 Power Systems Computation Conference (PSCC)*. IEEE, June 2018.

[98] N. Meyer-Hübner, M. Suriyah, and T. Leibfried. On efficient computation of time constrained optimal power flow in rectangular form. In *2015 IEEE Eindhoven PowerTech*. IEEE, June 2015.

[99] N. Meyer-Hübner, M. Suriyah, and T. Leibfried. N-1-secure optimal generator redispatch in hybrid AC-DC grids with energy storage. In *2018 IEEE PES Innovative Smart Grid Technologies Conference Europe (ISGT-Europe)*. IEEE, October 2018.

[100] N. Meyer-Hübner, M. Suriyah, T. Leibfried, V. Slednev, V. Bertsch, W. Fichtner, P. Gerstner, M. Schick, and V. Heuveline. Optimal storage operation with model predictive control in the German transmission grid. In Valentin Bertsch, Wolf Fichtner, Vincent Heuveline, and Thomas Leibfried, editors, *Trends in Mathematics*, pages 31–45. Springer International Publishing, 2017.

[101] N. Meyer-Hübner, M. R. Suriyah, T. Leibfried, V. Slednev, V. Bertsch, W. Fichtner, P. Gerstner, M. Schick, and V. Heuveline. Time constrained optimal power flow calculations on the German power grid. In *International ETG Congress 2015; Die Energiewende - Blueprints for the new energy age*, pages 1–7, November 2015.

[102] N. Meyer-Hübner, S. Weck, F. Bennewitz, M. Suriyah, K. Bhalodi, M. Giuntoli, V. Biagini, A. Krontiris, A. Wasserrab, M. Ndreko, M. Wiest, T. Leibfried, and J. Hanson. N-1-secure dispatch strategies of embedded HVDC using optimal power flow. In *2018 IEEE Power & Energy Society General Meeting (PESGM)*. IEEE, August 2018.

E.2.3 Co-authored articles

[103] T. Leibfried, T. Mchedlidze, N. Meyer-Hübner, M. Noellenburg, I. Rutter, P. Sanders, D. Wagner, and F. Wegner. Operating power grids with few flow control buses. In *Proceedings of the 2015 ACM Sixth International Conference on Future Energy Systems*, e-Energy '15, pages 289–294, New York, NY, USA, 2015. ACM.

[104] N. Schween, N. Meyer-Hübner, P. Gerstner, and V. Heuveline. A time step reduction method for multi-period optimal power flow problems. In *EMCL Preprint Series 2019-02*, 2019.

[105] V. Slednev, M. Ruppert, V. Bertsch, W. Fichtner, N. Meyer-Hübner, M. Suriyah, T. Leibfried, P. Gerstner, M. Schick, and V. Heuveline. Regionalizing input data for generation and transmission expansion planning models. In Valentin Bertsch, Wolf Fichtner, Vincent Heuveline, and Thomas Leibfried, editors, *Advances in Energy System Optimization*, pages 31–45, Cham, 2017. Springer International Publishing.

E.3 Supervised student theses

[106] I. Batsioudis. Analyse regionaler Lastprofile im deutschen Hochspannungsnetz. Diplomarbeit, KIT, 2015.

[107] J. Bocklisch. Vergleich von Software zur Netzberechnung am Beispiel der Übertragungsnetze von Spanien und Portugal. Bachelorarbeit, KIT, 2017.

[108] F. Erlewein. Möglichkeiten zur Speicherung von Energieüberschuss aus erneuerbaren Energiequellen und kombinierter optimaler Lastuss von Gas- und Elektrizitätsnetz. Diplomarbeit, KIT, 2016.

[109] D. Fetzner. Photovoltaik-Kraftwerke im FACTS-Betrieb. Masterarbeit, KIT, 2014.

[110] F. Gielnik. Speichereinsatz in gemischten AC/DC-Netzen durch zeitlichen Optimal Power Flow. Bachelorarbeit, KIT, 2016.

[111] M. Haas. Speicherdimensionierung und -betrieb in Niederspannungsnetzen durch zeitlichen optimalen Lastfluss. Masterarbeit, KIT, 2016.

[112] C. Ichoku. Modellierung des elektrischen Transportnetzes osteuropäischer Länder und Auswirkungen auf den Lastfluss bei Verbindung mit der 50Hertz-Regelzone. Bachelorarbeit, KIT, 2017.

[113] M. Körner. Bestimmung des Arbeitspunktes von gemischten AC/DC-Netzen durch Optimal Power Flow. Bachelorarbeit, KIT, 2015.

[114] S. Linke. Analyse des Stromverbrauchs in der Industrie über CO2-Zertikate. Masterarbeit, KIT, 2016.

[115] M. Mahmood. Modeling of the electrical transmission grid of northern germany. Masterarbeit, KIT, 2014.

[116] T. Quach. Kooperatives Lösungsverfahren zur optimalen Speichernutzung in gekoppelten elektrischen Netzen. Diplomarbeit, KIT, 2017.

[117] K. Sand. Bestimmung von Potential und Grenzen der KWK-Nutzung in Niederspannungsnetzen in Karlsruhe. Bachelorarbeit, KIT, 2015.

[118] T. Sandmeier. Berücksichtigung transienter Stabilität im optimalen Lastfluss. Masterarbeit, KIT, 2018.

[119] C. Schäfer. Modellierung und Lastflussanalyse südosteuropäischer Übertragungsnetze. Bachelorarbeit, KIT, 2018.

[120] J. Ungerland. Modellierung und Validierung des elektrischen Transportnetzes von Süddeutschland. Bachelorarbeit, KIT, 2014.

[121] F. Zghal. Netzstützender Betrieb von Speichern durch zeitlich unsymmetrischen optimalen Lastfluss. Masterarbeit, KIT, 2017.

Nomenclature

Abbreviations

AC	Alternating Current
ADMM	Alternating Direction of Multipliers Method
ALADIN	Augmented Lagrangian based Alternating Direction Inexact Newton
APP	Auxiliary Problem Principle
D-OPF	Dynamic Optimal Power Flow
DC	Direct Current
ESS	Energy Storage
FACTS	Flexible AC Transmission Systems
HVDC	High Voltage Direct Current
KKT	Karush-Kuhn-Tucker
MILP	Mixed Integer Linear Problem
NLP	Nonlinear Problem
OCD	Optimality Condition Decomposition
OPF	Optimal Power Flow
PST	Phase Shifting Transformer
PV	Photovoltaic
QP	Quadratic Problem
RES	Renewable Energy Source
SC-D-OPF	Security-Constrained Dynamic Optimal Power Flow

SC-OPF	Security-Constrained Optimal Power Flow
TSO	Transmission System Operator
UPFC	Unified Power Flow Controller
VSC	Voltage Source Converter

Dual variables

κ, ω	Dual variables of constraints in the interior point method
λ	Dual variables in distributed optimization
λ_{QP}	Dual variables of quadratic problem in ALADIN
z	Exchange variables in distributed optimization

Functions

$f(s)$	Nodal cost function
$F(x)$	Cost function in distributed optimization
$h(x)$	Equality and inequality constraints
$\mathit{Basics}(x)$	Collection of basic constraints
$\mathit{Costs}(x)$	Cost function
$\mathit{Dynamics}(x)$	Collection of dynamic constraints
$\mathit{N\text{-}1\ Coupling}(x)$	Collection of N-1 coupling constraints

Indices

$[\cdot]^c$	Topology ($c \in \mathcal{C}$)
$[\cdot]^t$	Time step ($t \in \mathcal{T}$)
$[\cdot]_{\mathcal{N}}$	Considered node set
$[\cdot]_k$	Region ($k \in \mathcal{R}$)

Parameters (I) – General

Δt	Time duration between two time steps
$\underline{X}, \overline{X}$	Lower and upper limit of element X
ξ	Occurrence of outage between two time steps ($0 \leq \xi \leq 1$)
a_{q}	Quadratic cost coefficient for reactive variable

a_X	Quadratic cost coefficient of variable X
b_X	Linear cost coefficient of variable X
C	Number of contingencies
g_{DC}	DC branch conductance
p	Cost weighting factor for a scenario
$P_{\mathrm{G,Disp}}$	Generator active power dispatch
R	Number of regions
$R_{\mathrm{N\text{-}1},X}$	Limit for curative action of variable X
$R_{\mathrm{T\text{-},G}}, R_{\mathrm{T+,G}}$	Lower and upper limit for generator ramping over time
T	Total number of time steps ($= T_{\mathrm{N\text{-}1}} + T_{\mathrm{N\text{-}0}}$)
$T_{\mathrm{N\text{-}0}}$	Number of N-0 secure time steps
$T_{\mathrm{N\text{-}1}}$	Number of N-1 secure time steps
Y_{AC}	Complex admittance matrix of AC network
Y_{DC}	Real admittance matrix of DC network
y_{P}	Parallel branch admittance
y_{Sh}	Shunt admittance
y_{SP}	Serial and parallel branch admittance ($= y_{\mathrm{P}} + y_{\mathrm{S}}$)
y_{S}	Serial branch admittance
Parameters (II) – Distributed Optimization	
μ	Stabilization parameter in ALADIN
ρ	Penalty parameter in ADMM and ALADIN
τ, Θ	Update parameters in ADMM
A	Consensus matrix in distributed optimization
r_μ	Iterative ramping of μ in ALADIN
W	Diagonal weighting matrix in distributed optimization
$W(S)$	Entries in W related to power
$W(V)$	Entries in W related to voltage

Sets

$\mathcal{C}$	Contingency scenarios ($= \{0, 1, .., C\}$)
$\mathcal{E}^{\mathrm{CL}}$	Considered lines for cost function
$\mathcal{E}^{\mathrm{D,Shed}}$	Sheddable loads
$\mathcal{E}^{\mathrm{D}}$	Loads
$\mathcal{E}^{\mathrm{ESS}}$	Energy storage systems
$\mathcal{E}^{\mathrm{G,Disp}}$	Dispatchable generators ($\mathcal{E}^{\mathrm{G,Disp}} \subseteq \mathcal{E}^{\mathrm{G}}$)
$\mathcal{E}^{\mathrm{G,Redisp}}$	Redispatchable generators ($\mathcal{E}^{\mathrm{G,Redisp}} \subseteq \mathcal{E}^{\mathrm{G}}$)
$\mathcal{E}^{\mathrm{G}}$	Generators
$\mathcal{E}^{\mathrm{Shunt}}$	Shunts
$\mathcal{E}^{\mathrm{VSC}}$	AC-DC converters
$\mathcal{N}$	All nodes
$\mathcal{N}^{\mathrm{AC}}$	AC nodes ($\mathcal{N}^{\mathrm{AC}} \subseteq \mathcal{N}$)
$\mathcal{N}^{\mathrm{DC}}$	DC nodes ($\mathcal{N}^{\mathrm{DC}} \subseteq \mathcal{N}$)
$\mathcal{N}^{\mathrm{Ref}}$	Reference (slack) nodes ($\mathcal{N}^{\mathrm{Ref}} \subseteq \mathcal{N}$)
$\mathcal{R}$	Regions ($= \{1, .., R\}$)
$\mathcal{S}$	Considered combinations of (t, c) where $t \in \mathcal{T}, c \in \mathcal{C}$
$\mathcal{T}$	Time steps ($= \{1, 2, .., T\}$)

Optimization variables

ψ_{PST}	Complex tap ratio of phase shifting transformer
E_{ESS}	Storage energy
I_{Br}	Complex AC branch current
P_{AC}	Injected active power at an AC node
P_{DC}	Injected active power at a DC node
P_{Br}	Active AC branch power flow
$P_{\mathrm{D,Shed}}$	Shedded active power from a load
P_{DCBr}	Active DC branch power flow

$P_{\mathrm{ESS,C}}$	Storage charging active power
$P_{\mathrm{ESS,D}}$	Storage discharging active power
$P_{\mathrm{G,Down}}$	Generator downward redispatch
$P_{\mathrm{G,Up}}$	Generator upward redispatch
P_{G}	Generator active power
$P_{\mathrm{VSC,L}}$	AC-DC converter losses
P_{VSC}	AC-DC converter active power on AC side
Q_{AC}	Injected reactive power at an AC node
$Q_{\mathrm{D,Shed}}$	Shedded reactive power from a load
Q_{ESS}	Storage reactive power
Q_{G}	Generator reactive power
Q_{VSC}	AC-DC converter reactive power on AC side
s	Variables assigned to a node
s_{AC}	Variables assigned to an AC node
s_{DC}	Variables assigned to a DC node
S_{Sh}	Apparent shunt power injection
S_{Br}	Apparent AC branch power flow
S_{VSC}	AC-DC converter apparent power on AC side
V_{AC}	Complex AC bus voltage
V_{DC}	Real DC bus voltage
x	All optimization variables

The future transmission grid for electrical power will face challenges on an unprecedented scale as the transformation of the energy system progresses. The massive integration of renewable energy sources will require new methods and additional equipment to maintain the system secure and cost-efficient. This doctoral thesis presents an approach to securely operate a transmission grid based on optimal power flow. Optimal control of phase shifting transformers, overlaying HVDC grids and large-scale energy storage lead to reduced operating costs. Furthermore, this work discusses efficient approaches to optimally coordinate multiple inter-connected control areas, if one central controller is undesirable for political or technical reasons.